APPLICABILITY STUDY OF ELECTROLYTE CARRIERS USED IN SACRIFICIAL ANODE CATHODIC PROTECTION FOR STRUCTURAL STEEL MEMBERS IN ATMOSPHERIC ENVIRONMENTS

徐, 捷

APPLICABILITY STUDY OF ELECTROLYTE CARRIERS USED IN SACRIFICIAL ANODE CATHODIC PROTECTION FOR STRUCTURAL STEEL MEMBERS IN ATMOSPHERIC ENVIRONMENTS

Jie Xu

Applicability Study of Electrolyte Carriers Used in Sacrificial Anode Cathodic Protection for Structural Steel Members in Atmospheric Environments

A Thesis Submitted
In Partial Fulfillment of the Requirements
For the Degree of
Doctor of Engineering

By

Jie Xu

九州大学

to the
DEPARTMENT OF CIVIL ENGINEERING
GRADUATE SCHOOL OF ENGINEERING
KYUSHU UNIVERSITY
Fukuoka, Japan
September, 2024

DEPARTMENT OF CIVIL ENGINEERING
GRADUATE SCHOOL OF ENGINEERING
KYUSHU UNIVERSITY
Fukuoka, Japan

CERTIFICATE

The undersigned hereby certify that they have read and recommended to the Graduate School of Engineering for the acceptance of this Thesis entitled, "***Applicability Study of Electrolyte Carriers Used in Sacrificial Anode Cathodic Protection for Structural Steel Members in Atmospheric Environments***" by **Jie Xu** in partial fulfillment of the requirements for the degree of **Doctor of Engineering**.

Dated: September, 2024

Thesis Supervisor:

Prof. Shigenobu Kainuma, Dr. Eng.

Examining Committee:

Prof. Hiroaki Nakano, Dr. Eng.

Prof. Takahiro Nishida, Dr. Eng.

ABSTRACT

Corrosion in atmospheric environments degrades the mechanical properties and durability of steel members. While methods like coating aim to enhance corrosion resistance, they may have limitations. The sacrificial anode cathodic protection (SACP) method, utilizing electrolyte carriers, emerges as a potential choice for corrosion protection without the need for surface treatment. However, its effectiveness in the atmospheric environment can be constrained by factors like electrolyte scarcity or high resistance of the electrolyte carrier. Therefore, the development of the electrolyte carriers with superior electrolyte absorption and retention capacities and high ionic conductivity is crucial for the application of the SACP method in the atmospheric environment. Moreover, the environment surrounding steel structures plays a pivotal role in their corrosion behavior, with factors such as humidity, temperature, airborne salts, and proximity to marine or industrial zones exerting distinct influences. Therefore, the development of the electrolyte carriers is also necessary to adapt the surrounding environments.

The development of electrolyte carriers for SACP methods used in the atmospheric environment is presented in this dissertation. Water-swelling rubber, cotton-like fiber and PANa-CMC hydrogels selected as electrolyte carriers were utilized in corrosion locations of in boundary with ground, enclosed sections, and high-humidity areas, respectively. The effectiveness of the SACP method with the above electrolyte carriers were evaluated by electrochemical experiments and SACP tests. Furthermore, the configuration, fixation with electrodes, hydrophilicity and ionic conductivity of the electrolyte carriers were also discussed, based on experiments such as water absorption and retention tests, adhesion tests.

The results showed that effectiveness of the three types of electrolytes, including water-swelling rubber, cotton-like fiber, and PANa-CMC hydrogels, in the SACP method were enough to protection steel members in corrosion locations of boundary with ground, enclosed sections, and high-humidity areas in the atmospheric environment. In the SACP method using water-swelling rubber for steel members located in boundary with ground, unless completely dry, rubber retains sufficient moisture for the maintenance of the sacrificial anode corrosion protection circuit. Besides, transitioning from a water-submerged to a dry environment is facilitated by the high-water retention capability of the rubber, ensuring the continuity of sacrificial anode action. Furthermore, the OCP of the Al-3Zn sacrificial anode was approximately −0.2 V relative to steel when immersed in the cotton-like fiber, indicating the effectiveness of the SACP method with cotton-like fiber applied for steel members in closed section. Meanwhile, the Al-3Zn alloy exhibited the ability to provide adequate and relatively stable protective current density and potential for steel members, mitigating corrosion risks within the cotton-like fiber environment. Moreover, PANa–CMC hydrogels coupled with Al–3Zn alloy generate and sustain a protective current to safeguard steel in high-humidity environments. Adding 5% CMC in hydrogels increases the density of the protective current up to about 3 μA/cm². These innovative applications pave the way for expanding SACP methods in atmospheric environments.

In addition, the suitability of the configuration of the three electrolyte carriers and the fixation to the electrodes for specific corrosion sites was discussed. Furthermore, the above electrolyte carriers showed superior water absorption and retention capacities, to sustain the SACP in the atmospheric environment. Moreover, the ionic conductivity of the electrolyte carriers was high enough to obtain protective current density for steel

members in atmospheric environment.

Keywords: Electrolyte carrier, Sacrificial anode cathodic protection (SACP), Atmospheric Corrosion, steel

Highlights:

(1) Electrolyte carriers were developed in the SACP method for steel members in atmospheric environments considering specifical corrosion locations.

(2) The suitability of the configuration of the three electrolyte carriers and the fixation to the electrodes for specific corrosion sites was discussed

(3) Water absorption and retention capability shows the potential applicability of electrolyte carriers in atmospheric environments.

(4) The ionic conductivity of the electrolyte carriers was high enough to obtain protective current density for steel members, coupling with sacrificial anodes.

TABLES OF CONTENTS

LIST OF TABLES

LIST OF FIGURES

CHAPTER 1 INTRODUCTION

1.1 Background

The realm of steel structural atmospheric corrosion represents a pivotal domain of inquiry encompassing multifaceted chemical, electrochemical, and physical transformations evident upon steel exposure to atmospheric elements[1-3]. Predominantly instigated by elements such as oxygen, water vapor, atmospheric oxides, acid rain, and saline compounds, this corrosion profoundly influences not only the aesthetic integrity of structural steel but also portends potential diminutions in its mechanical robustness and longevity, thus imperiling the dependability and safety of steel-based constructions[4-7].

The impetus for investigating atmospheric corrosion of steel emanates from the pragmatic repercussions of economic losses and safety hazards stemming from corrosive manifestations in real-world applications of steel[8-10]. Given the burgeoning demand for steel-infused structures—be it in the form of edifices, bridges, or maritime platforms—exposed to a gamut of environmental exigencies within engineering contexts, unraveling and governing atmospheric corrosion within steel matrices assumes paramount importance[11, 12].

The comprehensive investigation of atmospheric corrosion in steel structures necessitates a nuanced exploration of corrosion catalysts and mechanisms across diverse positions and environmental contexts[16, 17]. The disparate locations of steel exposure within a structure engender distinct corrosion dynamics, notably discernible at steel members in boundary with ground, enclosed sections, and high-humidity areas[9, 18-23], as shown in the Figure 1- 1.

Figure 1- 1 Representative atmospheric corrosion locations of steel members including: (a) steel members in boundary with ground[13], (b) enclosed sections [14], (c) high-humidity areas[15].

Primarily, the study of corrosion at the steel-concrete interface involves investigating the corrosion phenomena and associated mechanisms arising from the contact between two different materials[15]. Research in this field focuses on exploring the chemical, electrochemical, and physical reactions at the interface between concrete and steel, and their impact on structural durability and stability.

Common types of corrosion at this interface include electrochemical corrosion, alkali attack, and chemical corrosion. Electrochemical corrosion often arises from inter-metallic currents at different potentials, leading to corrosion on the surface of the steel. Additionally, alkali substances from concrete may penetrate the steel surface, causing alkali attack and surface damage to the steel[16, 17]. Furthermore, potential chemical ingress and reactions may result in corrosion at the steel-concrete interface.

Researchers aim to understand the mechanisms and characteristics of corrosion at this interface, proposing preventive and restorative measures accordingly. This involves mitigating the risk of interface corrosion through improved interface designs, specialized materials, and adjustments in concrete formulations[18-20]. Additionally, efforts are directed towards developing new coatings, protective measures, and monitoring

techniques to enhance the durability of steel-concrete interactions, ensuring long-term structural stability and reliability[20-22].

Secondly, the investigation into corrosion at enclosed sections delves into regions within structures that pose challenges in direct accessibility and protection, encompassing welded joints, obscured sections, and analogous areas. These zones, hindered in observation and safeguarding, are inherently predisposed to heightened susceptibility to corrosion, potentially manifesting distinct corrosion mechanisms and attributes in contrast to their exposed counterparts. Enclosed sections present a spectrum of corrosion types, including microbiological corrosion, stress corrosion cracking, anaerobic corrosion, and more[23-25]. For instance, the microenvironment prevailing within these concealed spaces, devoid of adequate oxygen and moisture, fosters conducive conditions for microbial proliferation, thereby instigating microbiological corrosion and expediting material degradation. Additionally, the interplay between structural stress and environmental influences could incite stress corrosion cracking in such concealed domains.

The core objective underpinning the exploration of corrosion at enclosed sections revolves around attaining an intricate understanding of corrosion mechanisms and contributory factors intrinsic to their specialized environments. This pursuit is geared toward devising more efficacious preventive and remedial strategies, necessitating the formulation of tailored protective methodologies. These encompass specialized coatings, judicious selection of alloy materials, enhancements in welding methodologies, and advancements in monitoring and assessment techniques tailored to appraise corrosion conditions within concealed areas.

Hence, the inquiry into corrosion at enclosed sections endeavors to meticulously probe

the challenges inherent in these challenging-to-surveil and safeguard spaces, striving to proffer more adept solutions to ensure structural integrity and reliability.

The scholarly inquiry into atmospheric corrosion at exposed surface areas is centered on the systematic exploration of corrosion dynamics and their ramifications on the surfaces of steel structures directly confronted with atmospheric elements[26]. These regions inherently exhibit heightened vulnerability to corrosion owing to the direct impact of constituents such as oxygen, moisture, salts, acid rain, oxidizing agents, and other atmospheric components[27, 28]. Within these exposed domains, pivotal factors encompassing humidity levels, temperature fluctuations, and chemical concentrations prevailing in the atmospheric milieu wield substantial influence over corrosion dynamics. Elevated humidity levels, when coupled with the presence of oxygen, expedite corrosion mechanisms. Furthermore, the deposition of salts, particularly pronounced in coastal or industrially polluted locales, accelerates the corrosion trajectory. Moreover, acidic compounds and oxidizing agents present in acid rain constitute pivotal contributors to corrosion incidence at exposed surfaces[29]. These agents instigate chemical reactions upon interaction with the steel surface, culminating in metal dissolution, oxidation processes, and subsequent corrosion affliction.

The paramount goal underscoring the investigation of atmospheric corrosion at exposed surface areas revolves around attaining a comprehensive grasp of corrosion mechanisms and influential determinants, concomitant with the formulation of targeted preventive and management protocols. The endeavors of scientists and engineers converge on the development of materials fortified against corrosion, specialized surface coatings, protective interventions, and proficient monitoring and assessment methodologies. These concerted initiatives are geared toward augmenting the longevity

of steel structures, fortifying their corrosion resilience, and ensuring steadfast stability and reliability even amidst adversarial atmospheric conditions.

Research endeavors targeting countermeasures against atmospheric corrosion are rooted in addressing the corrosion challenges confronting steel structures exposed to diverse atmospheric conditions. These strategic approaches encompass a spectrum of interventions, including material innovation, protective coatings, design refinement, monitoring methodologies, and maintenance strategies, all aimed at mitigating or impeding the deleterious impact of atmospheric corrosion on steel structures.

Central to these endeavors is material innovation, a pivotal facet entailing the advancement of more corrosion-resistant alloy materials, coatings, and protective surface treatments. This encompasses a multifaceted approach encompassing alloy refinement, bolstering steel's resistance against oxidation, weathering, and chemical degradation, alongside the creation of innovative protective coatings or films to fortify steel surfaces against atmospheric corrosion[30, 31]. Design optimization emerges as another critical sphere, involving a proactive integration of corrosion considerations during the structural design phase. Implementing apt structural designs and protective measures serves to curtail the susceptibility of structures to corrosion. This may encompass optimizing structural configurations, deploying suitable protective methodologies, and refining the design of structural constituents[32]. Furthermore, the development of monitoring techniques stands as a significant stride in the pursuit of countermeasures against atmospheric corrosion[33]. This aims at augmenting monitoring and diagnostic capabilities vis-à-vis the corrosion process. Refined monitoring methodologies enable prompt detection and assessment of corrosion degrees, furnishing crucial data support for preemptive maintenance and remedial actions.

However, persistent challenges and constraints persist within extant research on countermeasures against atmospheric corrosion. The diverse atmospheric exposures encountered by steel structures necessitate a nuanced approach, as a singular protective method may not comprehensively mitigate corrosion under varied environmental conditions. There exists an exigency for a deeper comprehension of corrosion mechanisms, fostering targeted protective technologies to fortify the durability and corrosion resistance of steel structures. Additionally, refining monitoring techniques remains pivotal, demanding greater precision and comprehensiveness to discern corrosion indicators early and facilitate more precise maintenance and repair interventions. In essence, sustained endeavors spanning diverse facets of research on countermeasures against atmospheric corrosion are imperative to confront the intricate corrosion challenges prevalent across heterogeneous environmental terrains.

1.2 Research objectives and scope

The primary objective of this dissertation is to advocate a specific remedy addressing atmospheric corrosion concerns in diverse segments of steel structures. This proposed solution centers on leveraging sacrificial anode cathodic protection (SACP) methodologies that employ electrolyte carriers within the atmospheric environment. Validating the viability of SACP protection technology within the atmospheric domain necessitates an initial comprehension of the corrosion milieu, its diverse conditions, and the underlying mechanisms influencing steel in varied locations. Unlike marine or soil settings, the atmospheric environment often lacks ample electrolytic components, accentuating the pivotal role of the electrolyte carrier's water-absorption capacity. This attribute stands as paramount to ensure the efficacy and enduring functionality of the SACP system. Moreover, the efficacy of this carrier, acting as an electrolyte conduit,

hinges significantly upon its conductivity and electrochemical interplay between the anode and cathode materials, profoundly influencing the efficiency and reliability of the system. Ultimately, comprehensive experimental validation assumes utmost importance to authenticate the genuine reliability and efficacy of the sacrificial anode system operating within the atmospheric environment.

The paper conducts an inquiry into three prevalent atmospheric corrosion scenarios—steel members in boundary with ground, enclosed sections, high-humidity areas—scrutinizing their respective environments and corrosion mechanisms. The proposition introduces rubber, cotton fibers, and hydrogels as prospective electrolyte carriers, subjecting them to rigorous examination of fundamental traits like water absorption rate, water retention capabilities, and ion conductivity. Subsequent phases of the research delve into the application of SACP technology within each of these scenarios, employing a combination of electrochemical analyses and exposure experiments. Ultimately, the study culminates in an evaluation of the technology's adaptability and efficacy within the atmospheric corrosion environment, grounded upon the findings derived from the experimental results.

This dissertation is organized basing on the objectives listed below:

(1) Investigate the corrosion characteristic and mechanism of steel members in different atmospheric environment. The corrosion occurrences at steel-concrete interfaces primarily result from the interaction between dissimilar materials. This intersection is susceptible to various mechanisms, including electrochemical corrosion and erosion triggered by alkali substances. Besides, enclosed sections encompass a range of corrosion types, spanning from long-term stagnant water to lacking sufficient oxygen and moisture. Furthermore, within high-humidity areas, steel components consistently experience

cycles of wetting and drying. Hence, the investigation serves to deepen our comprehension of the diverse corrosion traits and mechanisms exhibited by steel across various settings. This understanding fosters informed guidance for the selection of suitable electrolyte carriers in SACP technology, particularly within the atmospheric environment.

(2) Performing an in-depth analysis of the material properties inherent in the three primary electrolyte carriers—water-swelling rubber, cotton-like fibers, and hydrogels—stands as a pivotal endeavor. Grasping their water absorption capacities, retention capabilities, and ion conductivity assumes paramount significance for their effective deployment within SACP technology, specifically tailored to the atmospheric setting. Anticipated outcomes encompass tailored recommendations delineating application scenarios, derived from the inherent characteristics of these materials, and gleaned from the experimental findings.

(3) Carry out extensive electrochemical performance evaluations and validation experiments for the SACP system, utilizing the three specified electrolyte carriers: water-absorbent rubber, cotton-like fibers, and hydrogels, within atmospheric environments surrounding steel members adjacent to the ground, enclosed sections, and high-humidity areas. Focus these tests and experiments on thoroughly assessing the effectiveness and appropriateness of these carriers concerning the steel-concrete interface, enclosed surfaces, and exposed steel regions.

(4) SACP technology exhibits varying applicability within atmospheric conditions across three typical corrosion sites. Considerations encompass corrosion characteristics, mechanisms, the relationship between the electrolyte carrier and the anode metal plate, interconnection among steel plates, and the resultant protective effects. Drawing from

these factors, reasonable suggestions for the application of sacrificial anode cathodic protection methods in atmospheric settings can be proffered.

1.3 Literature review

1.3.1 Atmospheric corrosion and factors

Atmospheric corrosion denotes the intricate process by which metal materials undergo surface deterioration or chemical transformations upon exposure to diverse constituents prevalent within the atmospheric milieu, encompassing oxygen, water vapor, airborne particulates, and chemical species[34, 35]. The scholarly investigation into atmospheric corrosion holds paramount significance across multifarious domains, including but not limited to material degradation and its ensuing economic ramifications, the assurance of safety and reliability in engineering applications, the imperative mandate for environmental conservation and sustainable development, as well as the advancement of scientific inquiry[36, 37].

Atmospheric corrosion is a form of metal degradation that occurs when metal materials are exposed to factors such as oxygen, water vapor, particulates, and chemicals in the atmosphere. Its mechanism primarily involves electrochemical reactions and physicochemical processes:

Atmospheric corrosion predominantly involves electrochemical reactions between the metal surface and elements like oxygen and water vapor in the environment[1, 38]. In a typical electrochemical corrosion process, the metal surface undergoes oxidation reactions, producing metal ions (e.g., iron ions), alongside reduction reactions, where oxygen or water is reduced to hydrogen gas or ions[39, 40]. These electrochemical reactions lead to corrosion and loss on the metal surface.

Atmospheric corrosion is also influenced by physicochemical processes in the environment[41]. For instance, humid conditions or salt-laden atmospheres containing chloride ions may expedite corrosion by enhancing conductivity and ion migration rates, thereby increasing the rate of metal corrosion. Variations in climate conditions, such as fluctuations in temperature, humidity, and oxygen content, also affect the extent of corrosion[42].

During the corrosion process, a corrosion product layer like oxides or carbonates may form on the metal surface[43]. Sometimes, these layers act as protective barriers, slowing down the corrosion rate. However, in certain situations, they might accelerate corrosion because they can be unstable or detach, exposing new metal surfaces[44].

Overall, atmospheric corrosion is a complex process influenced by the characteristics of the metal material, environmental conditions, and the interplay of electrochemical and physicochemical factors. Different metals may exhibit varied corrosion behaviors in different environments. Understanding the mechanisms of corrosion aids in devising effective preventive and protective measures to mitigate or prevent corrosion.

1.3.2 Mechanism of atmospheric corrosion of steel members considering locations

In structural engineering and materials science, the susceptibility of steel structures to atmospheric corrosion is a critical concern that directly impacts their durability and safety. Atmospheric corrosion, a complex process influenced by various environmental factors, can vary significantly based on geographical locations. This study embarks on a comprehensive investigation into the intricate mechanisms underlying the atmospheric corrosion of steel members, with a keen focus on the role of specific locations.

The environment surrounding steel structures plays a pivotal role in their corrosion behavior, with factors such as humidity, temperature, airborne salts, and proximity to

marine or industrial zones exerting distinct influences. This research seeks to unravel the nuanced interactions between these environmental elements and the corrosion processes affecting steel members, emphasizing the importance of considering diverse geographical locations in our analysis.

By delving into the specifics of atmospheric conditions prevalent in different regions of steel structures, this investigation aims to identify patterns and correlations between environmental factors and the corrosion rates observed in steel structures. Understanding these location-dependent mechanisms is imperative for designing corrosion-resistant materials, implementing effective maintenance strategies, and enhancing the overall longevity and structural integrity of steel members.

Furthermore, the findings of this study hold substantial implications for industries, infrastructure development, and urban planning, where accurate assessments of corrosion risk are crucial for ensuring the safety and sustainability of structures over their operational lifetimes. As we explore the multifaceted aspects of atmospheric corrosion, this research endeavors to contribute valuable insights that can inform practical solutions for mitigating corrosion-related challenges, tailored to specific geographical contexts.

(1) Corrosion characteristics of steel members in the boundary ground

Understanding the intricate corrosion phenomena at the juncture between steel and concrete stands pivotal, given its profound implications not only on material engineering performance but also on the structural integrity and longevity of constructions. The corrosion mechanisms within this interface are governed by a confluence of factors, inclusive of environmental parameters, concrete quality, steel properties, and their interplay.

Primarily, stagnant water is prone to occur in areas of steel members in boundary with

ground[45, 46], as depicted in Figure 1- 2. The porosity inherent in concrete facilitates the ingress of water, oxygen, and chemicals around steel reinforcements. The presence of moisture carrying salts precipitates an acceleration of the corrosion process. Meanwhile, the alkaline milieu intrinsic to concrete fosters the formation of a shielding oxide layer on steel surfaces; however, this protective shield is compromised in the wake of fissures or impairments.

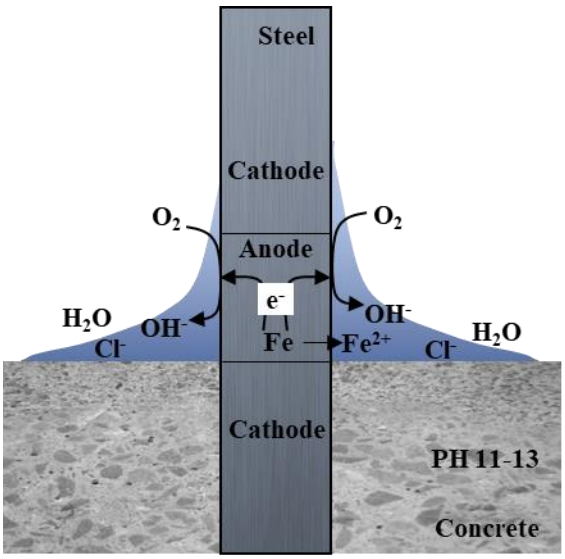

Figure 1- 2 Stagnant water in areas of steel members in boundary with ground.

Secondarily, the disparate coefficients of thermal expansion between steel and concrete lead to the formation of minute fissures, serving as conduits for moisture and oxygen infiltration[47]. These fissures offer a passage for these agents to reach the steel surface, thereby catalyzing corrosion reactions, as shown in Figure 1- 3. Electrochemical mechanisms also play a pivotal role, especially in the presence of electrolytes like salts within the concrete matrix. Differential electrochemical regions on steel surfaces lead to localized corrosion, potentially culminating in steel structural failures.

The pursuit of effective corrosion prevention strategies has spurred extensive research endeavors. This encompasses advancements in concrete formulations to curtail

permeability and stabilize the alkaline environment. Additionally, technologies spanning corrosion-resistant coatings, inhibitors, and SACP have garnered significant attention to fortify steel resilience at the steel-concrete interface.

In summary, comprehending the intricate corrosion mechanisms at the steel-concrete junction necessitates a nuanced grasp of material attributes, structural design, and prevailing environmental conditions. Through the diligent application of tailored protective measures informed by such understanding, the endurance and safety of concrete structures witness significant elevation.

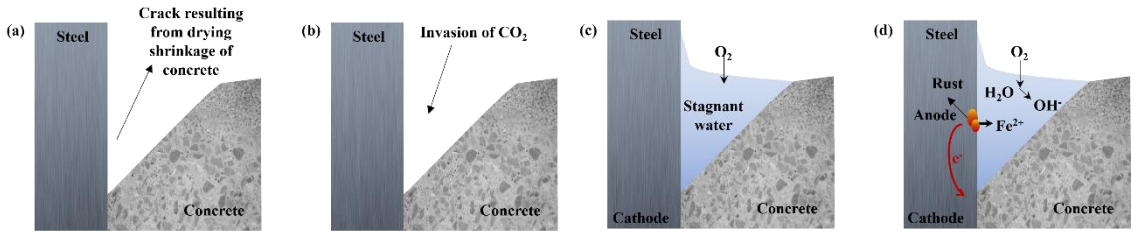

Figure 1- 3 Corrosion characteristics of steel members in boundary with ground.

(2) Corrosion characteristics of steel members in enclosed sections

The corrosion of enclosed sections in steel is a crucial yet intricate issue, often referring to the interior or concealed areas of steel components that cannot be directly observed due to environmental factors or other reasons. This form of corrosion poses a potential threat to the stability and durability of structures as its development is concealed and difficult to detect, leading to severe structural damage.

Corrosion in enclosed sections is primarily influenced by various factors. Firstly, environmental elements such as humidity, temperature, oxygen, and salts play a crucial role. Enclosed or sealed spaces often contain oxygen and moisture that are difficult to eliminate, providing the foundational conditions for corrosion. When a humid atmosphere contains salts or other chemical substances, they accelerate the corrosion process.

Secondly, the occurrence of corrosion in enclosed sections is also affected by the

material's characteristics and quality control. Defects, cracks, oxides, as well as residual dirt or salts from manufacturing processes, could serve as starting points for corrosion. Factors such as the material's chemical composition, microstructure, residual stresses, etc., can also influence the rate and extent of corrosion.

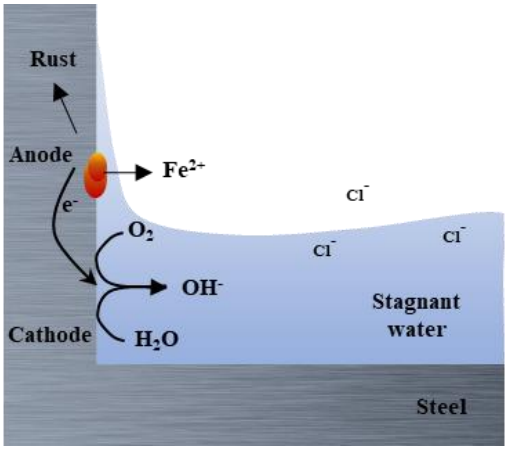

Figure 1- 4 Corrosion characteristics in closed sections.

The mechanism of corrosion in enclosed sections also involves electrochemical reactions. In a moist environment, different electrochemical zones can form on the steel surface, where some areas act as anodes while others serve as cathodes, resulting in localized corrosion. Since enclosed sections are difficult to observe and maintain, corrosion reactions may propagate internally without timely detection and intervention.

To prevent and control corrosion in enclosed sections, engineers and researchers focus on developing various detection techniques and protective measures. Techniques like non-destructive testing such as ultrasonic, X-ray, and magnetic particle inspection are employed to assess corrosion in concealed areas. Additionally, measures like corrosion-resistant coatings, corrosion inhibitors, cathodic protection, among others, are extensively studied and applied to slow down or impede the corrosion process in enclosed sections.

In conclusion, corrosion in enclosed sections of steel poses challenges in detection and

control, requiring diverse technical means and protective measures. A comprehensive understanding of corrosion mechanisms and the implementation of effective preventive and monitoring measures are crucial in enhancing structural durability and safety.

(3) Corrosion characteristics of steel members in high-humidity areas

The corrosion characteristics of steel components in the exposed surface area are primarily influenced by environmental factors and the exposure conditions of the components. These characteristics include, but are not limited to, the following aspects:

Firstly, the corrosion of steel components in the exposed surface area is directly affected by atmospheric conditions. Humidity, temperature, oxygen content, and the concentration of pollutants in the atmosphere all play a crucial role in the corrosion rate of steel components, as shown in Figure 1- 5. High humidity and high temperatures often accelerate the corrosion process, while pollutants such as oxides and chloride ions may further exacerbate the corrosion rate. Secondly, the shape and design features of steel components in the exposed surface area also influence the degree and form of corrosion. Factors such as surface irregularities, angles, seams, and connection methods may lead to localized corrosion, such as pitting and intergranular corrosion. Additionally, surface treatment and protective measures also significantly impact the corrosion characteristics. For example, coatings, corrosion-resistant paints, plating, and other protective measures can effectively shield the steel component surfaces from corrosion, slowing down the corrosion rate and severity. However, the quality and durability of these protective measures are crucial factors affecting corrosion characteristics.

In summary, the corrosion characteristics of steel components in the exposed surface area are influenced by a combination of factors, including atmospheric conditions, component design, surface treatment, and protective measures. A thorough understanding

of these characteristics and the implementation of effective protective measures are essential for prolonging the service life and maintenance intervals of steel components.

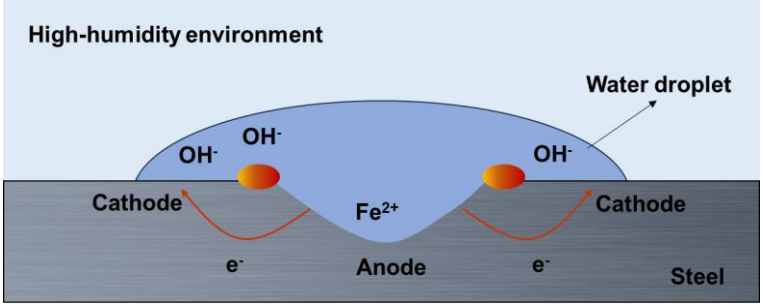

Figure 1- 5 Corrosion characteristics in high-humidity areas.

1.3.3 Corrosion resistance methods for atmospheric corrosion

Atmospheric corrosion protection involves various strategies and measures, including but not limited to the following aspects:

(1) Metal surface coatings or protective films: Metal surface coatings or protective films are one of the common protective measures against atmospheric corrosion[48]. This method involves forming a layer of coating or protective film on the metal surface, serving as a barrier to isolate the external corrosive environment and protect the metal substrate. These coatings can employ various chemical compositions and application techniques[49, 50].

Coating techniques like spraying, electroplating, hot-dip galvanizing, painting, or powder coating serve as effective methods to establish protective layers on metal surfaces[51-53]. These applied layers function as formidable barriers, shielding the metal from exposure to atmospheric elements such as oxygen, water, and various chemicals. By creating this protective barrier, these coatings impede or slow down the corrosion process, effectively prolonging the lifespan of metal materials in diverse atmospheric conditions. Each coating method offers unique advantages and applicability, contributing to the

overall arsenal of corrosion protection techniques available for metal surfaces. Some coatings also possess properties such as abrasion resistance, high-temperature resistance, corrosion resistance, UV resistance, and chemical stability, enhancing the protective effect on metal surfaces[54-56].

Despite the significant advantages of metal surface coatings or protective films as a defense against atmospheric corrosion, they also come with certain drawbacks or limitations[57]. Firstly, when exposed to harsh environmental conditions over an extended period, such as high temperatures, humidity, or exposure to chemical gases, coatings might experience wear, peeling, or cracking, thereby reducing their protective efficacy[58]. Secondly, improper application or variations in coating quality may result in unevenness or defects, leaving certain areas of the metal surface exposed to corrosive environments[59]. Additionally, certain coatings might not offer adequate resistance to specific corrosive agents, leading to the potential for localized or accelerated corrosion[60]. Lastly, maintaining and repairing coatings pose challenges[61]. Once damaged or aged, coatings require prompt repairs to sustain their effectiveness, often demanding substantial time and cost[62]. Hence, while coatings serve as effective corrosion prevention measures, regular monitoring and maintenance are essential to ensure their enduring corrosion protection.

(2) Alloys or corrosion-resistant metal materials: In the protection against atmospheric corrosion, choosing alloys or corrosion-resistant metal materials is an effective measure[63]. These materials typically exhibit higher corrosion resistance by adjusting their chemical composition or incorporating specific alloying elements, imparting enhanced corrosion resistance to the material itself. For instance, stainless steel, nickel-based alloys, aluminum alloys, and others are widely utilized to resist atmospheric

corrosion[64, 65]. During the alloying process, corrosion-resistant elements such as chromium, nickel, molybdenum, etc., are introduced, forming a dense oxide layer or other corrosion-resistant compounds, thereby improving the metal surface's resistance to corrosive media like oxygen and water vapor[66]. However, it is important to note that different environmental conditions may impact various alloy materials differently. Therefore, careful consideration based on the specific usage environment and the characteristics of the corrosive medium is necessary when selecting materials to maximize their corrosion resistance.

Although alloys or corrosion-resistant metal materials possess good corrosion resistance in protecting against atmospheric corrosion, their applications still have some drawbacks and limitations[67]. Firstly, high-performance alloys typically come with higher costs, which increase engineering and manufacturing expenses, posing economic challenges for large-scale applications[68]. Secondly, under certain extreme environmental conditions such as extremely high temperatures, strong acids, strong alkalis, even corrosion-resistant alloys might face corrosion, necessitating additional protective measures or the selection of special materials[69]. Moreover, certain alloys may exhibit sensitivity in specific environments, offering limited resistance to corrosive media, demanding more complex material selection and protective measures[70]. Finally, the processability and availability of alloy materials might also be limited, sometimes failing to meet the requirements of complex structures or specific processes, which could restrict their widespread application. Therefore, despite the corrosion resistance of alloys or corrosion-resistant metal materials, a comprehensive consideration of their cost, environmental conditions, and specific application requirements is essential in selecting the most suitable corrosion prevention measures.

(3) Cathodic protection: Cathodic protection (CP), as an effective method against atmospheric corrosion, works by introducing an external current to the metal surface, turning it into the cathode in electrochemical reactions, thus slowing down or inhibiting metal corrosion[71]. It mainly consists of sacrificial anodes and impressed current methods. In SACP methods, a more easily corroded metal (usually zinc or aluminum) is introduced as the anode, sacrificing itself to protect the primary metal structure[72]. On the other hand, impressed current cathodic protection (ICCP) applies a negative current from an external power source to maintain the metal surface in a reduced state, thereby suppressing the oxygen reduction reaction and slowing down the corrosion process[73].

One challenge faced by CP methods in atmospheric corrosion prevention is the lack of sufficient electrolyte[74]. In certain environmental conditions, such as dry or low-humidity atmospheric environments, conductive electrolytes (like rain water) may be insufficient. In such cases, cathodic protection requires an adequate electrolyte to sustain current transfer, ensuring the metal surface effectively functions as the cathode. However, insufficient moisture or electrolyte content in the environment may affect the efficiency of the CP system since the lack of electrolyte reduces current transmission and distribution, thereby compromising its protective effect.

Despite the significant challenges faced by CP systems in atmospheric environments, researchers have explored its application in preventing corrosion of steel reinforcement in reinforced concrete structures. In terms of cathodic protection for reinforcing bars in concrete structures, research indeed focuses on several key aspects. Firstly, it centers on the design and optimization of cathodic protection systems, concentrating on determining the optimal current density, protection potential, and electrode materials[75-77]. This work aims to ensure the cathodic protection system effectively safeguards the reinforcing

bars while minimizing adverse effects on the concrete structure[78]. Secondly, the research looks into the impact of cathodic protection on the mechanical performance and durability of concrete[79, 80]. This line of study strives to ascertain the degree of influence of the cathodic protection process on concrete performance to mitigate potential negative impacts. In practical engineering, these systems must sustain effective operation continually and adapt to varying environmental conditions to ensure the long-term corrosion resistance of concrete structures[81]. Overall, the current research focus lies in exploring cathodic protection technologies that are more effective, reliable, and have minimal impact on concrete structures[82]. These endeavors aim to enhance the durability and reliability of concrete structures, ensuring their long-term resistance to corrosion.

The issue of inadequate electrolytes might be particularly pronounced in dry or low-rainfall areas, where atmospheric moisture content is relatively low. In such scenarios, alternative methods to enhance electrolyte supply, such as adding water or other conductive fluids, might be necessary to ensure the continual effective operation of the CP system. Consideration of environmental conditions and electrolyte supply is crucial in designing and implementing cathodic protection systems to ensure their stability and effectiveness.

(4) Environmental control and maintenance: Environmental control and maintenance in atmospheric corrosion protection are key strategies aimed at regulating and managing the conditions under which metals are exposed to the atmosphere to reduce or delay the corrosion rate[83, 84]. This method involves managing several aspects:

Firstly, controlling environmental conditions is crucial, including temperature, humidity, and gas composition[85-87]. By maintaining appropriate humidity and temperature levels, as well as controlling the oxygen content and concentrations of other

corrosive substances in the air, the exposure time of metals to corrosive environments can be reduced, thereby slowing down the corrosion process. Secondly, regular cleaning and maintenance are also crucial. Timely removal of impurities, dirt, and deposits from the metal surface helps prevent them from becoming the starting point or accelerant for corrosion[88, 89]. This practice contributes to maintaining the cleanliness and smoothness of the metal surface, slowing down corrosion. Additionally, standard maintenance measures include inspecting and repairing surface coatings or protective films. Periodically checking the integrity and quality of coatings and repairing or replacing worn, cracked, or peeled sections ensures that the coatings continue to provide protection.

Indeed, the comprehensive approach to corrosion prevention often involves a combination of various measures tailored to specific circumstances and environmental demands. By integrating multiple strategies, such as coatings, SACP, coating, or other methods, tailored solutions can be devised to safeguard metal materials effectively. This multifaceted approach aims not only to prolong the lifespan of metal materials but also to mitigate the detrimental effects posed by atmospheric corrosion. However, despite the breadth of available corrosion prevention measures, as highlighted in the literature review, several persistent challenges hinder their practical application. These unresolved issues often encompass practical limitations, technological barriers, or deficiencies in current methodologies. Addressing these challenges becomes pivotal for advancing the effectiveness and efficiency of corrosion prevention strategies, ensuring their adaptability across diverse environmental conditions and operational contexts. Resolving these persisting issues stands as a critical frontier in advancing the field of corrosion prevention, aiming for more robust, sustainable, and reliable protection of metal materials against

atmospheric corrosion.

1.3.4 Electrolyte carriers and application in SACP in atmospheric environment

As mentioned in section 1.3.2, the role of electrolytes in sacrificial anode cathodic protection methods is particularly crucial. Hence, research on electrolytes carriers in the atmospheric environment or substances capable of serving as carriers of electrolytes becomes highly significant. An electrolyte refers to a compound present in a solution or solid state in the form of ions, capable of conducting electricity under the influence of an electric field[90]. Based on their physical state and conductivity, electrolytes can be divided into two categories: liquid electrolytes and solid electrolytes[91-93].

Liquid electrolytes are electrolyte systems formed in a liquid solvent, typical examples include salts dissolved in water or acid-base solutions. In liquid electrolytes, the solvent serves as a medium, aiding the movement of electrolyte molecules or ions, facilitating electrical conduction[94, 95].

Solid electrolytes refer to electrolyte systems existing in a solid state that possess ion migration capability[96]. This type of electrolyte is commonly found in solid materials such as oxides, sulfides, polymers, among others[97, 98]. Solid electrolytes conduct electricity in their solid state as well and find extensive applications in batteries, sensors, electrochemical devices, and more[99, 100].

The classification of electrolytes is not only based on their physical state but also on their ionic properties, conductivity, and chemical composition. The distinct characteristics of liquid and solid electrolytes enable their significant roles in various fields and applications, offering extensive prospects in energy storage, electrochemical reactions, chemical sensing, and beyond.

As stated in section 1.3.2, liquid electrolytes are difficult to sustain in the atmospheric

environment to maintain protective currents in the SACP method. Therefore, solid-state electrolytes or materials capable of long-term maintenance of liquid electrolytes (hereafter collectively referred to as electrolyte carriers for ease of reference) are gradually emerging as a new alternative.

Efforts have been made to extend the application of SACP method to environments where there is no standing water or limited access to an electrolyte. For instance, SACP has been employed in the protection for reinforcement bars in the concert. The introduction of SACP involves creating a protective electric field around the reinforcement bars, converting the surface of the bars into a cathode and generating an anodic zone around them, thereby slowing down or preventing the corrosion process of the reinforcement bars[101, 102]. Literature has reported the application of SACP in laboratory settings and practical engineering, confirming its effective anti-corrosion effects on reinforced concrete structures[103-105]. Furthermore, studies delve into the working mechanism of SACP, including aspects like current density, potential control, and electrochemical reactions, providing theoretical support for its application in engineering practice[106-108]. Studies indicate that SACP method not only effectively extends the service life of structures and reduces maintenance costs but also significantly improves the durability and reliability of concrete structures[109, 110]. This provides reliable grounds for the widespread application and promotion of SACP in practical engineering. Despite demonstrating tremendous potential in the field of corrosion prevention, the application of SACP still faces some challenges[77, 111]. The literature points out issues related to the implementation difficulty, long-term stability, and cost-effectiveness of SACP method in large-scale projects[112-114]. In the future, researchers are seeking to improve the method, address these challenges, and continuously explore

new materials and processes to enhance the performance and reliability of SACP. These reviews in the literature summarize the application scenarios, achievements, and challenges of SACP technology in reinforced concrete structures, providing valuable references for further research and engineering practices of this technology.

Another approach to expand the application of SACP method is the use of hydrophilic materials, such as absorbent fiber sheet as electrolyte carriers or even as electrolytes themselves[74, 114]. These hydrophilic materials can absorb and retain water from rain, dew and even moisture, allowing them to serve as effective electrolyte carriers in environments where traditional electrolytes may be limited or inaccessible[115, 116]. This approach offers a promising solution to extend the reach of SACP method to a wider range of conditions and substrates[117, 118]. However, challenges persist in the application of hydrophilic materials. The use of a fiber sheet requires bolting to steel members, potentially compromising their mechanical strength[119].

In conclusion, SACP has been applied to some extent in the atmospheric environment. Its key aspect still revolves around the presence and maintenance of the electrolyte. Hence, it is necessary to develop more electrolyte carriers to adapt to various atmospheric corrosion environments.

1.4 Organization and outline

In the subsequent chapters of this dissertation, a comprehensive exploration of the subject matter unfolds, delineating various aspects in detail across chapters 2 through 6. The thematic breakdown across these chapters offers an in-depth examination and analysis as follows:

Chapter 2: This chapter delves into the properties and potential of water-swelling rubber, notable for its high elastic modulus and capacity to retain moisture, such as

rainwater, over extended durations. The core strategy revolves around the sacrificial anode corrosion protection method, which employs hydrophilic rubber. This innovative approach takes advantage of the rubber's moisture-absorbing capabilities when exposed to waterlogged conditions near the ground, offering continuous corrosion protection. During drier periods, the retained moisture within the rubber still provides a protective barrier. Crucially, the swelling behavior of the rubber is expected to significantly improve the bond between the anode material and the steel, potentially enhancing the overall effectiveness of anode corrosion protection. The primary objective of this research is to assess the fundamental influence of hydrophilic rubber on the performance of anode corrosion protection in proximity to the ground for steel members, aiming for a comprehensive understanding of its protective benefits and implications for structural integrity.

Chapter 3: An absorbent cotton-like fiber coupling with Al-3Zn alloy (acting as anode) was used in SACP method for corrosion protection for steel members in closed section. To verify the applicability of the cotton-like fiber, experiments on water absorption and retention capacity, electrochemical properties, and corrosion resistant performance in SACP method were carried out. The results indicated that the open circuit potential (OCP) and Nyquist plots of steel and Al-3Zn alloy, underscored the promising potential of the cotton-like fiber as a highly effective electrolyte carrier for facilitating the implementation of the SACP method for closed-sectional steel members in atmospheric environment. The Al-3Zn alloy exhibited a sufficient and consistent protective current density and potential for steel members against corrosion within the cotton-like fiber environment.

Chapter 4: This chapter focused on the development of PANa–CMC hydrogels as electrolytes for the SACP method, with the objective of safeguarding steel against

corrosion in high-humidity environments. Various evaluations were performed to assess the efficacy of the SACP method using PANa–CMC hydrogels. The results shows that the electrochemical performance of the hydrogels was analyzed using Electrochemical impedance spectroscopy (EIS) and polarization curves, focusing on parameters such as ionic conductivity, equivalent circuit, corrosion current density of Al-3Zn anodes, and steel. Constant exposure tests were also conducted to evaluate the time-dependent anti-corrosion performance of the hydrogels, considering the characteristics of the steel surface condition and protective current density. Additionally, the impact of PANa–CMC hydrogels on fixing metal ions from anodes and reducing the formation of passive film in the SACP method was discussed. Overall, the results indicate that PANa–CMC hydrogels exhibit promising characteristics as eco-friendly electrolytes and expand the application of the SACP method to high-humidity environments.

Chapter 5: This chapter delves into the nuanced aspects that significantly influence the performance of electrolyte carriers within the challenging context of atmospheric environments. A comprehensive exploration encompasses the configuration of these carriers, the fixation between carriers and electrodes, considerations of hydrophilicity, and an in-depth examination of ionic conductivity. Understanding these critical factors is pivotal for optimizing the effectiveness of SACP systems and ensuring the enduring protection of metallic structures against the pervasive threat of corrosion. The results shows that the configuration of three electrolyte carriers can be adapted to their application environments, respectively. Moreover, these three electrolyte carriers exhibit a level of adhesion to steel members to sustain cathodic protection current. Notably, the PANa-5%CMC hydrogel demonstrates a higher bonding strength, reaching 603.6 kPa. Furthermore, each materials shows remarkable water absorption and retention capability,

due to the functional groups such as -OH and -COOH. Additionally, the electrochemical properties including OCP, ionic conductivity ensure that the effectiveness of SACP reaction can also be guaranteed in atmospheric environments.

Chapter 6: This chapter summarized the work presented in this dissertation, future research topics emerged from this work were also proposed.

The flowchart of work in this dissertation is shown in Figure 1- 6.

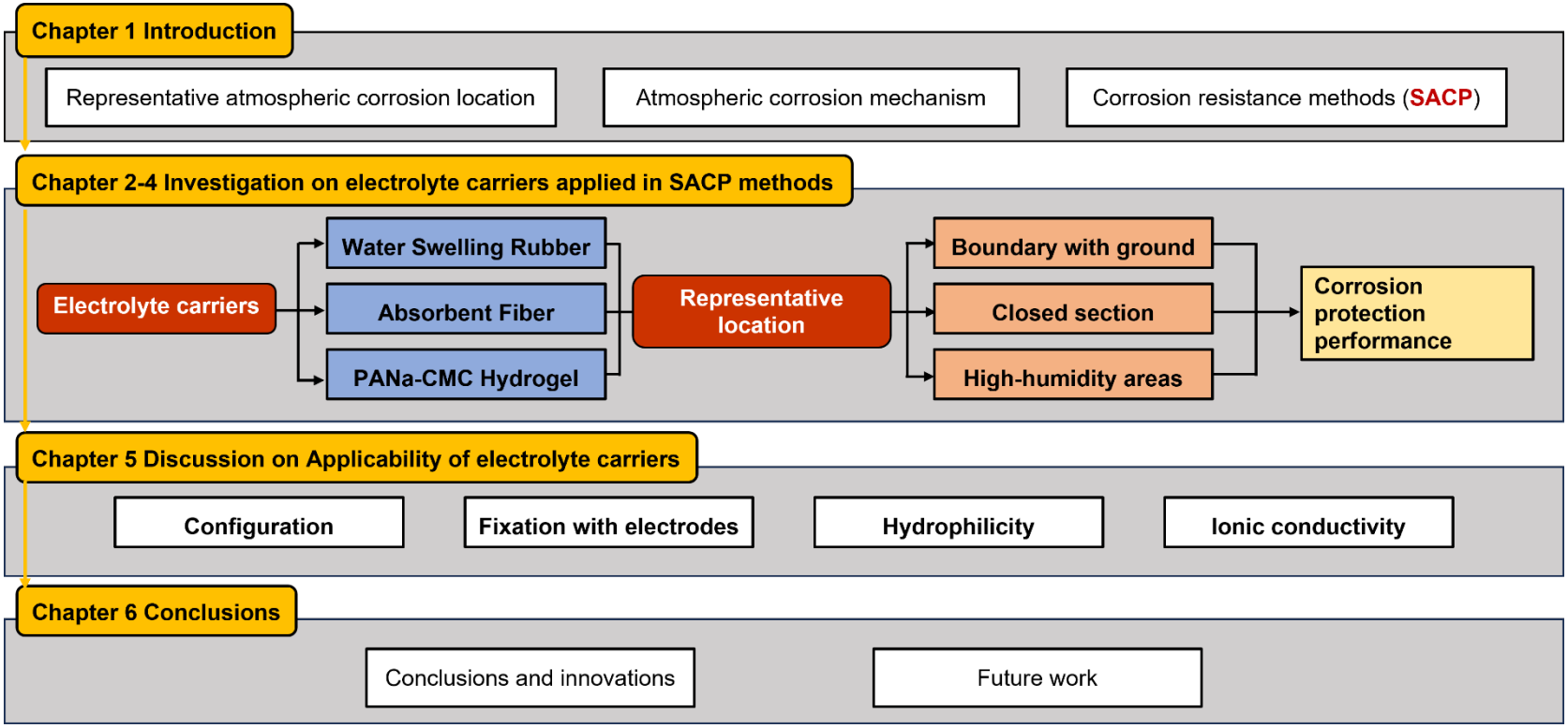

Figure 1- 6 Flowchart of the dissertation.

CHAPTER 2 FUNDAMENTAL STUDY ON WATER-SWELLING RUBBER IN SACP METHOD APPLIED FOR STEEL MEMBERS IN BOUNDARY WITH GROUND

2.1 Introduction

In the ground interface of steel structural members, extended exposure to environmental elements, particularly rainwater, can trigger highly aggressive localized corrosion. Numerous instances have been documented where this localized corrosion has culminated in structural failures[120-122].

The corrosion of steel members in contact with the ground poses a significant challenge. It not only diminishes the cross-sectional area of the steel but also alters the bond behavior between steel and concrete[123]. Corrosion-induced changes in material properties at the interface are noteworthy[124]. Moreover, the volumetric expansion of steel due to corrosion can lead to concrete cover cracking and spalling. This compromises the effective confinement of steel, subsequently weakening the bond between corroded steel and concrete[125].To prevent corrosion in the interface between steel members and concrete, coatings are commonly employed. However, the application of anti-rust coatings on the steel surface always leads to a reduction in the adhesion between the steel and concrete[126, 127]. For the other hand, corrosion is prone to occur, where the coating is vulnerable to deterioration[128]. In addition, dew and stagnant water with chloride from antifreeze at the corner of the structure contribute to corrosion of steel members, especially[129].

Apart from the coating, SACP is the most broadly utilized strategy to diminish corrosion. However, an electrolyte is necessary, so that SACP is preferred for protection

for steel structures buried in soil or submerged in water[130]. Its application in a dry environment is still raw and problems exist[131]. Recently, S. Kainuma fixed sacrificial anode and fiber sheet with high water absorption and retention properties together, to achieve the anti-corrosion effect for steel plates[74]. However, the fiber sheet is difficult to fit with steel members at the corner of the structure tightly over a long period of time. In this study, instead of fiber sheet, water swelling rubber with higher elastic modulus was applied in the SACP system. The water swelling rubber was expected to act as an electrolyte carrier with high absorption and retention capacity to prevent corrosion under different environmental conditions. The rubber acts as a moisture supply material necessary for SACP. During stagnant water conditions, it absorbs and retains moisture, providing corrosion protection. In dry conditions, corrosion protection is facilitated through the water content within the rubber. The swelling of the rubber is expected to enhance adhesion between the anode material and the steel.

2.2 Material and SACP method using the water-swelling rubber

2.2.1 Material and the SACP system

The water-swelling rubber (40 × 40 × 5 mm) utilized in this study, as depicted in Figure 2- 1 and detailed in Table 2- 1, serves as a water-swelling sealing agent commonly employed in shield tunneling methods. For additional information, please refer to the corresponding patent or utility model number.

Table 2- 1 Properties of water-swelling rubber.

Density (kg/dm^3)	Modulus of elasticity	Hardness H^*	Tensile strength	Stretching H_B(%)	Volume change rate
1.2	0.65	A40±5	4.0+	500+	200+

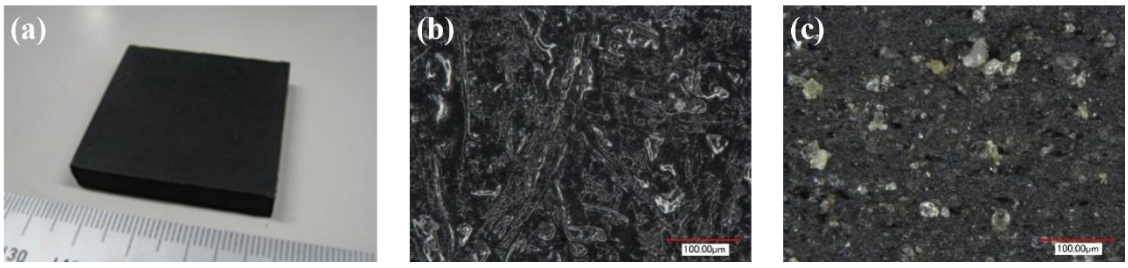

Figure 2- 1 (a) Appearance and (b) enlarged view of surface and (c) cross section view of the water- swelling rubber.

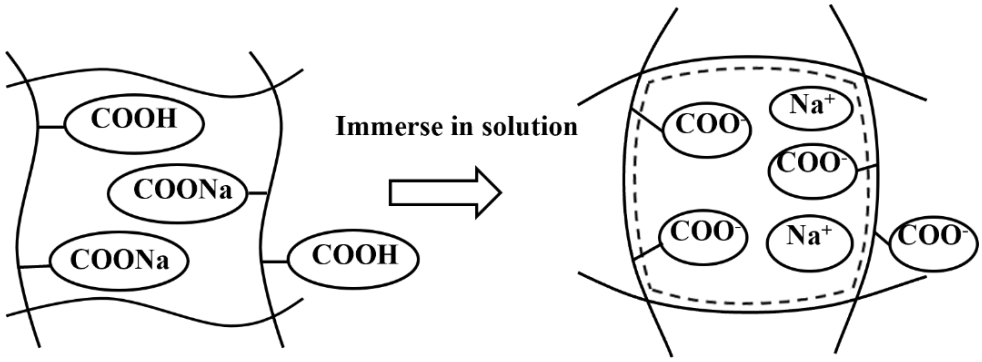

Figure 2- 2 Mechanism of superabsorbent polymer.

This water-swelling rubber is primarily composed of chloroprene synthetic rubber and is a vulcanized rubber-based water-swelling sealing material. To enhance its water-absorption capabilities, a high water-absorbing polymer with excellent electrolyte resistance (sodium salt-crosslinked acrylic acid polymer) is incorporated into the rubber network. This polymer absorbs water and swells, causing an increase in the rubber's volume. Furthermore, the inclusion of a hydrophilic polyurethane component enhances water permeability deep into the rubber.

Figure 2- 2 illustrates the water absorption mechanism of the high water-absorbing polymer. The polymer forms a mesh structure inside the rubber, and as cations within the polymer dissolve into water, osmotic pressure develops between the dissolved water and the water in the surroundings. Osmotic pressure continues until the concentration

difference of cations diminishes, allowing the absorption of a substantial amount of moisture. After absorbing water, the polymer undergoes gelation, effectively retaining moisture.

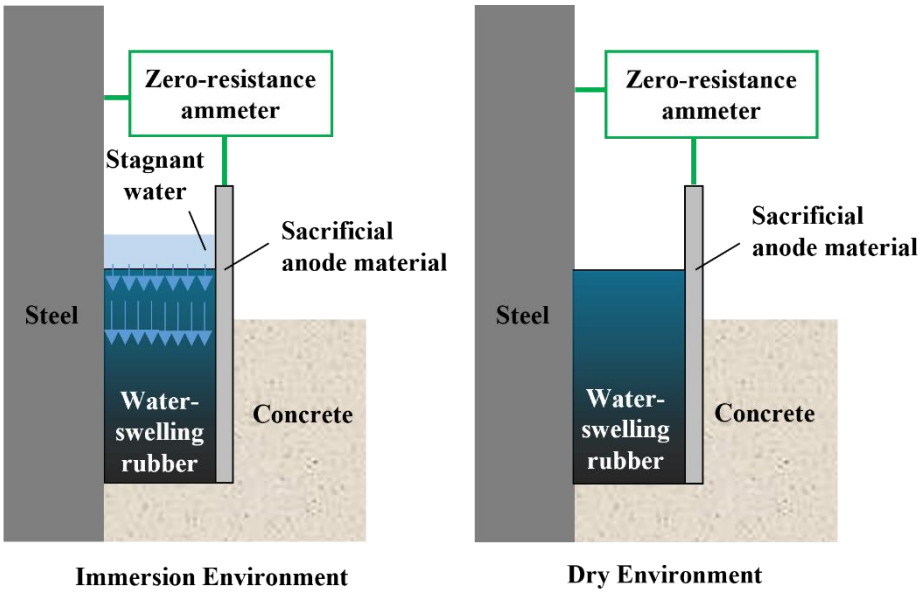

Figure 2- 3 Anti-corrosive method with sacrificial anode using water-swelling rubber.

Materials for the SACP system: A zinc plate was chosen as the sacrificial anode, the efficacy of which having been previously confirmed in atmospheric conditions. The SM490A steel, compliant with the Japanese Industrial Standard (JIS) G3106, was employed as the cathode. The sodium polyacrylate hydrogel acts as electrolyte carrier. The chemical composition of the steel is shown in Table 2- 2.

Table 2- 2 Chemical composition and dimensions of the steel.

Material	Chemical compositions (wt%)							
	Al	Zn	Fe	C	Si	Mn	P	S
Steel	-	-	balance	0.16	0.36	1.45	0.014	0.007

The CP system applied in this study includes a Zn plate and water swelling rubber, which are fixed together and attached to a surface-cleaned steel plate by a peek bolt and

an acrylic plate, as depicted in Figure 2- 3. The steel plate, acting as cathodic material, directly contacts with the rubber and is connected with the Zn plate acting as a sacrificial anode, by lead wires.

2.2.2 Wet- dry water absorption and retention tests

To comprehend the water absorption characteristics of water-swelling rubber, comprehensive water absorption and drying tests were executed. The water-swelling rubber (40 × 40 × 6 mm) underwent immersion in electrolyte, and temporal changes in water absorption were tracked, identifying the maximum water absorption as a distinctive feature. Distilled water and NaCl solutions at concentrations of 0.1, 3.5, and 7.0 wt% were employed in the water absorption tests. Following immersion, the rubber was extracted from the electrolyte, and after wiping off surface moisture, its weight was measured.

The immersion period for rubber soaked in distilled water and a 3.5 wt% NaCl solution was 60 days. To compare water absorption capacities at different NaCl concentrations, the immersion period for rubber soaked in 0.1 and 7.0 wt% NaCl solutions was set at 30 days. Water absorption tests were carried out in an atmospheric environment at approximately 17°C. To ensure a constant electrolyte concentration, electrolyte exchange transpired every 7 days.

Furthermore, drying tests involved letting the test samples, previously swollen in water absorption tests, stand in the atmosphere. Following the removal of surface moisture, the rubber was allowed to stand in the atmospheric environment, and weight measurements were conducted akin to water absorption tests. The drying period extended over 60 days, with drying occurring in an atmospheric environment at approximately 17°C. Refer to Table 2- 3 for the detailed test conditions for water absorption and drying.

Table 2- 3 Condition of the water absorbing and drying test.

Specimen	Steeping environment	Steeping period	Drying period	Initial weight (g)
A	Distilled water	60days	60days	12.09
B	3.5wt%NaCl aq			12.92
C	0.1wt%NaCl aq	30days	—	13.09
D	7.0wt%NaCl aq			12.76

2.2.3 Ionic conductivity of water-swelling rubber

To assess the SACP effect under different stress conditions, resistance measurements and sandwiched tests were conducted, varying the type and concentration of electrolyte within the rubber. The rubber was immersed in NaCl and $NaNO_2$ solutions with concentrations of 0.1, 1.0, 5.0, and 10.0 wt%, with an immersion period of 20 days. The resistance measurement system is depicted in Figure 2- 4(a), where a Pt plate served as the counter electrode (CE), and an ordinary steel plate was the working electrode (WE). The sandwiched test specimen, shown in Figure 2- 4(b), consisted of swollen rubber, an ordinary steel plate (60 × 60 × 9 mm, JIS G 3106 SM490A material), and a Zn plate (40 × 40 × 1 mm). Applying loads of 2 kg and 6 kg (uniform distributed stress: 1.2×10^{-2} and 3.7×10^{-2} N/mm^2) on the Zn plate maintained a constant distributed load on the rubber. The test duration was 24 hours, and the corrosion condition of the steel plate was examined post-test.

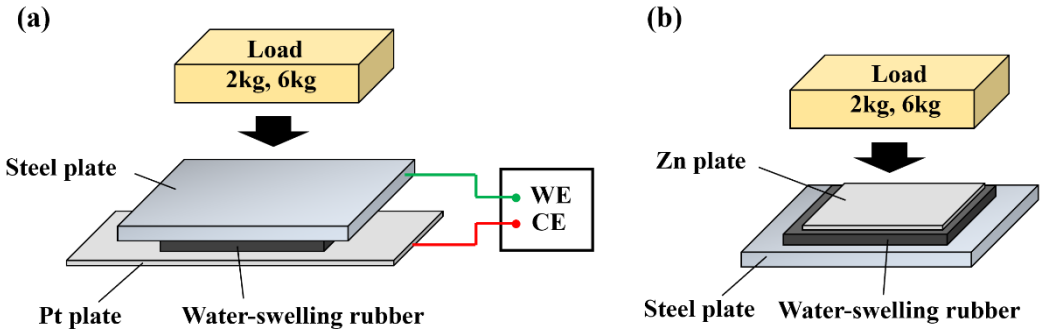

Figure 2- 4 (a) Components of (a) specific electrical resistance measurement system and (b) sacrificial anode specimen.

The specific resistance of each specimen can be calculated using Equation (3-1):

$$\rho = \frac{l}{R \cdot A} \tag{3-1}$$

Where R is the solution resistance of the swollen rubber, A is the area of the rubber, and l is the thickness of the rubber.

2.2.4 Wet- dry environmental SACP tests

To investigate the corrosion resistance of steel members at the concrete-ground interface in actual environments, tests simulating stagnant water and dry conditions were conducted. Specimens were created using rubber soaked in electrolyte, steel plates, and an anode material, and the characteristics of corrosion current in stagnant water and dry conditions were examined.

The specimens consisted of mild steel plates (JIS 3106 SM490A material, alumina blast-treated), Zn plates, water-swollen rubber, and PEEK bolts, as shown in Figure 2- 5. The water-swollen rubber was sandwiched between the steel plate and the anode plate, and the assembly was joined with PEEK bolts, with acrylic sheets used for positioning. The test utilized specimens soaked in 1.0 and 5.0 wt% NaNO2 aq for 30 days. Additionally, to verify the characteristics of the corrosion current based on the amount of

electrolyte in the rubber, specimens were prepared by soaking rubber for 60 days and drying it for 40 days. For comparison with specimens containing an anode material, specimens without a Zn plate were also set up.

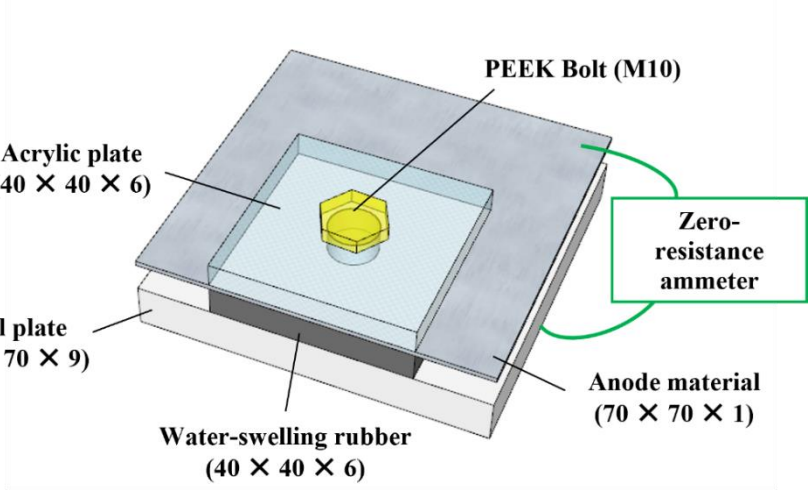

Figure 2- 5 Configuration and dimensions of the specimens (Unit: mm).

Table 2- 4 Test conditions of SACP tests.

Specimens	Electrolytes		Absorption period (day)	Drying period (day)	Immersion environment	Sacrificial anode material
	Electrolyte	Concentration (wt%)				
Dew1.0	$NaNO_2$	1.0	30	—	3.5wt% NaCl aq	Zn plate
Dew5.0		5.0				
Dry1.0		1.0	60	40		
Dry5.0		5.0				
Dew1.0-0.1		1.0	30	—	0.1wt% NaCl aq	
Dew1.0-X		1.0	30	—	3.5wt% NaCl aq	—

To simulate the conditions of water stagnation and drying at the ground interface in real environments, the following steps (1) to (3) were performed in order. The test specimens were placed in a constant temperature and humidity chamber at 18°C and 75% relative humidity.

(1) Air Curing (Dry Environment, 0–120 hrs.)

The specimens were left in a constant temperature and humidity chamber for measurement. The measurement period was 120 hours.

(2) Immersion Test (Stagnant Water Environment, 120–240 hrs.)

The specimens were immersed in 3.5 wt% NaCl aq for measurement. Additionally, one specimen with rubber swollen in 1.0 wt% $NaNO_2$ aq was immersed in 0.1 wt% NaCl aq. The measurement period was 120 hours.

(3) Air Curing (Dry Environment, 240–360 hrs.)

The specimens immersed in step 2 were removed, and air curing tests were conducted in an environment similar to step 1. The measurement period was 120 hours.

During the tests, external wires were connected to measure and record the corrosion current generated by the short circuit between the anode plate and the steel plate using a zero-resistance ammeter at 10-minute intervals. The conditions of the rubber during the test, the swelling and drying periods, and the immersion environment are presented in Table 2- 4.

2.3 Performance of the water-swelling rubber in the SACP method

2.3.1 Time-dependent protective current density

The temporal changes in corrosion current $I(\mu A)$ for each specimen are presented in Figure 2- 6. Note that 'Dry1.0' had poor contact around 280 hrs., and thereafter, I was

not measured. During the immersion test, is approximately 10-30 times higher than during air curing. This suggests that not only the electrolyte in the rubber but also the immersed electrolyte affects the corrosion current.

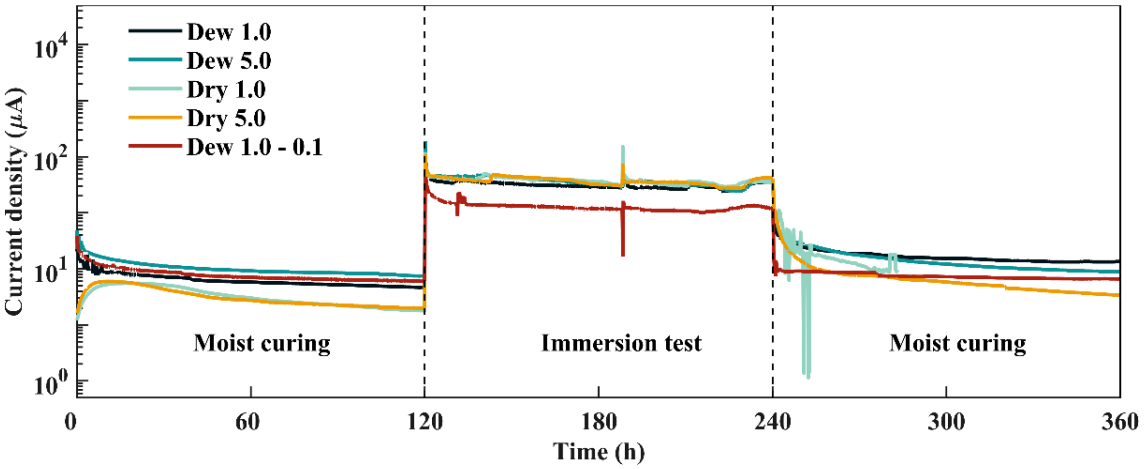

Figure 2- 6 The time-dependence of corrosion current for specimens.

The values of for Dew1.0, Dew5.0, and Dew1.0-0.1 during 0-120 hrs. are similar. Since these use swollen rubber, it is assumed that the concentration of the electrolyte in the rubber does not affect. Additionally, for Dry1.0 and Dry5.0, which use dried rubber, current density is measured from the beginning. This implies that unless the rubber is completely dry, sacrificial anode corrosion protection is manifested through the minute moisture within the rubber. The magnitude of I during air curing is influenced by the amount of water absorbed by the rubber. However, for concentrations above 1.0 wt%, the effect of concentration is considered small.

During the immersion period (120-240 hrs.), I for Dew1.0, Dew5.0, Dry1.0, and Dry5.0 follows a similar trend. Compared to Dew1.0-0.1 immersed in 0.1 wt% NaCl aq, the I for specimens immersed in 3.5 wt% NaCl aq is significantly higher. This indicates that when the corrosion circuit through the rubber is immersed in the electrolyte, the corrosion current depends on the surrounding immersion environment. The impact of

rubber's water absorption and concentration becomes minimal due to the significant influence of the immersion environment.

During the second air curing period (240-360 hrs.), I exhibits a similar trend to the first air curing period. Specimens using swollen rubber show higher I compared to Dry5.0, which uses dried rubber. Even with the transition from stagnant water to a dry environment, the I for each specimen remains stable, indicating that the rubber's high water retention capability sustains I.

2.3.2 The calculation of the total amount of electricity

The total electric charge Q during air curing and the total electric charge Q during the immersion test for each specimen are shown in Figure 2- 7. For specimens immersed in 3.5 wt% NaCl aq, Q during 240-360 hrs. is about 2-3 times higher than during 0-120 hrs. On the other hand, Dew1.0-0.1 shows a similar Q magnitude in both the first and second air curing periods. This suggests that Dew1.0, Dew5.0, Dry1.0, and Dry5.0 absorbed 3.5 wt% NaCl aq during the immersion test, leading to an increase in I compared to the first air curing period.

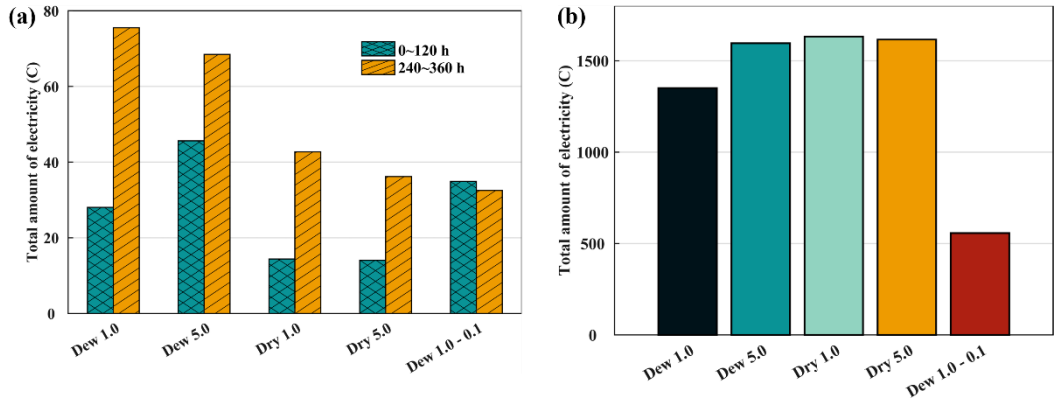

Figure 2- 7 The total amount of electricity for specimens of (a) moist curing and (b) immersion test.

2.3.3 Surface condition of the steel plate protected by the SACP method

The corrosion condition of the steel plates after 24 hours of the sandwiched test is shown in Table 2- 5. Based on the visual inspection of the steel plates, the impact of stress on the corrosion effect is minimal.

Table 2- 5 Corrosion protection situation of the steel surface.

	NaCl		$NaNO_2$	
	1.2×10^{-2} MPa	3.7×10^{-2} MPa	1.2×10^{-2} MPa	3.7×10^{-2} MPa
0.1 wt%	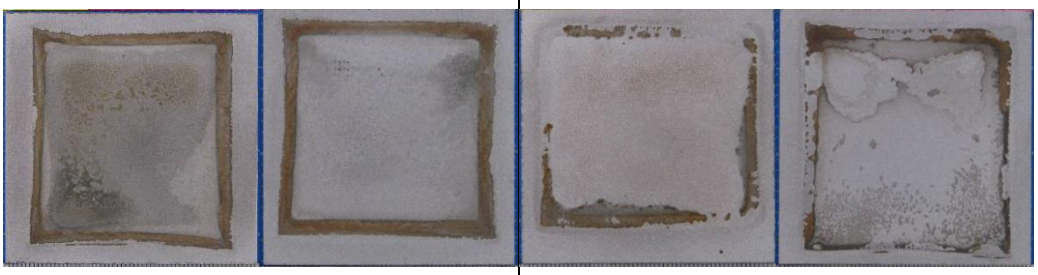			
1 wt%	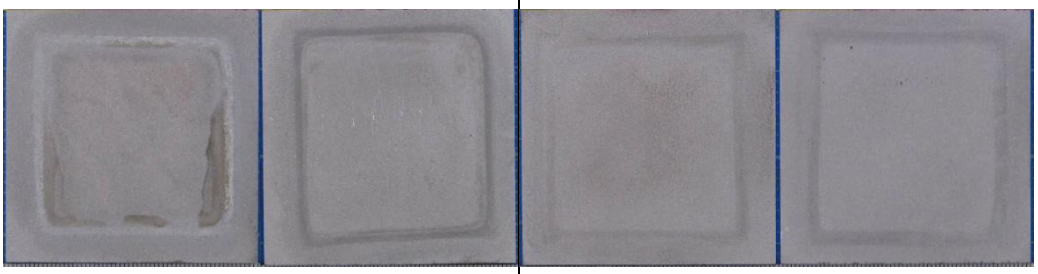			
5 wt%	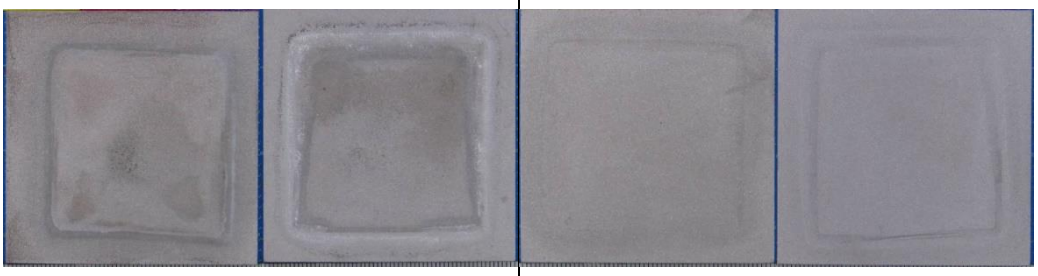			
10 wt%	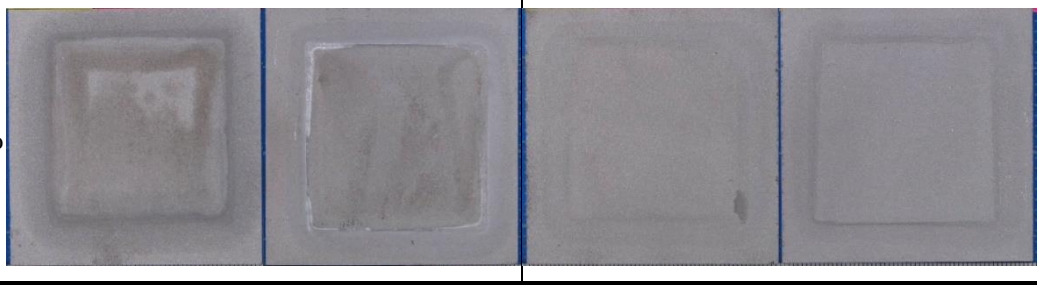			

In each electrolyte, the corrosion effect at 0.1 wt% concentration is the lowest, with the

outer surface of the rubber contact area in each specimen showing corrosion. When the concentration of the electrolyte inside the rubber is 0.1 wt%, the SACP effect is considered to be low. On the other hand, in specimens using rubber soaked in $NaNO_2$ aq, corrosion is almost absent at concentrations of 1.0– 10.0 wt%, indicating a high corrosion protection effect. $NaNO_2$ is commonly used as an oxidizing corrosion inhibitor, and in addition to this, the SACP effect mediated by moisture within the rubber is presumed to have influenced the corrosion protection effect on the steel plates.

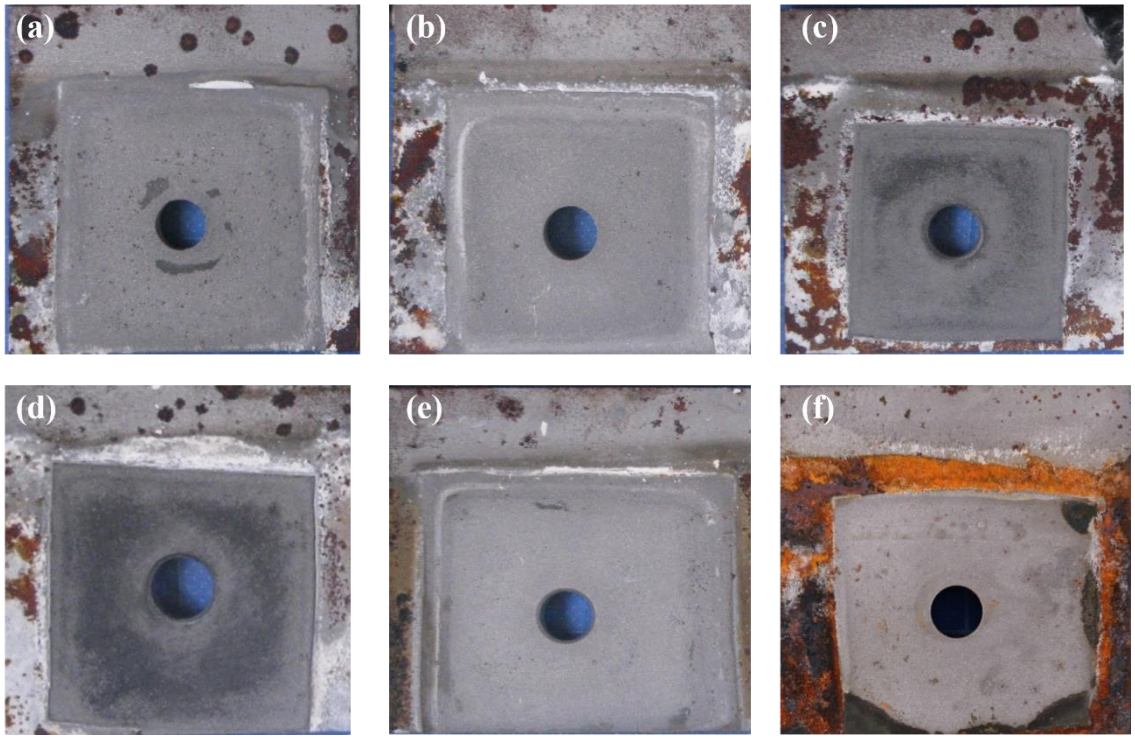

Figure 2- 8 Corrosion protection situation of the steel surface after the test.

SEM-EDX analysis results for Dew1.0 and Dew1.0-0.1 are presented in Figure 2- 9. In areas ①, ③, and ④ on the contact surface, residue of adhered rubber material (Si) is observed due to the tight adherence of the rubber. In the uncontacted area ②, chloride ions (Cl) from the 3.5 wt% NaCl aq immersion environment are observed, and oxide (O, Fe) is generated on the steel substrate. The upper black part ④ on the contact surface

has a high content of oxide (O), suggesting that due to the drying of the rubber during air curing, gaps occurred between the rubber and the steel plate.

The corrosion status of the rubber contact surface for each specimen is presented in Figure 2- 8. The corrosion status for specimens using swollen rubber is nearly identical. There is no observable corrosion on the rubber contact surface for each specimen, indicating sufficient corrosion protection. The corrosion status for specimens without a Zn plate is shown in Figure 2- 8(f). Similar to specimens with a Zn plate, most of the rubber contact area shows corrosion protection. This suggests that the adherence of the rubber to the steel plate reduces the dissolved oxygen (DO) at the contact site, enhancing sacrificial anode action.

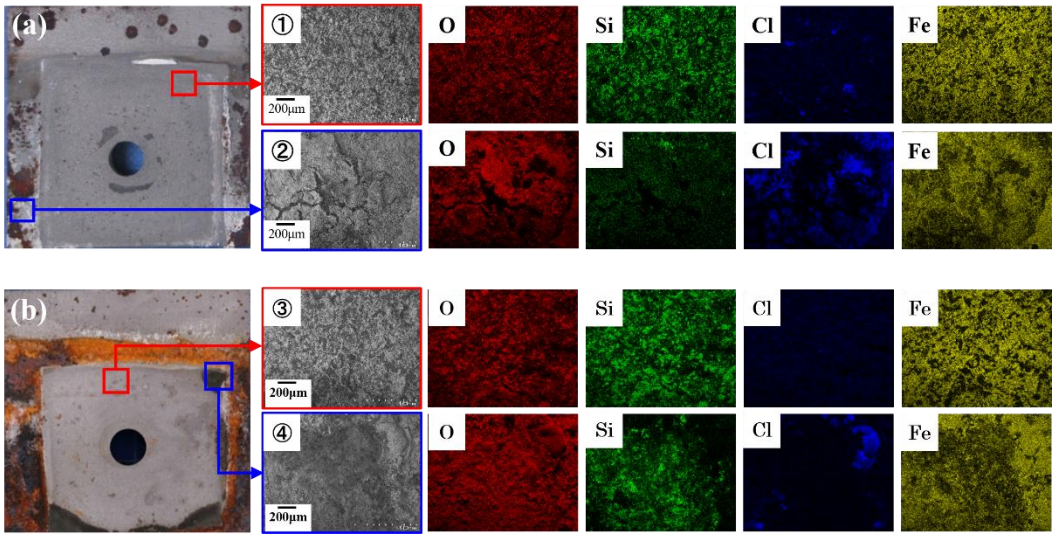

Figure 2- 9 Surface elemental analysis results of (a) Dew1.0 specimen and (b) Dew1.0-X specimen.

An enlarged view of the upper black part is shown in Figure 2- 10. In the red-framed area in Figure 2- 10, partial corrosion progression is visible. Unlike specimens with a Zn plate, no such corrosion progression is observed, indicating sufficient corrosion protection even at the edge of the steel plate. This is attributed to the use of an anode

material, which ensures corrosion protection even in minimal gaps through sacrificial anode action.

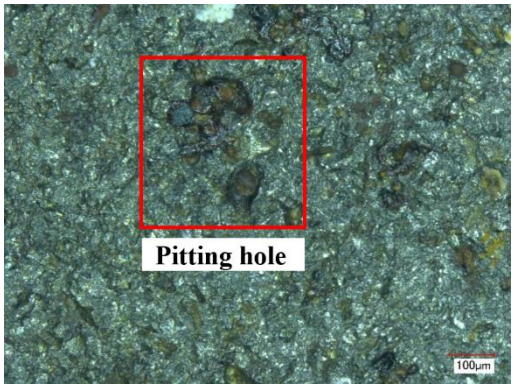

Figure 2- 10 Enlarged view of specimen Dew1.0-X. (×500).

2.4 Summary

In this investigation, we delve into the development of sacrificial anode corrosion protection technology utilizing water-swelling rubber for the concrete-ground contact area of steel members. The primary objective is to elucidate the influence of water-swelling rubber on the effectiveness of sacrificial anode corrosion protection. The key insights derived from this study include:

(1) Unless completely dry, rubber retains sufficient moisture for the maintenance of the sacrificial anode corrosion protection circuit.

(2) Transitioning from a water-submerged to a dry environment is facilitated by the high-water retention capability of the rubber, ensuring the continuity of sacrificial anode action.

CHAPTER 3 COTTON-LIKE FIBER ACTING AS ELECTROLYTE CARRIERS IN THE SACP SYSTEM FOR CLOSED-SECTIONAL STEEL STRUCTURES

3.1 Introduction

Common carbon steel has been widely employed in offshore structures, such as oil drilling platforms, ship hulls, and bridges[132, 133]. However, certain regions of these structures, particularly closed section parts such as steel light pole exposed to rain, are prone to stagnant water accumulation[134, 135]. Stagnant water, along with DO and chloride ions, accelerates the corrosion process of steel members of closed sections, as depicted in Figure 1- 1(b). The wet/dry cyclic process, attributed to the formation of a liquid film, is widely recognized as the primary cause of corrosion of steel members[136-138]. Additionally, corrosion has significant economic implications, with studies reporting national costs ranging from 1% to 5% of the gross national product (GNP)[48, 139]. Therefore, enhancing the corrosion resistance of carbon steel is crucial, and appropriate corrosion mitigation approaches need to be implemented.

In steel structures exposed to atmospheric environments, corrosion prevention typically relies on surface coatings such as paint[140-142]. However, during the repainting of steel structures, chloride ions from airborne sea salt or anti-freezing agents may persist on the steel substrates. The residual presence of chloride ions can trigger early sub-coating corrosion, significantly diminishing the longevity of the coating[143, 144]. Therefore, the coating may deteriorate prematurely, and instances of corrosion recurrence are common[145]. Consequently, the requirement for the development of corrosion prevention techniques is increasing, particularly for critical components in structures

situated in corrosive environments with intricate assemblies or confined spaces that do not require high-quality substrate preparation such as painting. SACP is widely acknowledged as a highly effective method for corrosion protection of offshore steel structures[146, 147]. The SACP system relies on the use of a more negative metal, such as aluminum (Al) or zinc (Zn), to generate a protective current naturally. However, SACP system is limited in aqueous and soil environments due to the requirement of an electrolyte for the continuity of the electrochemical circuit[148, 149].

Efforts have been made to extend the application of SACP method to atmospheric environments where there is no standing water or limited access to an electrolyte. One approach to extend SACP method involves utilizing its throwing power to protect the exposed portions of structures, such as marine concrete structures[103, 104]. Indeed, concrete has the potential to act as an electrolyte despite its relatively high resistivity. However, it is important to note that the protective area in which SACP method can be effectively applied may still be limited due to the high resistivity of concrete[111, 150]. Another approach to expand the application of SACP method is the use of hydrophilic materials, such as absorbent fiber sheet as electrolyte carriers or even as electrolytes themselves. These hydrophilic materials can absorb and retain water from rain, dew and even moisture, allowing them to serve as effective electrolyte carriers in environments where traditional aqueous electrolytes may be limited or inaccessible. This approach offers a promising solution to extend the reach of SACP method to a wider range of conditions and substrates. However, the application of hydrophilic materials remains challenging. The use of a fiber sheet necessitates bolting to steel members that could potentially compromise their mechanical strength[115]. Furthermore, under dry conditions, the water-swelling rubber contracts, creating a gap between the rubber and

the steel and resulting in inadequate protection of the steel. Additionally, the adhesive strength of the hydrogel is compromised by excessive water absorption during rainy periods. Consequently, these materials may not be ideal for improving the corrosion resistance of steel members in closed sections.

In this research, an absorbent cotton-like fiber coupling with Al-3Zn alloy (acting as anode) was used in SACP method for corrosion protection for steel members in closed section. To verify the applicability of the cotton-like fiber, experiments on water absorption and retention capacity, electrochemical properties, and corrosion resistant performance in SACP method were carried out. The results indicated that the cotton-like fiber exhibited remarkable water absorption capabilities, absorbing electrolyte nearly 7 times its weight within a 10-minute duration. Additionally, even after exposure to an environment at 26°C and 30% humidity for 15 days, it retained over 50% of its maximum water absorption capacity. Moreover, the electrochemical properties observed, including ion conductivities, the open circuit potential (OCP) and Nyquist plots of steel and Al-3Zn alloy, underscored the promising potential of the cotton-like fiber as a highly effective electrolyte carrier for facilitating the implementation of the SACP method for closed-sectional steel members in atmospheric environment. The Al-3Zn alloy exhibited a sufficient and consistent protective current density and potential for steel members against corrosion within the cotton-like fiber environment.

3.2 Experimental details

3.2.1 Materials and the SACP method using cotton-like fiber

The schematic illustration of the SACP method is depicted in the Figure 3- 1(a). In the SACP method, an Al-3Zn alloy (66 × 66 × 5 mm) and carbon steel (150 × 150 × 6 mm)

were selected as the anodic and cathodic materials, respectively. Chemical compositions of electrodes used in the method are listed in the Table 3- 1.

Table 3- 1 Chemical composition and dimensions of the Al alloy and steel.

Material	Chemical compositions (wt%)							
	Al	Zn	Fe	C	Si	Mn	P	S
Steel	-	-	balance	0.16	0.36	1.45	0.014	0.007
Al-3Zn	balance	3	-	-	-	-	-	-

To simulate low chloride (Cl^-) concentration corrosive environment within enclosed sections, a cotton-like fiber saturated with a 0.1 wt% NaCl aqueous solution was employed as an electrolyte carrier. This fiber is a composite blend comprising 70% bridged acrylate and 30% polyester fibers. Elaborate specifications and macroscopic representations of the fiber sheet are depicted in Table 3- 2 and Figure 3- 1(b), respectively. This acrylate fiber, characterized by elongated synthetic molecules, encompasses a composition of monomers including acrylic acid, sodium polyacrylate, and acrylamide-crosslinked polymers. The sophisticated crosslinked structure is achieved through inter-fiber bonding, engendering essential voids pivotal for water absorption within the fiber matrix.

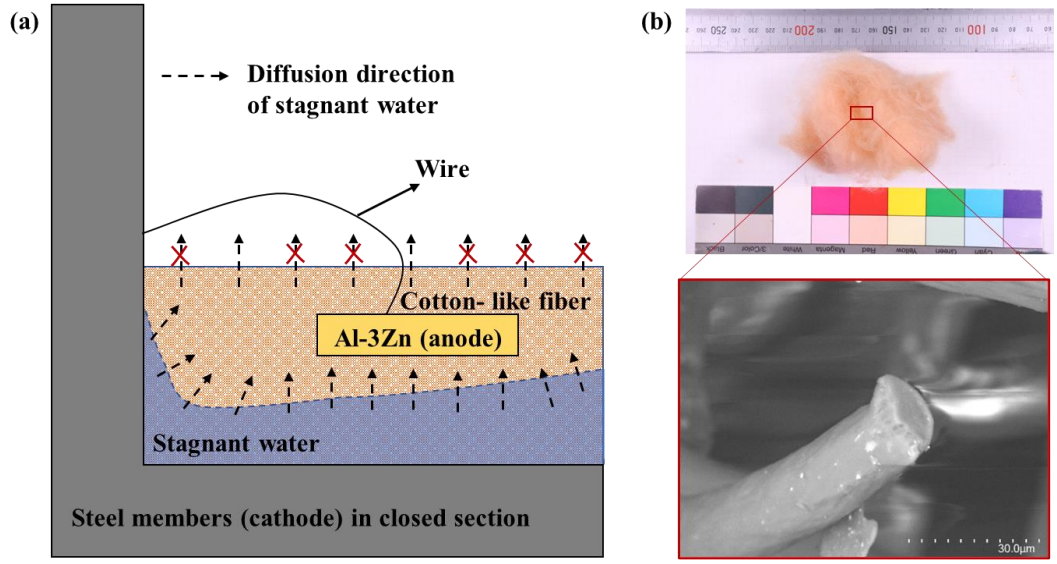

Figure 3- 1 (a) Schematic illustration of the SACP method using the cotton-like fiber acting as electrolyte carrier. (b) Photos of the cotton-like fiber.

As an electrolyte carrier in an atmospheric environment, the primary objective of cotton-like fibers is to achieve desirable water absorption and water retention properties. Second, the electrochemical performance of the electrodes in the cotton-like fiber medium in SACP systems requires further discussion. Finally, the effectiveness of the cotton-like fibers as electrolyte carriers in atmospheric environments must be validated using SACP experiments. The following experiments were conducted based on these objectives.

Table 3- 2 Material properties of the cotton-like fiber.

Fabric weight (g/m^2)	Mixed ratio (wt%)	
	Bridged acrylate fiber	Polyester fiber
600	70	30

3.2.2 Water absorption and retention test

To evaluate the water absorption ratio of the cotton-like fiber, the tea-bag method was chosen, as shown in the Figure 3- 2. The tea bag was made of nylon net with 250 mesh.

Before the experiment. The weight of tea bag was measured in conditions of dryness and fully-absorbing. Next, a certain amount cotton-like fiber was weighed and added into the dry tea bag. Then, tea bags with fiber were immersed in the 0.1 wt% NaCl aq. After a certain time, tea bags were picked up from solutions and hang on for ten minutes to measure the weight after absorption. Repeat this procedure until the weight of tea bags almost not change.

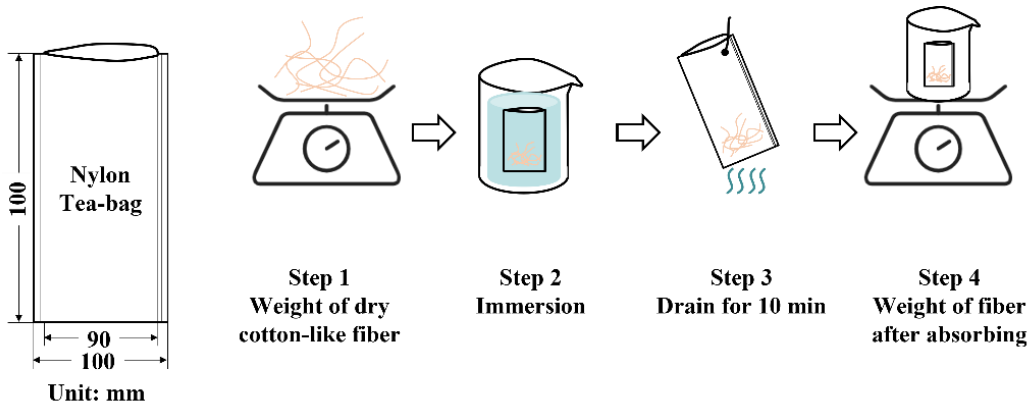

Figure 3- 2 Schematic illustration of measurement of water absorption ratio of cotton-like fiber.

The fully absorbent tea bags were hung in the constant temperature and humidity chamber to evaluate the water retention ratio of the cotton-like fiber. Every a certain time, tea bags were picked out to weight.

The water absorption and retention ratio can be calculated by equations as follows:

$$R_{ai} = (W_{ahi} - W_{a0})/W_{a0} \tag{3-1}$$

$$R_{ri} = \left(W_{rhi} - W_f\right)/W_f \tag{3-2}$$

Where R_{ai} and R_{ri} represent the water absorption and retention ratio, respectively. the W_{ahi}, W_{rhi} and W_{a0} are the weights of tea bag with cotton-like fiber after water absorption and retention test at time $= i$ and 0, respectively. W_f is the maximum weight of water of cotton-like fiber in the absorption test.

3.2.3 Electrochemical test

Cotton-like fiber absorbing NaCl solution, acting as electrolyte carrier, the ion conductivity of it is notably important for the SACP system. Although, the effectiveness of the fiber sheet has been varied by the previous research, the ion transportation capability of it is still unclear. The two stainless electrode method was selected to measure the ion conductivity of the cotton-like fiber, considering different electrolyte content of 100%, 50%, 25% and 10% (marking as Fiber-100, Fiber-50, Fiber-25, Fiber-10, respectively), as shown in the Figure 3- 3(a). The ion conductivity can be calculated by the equation as follows:

$$\sigma_{ion} = l/(R \cdot A) \quad (3\text{-}3)$$

Where l, R, A are the distance, resistance, and area of the cotton-like fiber between the two stainless electrodes, respectively.

Moreover, the open circuit potential (OCP) and electrochemical impedance spectroscopy (EIS) of Al-3Zn and steel immersed in the cotton-like fiber were measured by the three-electrode setup, as shown in Figure 3- 4(b). In the experimental setup, the working electrode consisted of either a steel or Al-3Zn alloy plate with an exposure area of 10 mm × 10 mm, while a platinum plate served as the counter electrode and Ag/AgCl was utilized as the reference electrode, respectively. The electrochemical performance of the SACP system was evaluated by conducting EIS and polarization curve measurements on the cotton-like fiber. The frequency range used was 105 to 10-2 Hz, with an amplitude set at 5 mV.

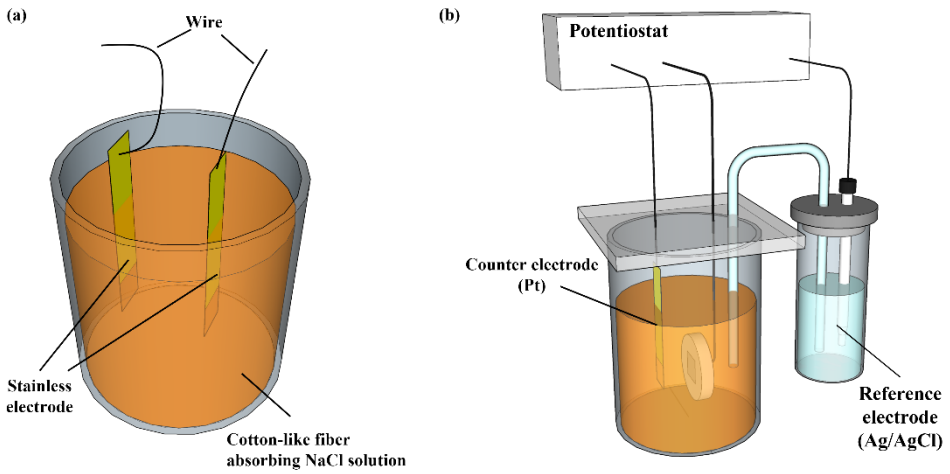

Figure 3- 3 (a) Measurement method of (a) ion conductivity of cotton-like fiber, (b) electrochemical impedance spectroscopy and polarization curves.

3.2.4 Performance of the SACP method with cotton-like fiber

To evaluate the working performance of the method employing cotton-like fiber, SACP tests were conducted in an indoor environment, as depicted in Figure 3- 4. The experimental setup involved an acrylic box measuring 200 × 200 × 200 mm. The Al-3Zn plate and steel plate were fully immersed in the cotton-like fiber, which absorbed a 0.1 wt% NaCl aq. A zero-resistance ammeter was utilized to measure the anti-corrosion current, recorded at 10-minute intervals for 168 hours. Variations in instant-off potential were also measured to assess whether the steel potential becomes more negative than the protective potential. a comparative analysis of the surface condition of steel with and without the SACP method was conducted.

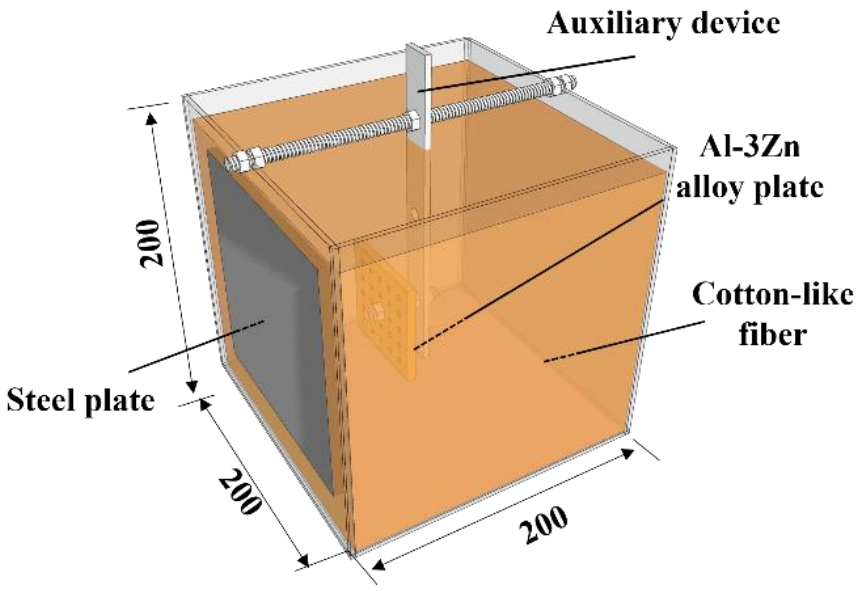

Figure 3- 4 Experimental setup of the SACP test employing cotton-like fiber.

3.3 Roles of the cotton-like fiber in the SACP system

3.3.1 Electrochemical characteristics of electrodes

Figure 3- 5(a) depicts OCP measurements conducted on carbon steel, an Al-3Zn sacrificial anode immersed in 0.1 wt% NaCl aq, and a cotton-like fiber fully absorbing 0.1 wt% NaCl aq over a 12-hour duration. Notably, the Al-3Zn sacrificial anode submerged in 0.1 wt% NaCl aq, and the fiber exhibited OCP values of approximately -0.85 V and -0.82 V, respectively, up to the 12-hour mark. In contrast, the carbon steel immersed in 0.1 wt% NaCl aq initially demonstrated an OCP of approximately −0.37 V, gradually declining over time to stabilize at a consistent OCP of approximately −0.68 V by the experiment's conclusion. Intriguingly, when introduced into the fiber, the OCP of the carbon steel promptly decreased to approximately -0.68V and maintained stability throughout the 12-hour period. Ultimately, an effective potential difference of approximately 0.2 V was established, suggesting the anticipated corrosion protection effect attributable to the sacrificial anode[151].

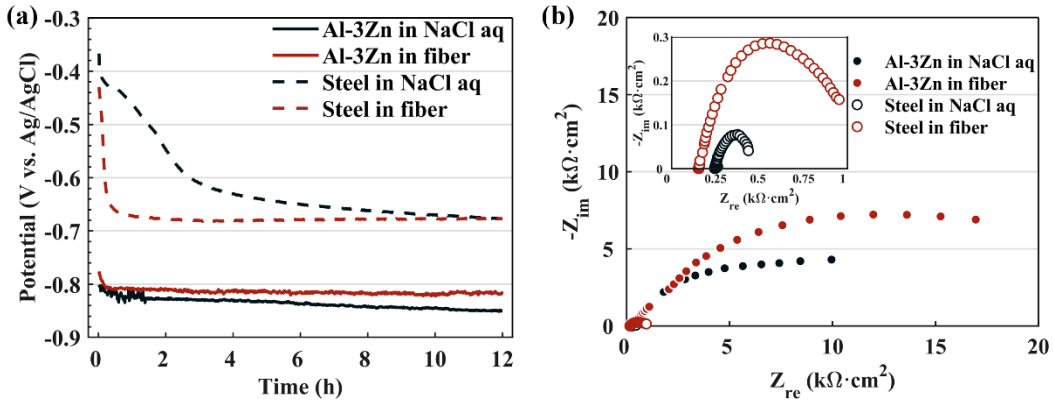

Figure 3- 5 Results of (a) OCP and (b) Nyquist plot of steel in 0.1 wt% NaCl aq and fiber after swelling.

EIS analysis was conducted on the carbon steel and Al-3Zn alloy to measure the impedance at the interface of the electrodes and cotton-like fiber varying electrolyte content, as shown in Figure 3- 6(b). Diameter in the Nyquist plot of both Al-3Zn alloy and carbon steel immersed in the fiber is much larger than that in aqueous solution, suggesting that electrodes are more difficult to dissolving. It's evident that this is more beneficial for corrosion protection of carbon steel but poses challenges for the operational performance of Al-3Zn alloys in the SACP.

3.3.2 Performance of cotton-like fiber in SACP method

The time-dependent variations of the anti-corrosion current densities in 120 h are illustrated in Figure 3- 6(a). The results clearly indicate that the Al-3Zn alloy exhibits the capability to provide adequate protective current against corrosion, albeit with a marginally lower anti-corrosion current density compared to that observed in 0.1 wt% NaCl aq. Meanwhile, the protective current in the fiber remains relatively stable. As shown in Figure 3- 6(b), the potential indicates that during the initial polarization phase, the steel potential undergoes a swift decline, stabilizing consistently at nearly -0.80V after approximately 24 hours. Notably, this value appears more negative than the typical

protective potential ((−0.73 V vs. Ag/AgCl/Sat.KCl)) observed in a neutral environment[152].

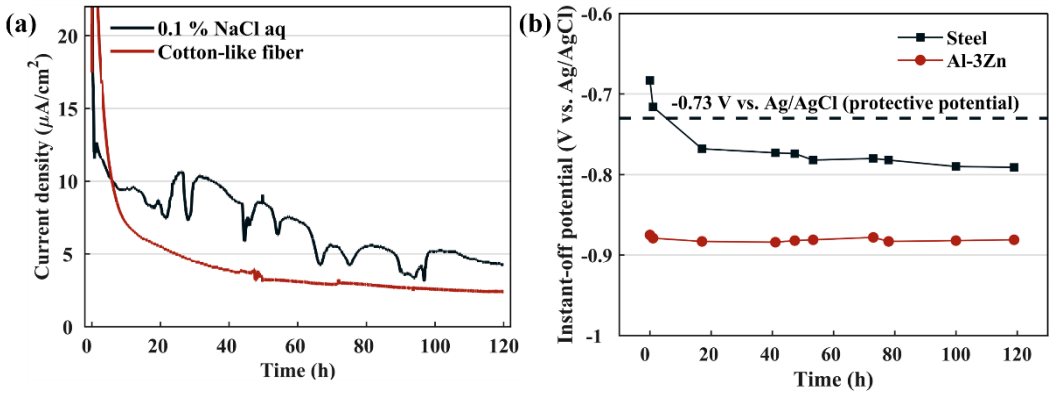

Figure 3- 6 (a) Anti-corrosion current densities and (b) instant-off potential in the SACP method.

The surface conditions of the steel members subjected to the control group and those under the protection of the SACP system are visually depicted in Figure 3- 8. As shown in Figure 3- 8(a), the particles on the surfaces of the steel members under SACP exhibit a similarity to those observed after abrasive blasting[193], displaying no discernible indications of rust or corrosion. However, after 120-h duration, the unprotected steel surface exhibited a prominent rust layer with uniform and dense corrosion pits, as shown in Figure 3- 8(b). The EDX results confirmed this observation; the steel plate protected by the SACP method exhibited an oxygen content of only 1.74%, whereas in the control group, this element accounted for as much as 10.79%.

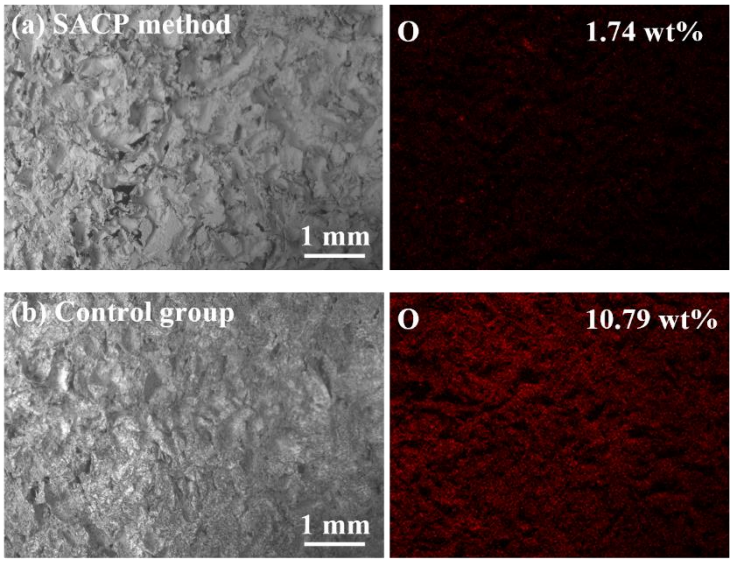

Figure 3- 7 SEM and element (O) mapping images of the steel surface in (a) control group and (b) SACP method.

3.4 Summary

In this investigation, a cotton-like fiber, serving as an electrolyte carrier, was innovatively incorporated into the SACP system to safeguard enclosed steel sections within the atmospheric milieu. The efficacy of the cotton-like fiber was rigorously assessed through comprehensive evaluations including water absorption and retention assessments, electrochemical analysis, and the actual SACP performance tests. The principal outcomes and findings can be summarized as follows:

(1) The OCP of the Al-3Zn sacrificial anode was approximately −0.2 V relative to steel when immersed in the cotton-like fiber, indicating the effectiveness of the SACP method.

(2) Both the Al-3Zn alloy and steel were more resistant to dissolution immersed in the cotton-like fiber, based on Nyquist plots.

(3) The Al-3Zn alloy exhibited the ability to provide adequate and relatively stable protective current density and potential for steel members, mitigating corrosion risks within the cotton-like fiber environment.

CHAPTER 4 SACP METHOD USING PANa-CMC HYDROGELS ACTING AS ELECTROLYTE CARRIERS FOR STEEL MEMBERS IN HIGH-HUMIDITY ENVIRONMENTS

4.1 Introduction

Corrosion of steel in high-humidity environments degrades its mechanical properties and durability[44, 138, 153]. Consequently, enhancing the corrosion resistance of steel is crucial, which requires appropriate corrosion mitigation strategies. Various methods have been explored, including anti-corrosion coating and dehumidification[154-158]. However, coating effectiveness can be compromised by film degradation and inadequate surface treatment, especially in high-humidity environments[74, 159-161]. Moreover, surface treatment and coating application pose challenges in complex plate joints and narrow areas[162, 163]. While dehumidification is effective, it consumes substantial energy[164, 165].

Hence, alternative options are being explored to prevent steel from corrosion. The SACP method has gained significant popularity for corrosion control in steel structures due to its cost-effectiveness and easy installation[166]. However, the application of the SACP method is mostly limited to marine and soil environments, such as oil drilling platforms and ship hulls, where the presence of an electrolyte is essential for facilitating ionic transport in the protection process[106, 167]. In atmospheric environments with limited rainfall or dew, maintaining the electrolyte on the steel surfaces becomes challenging, thus posing difficulties for the application of the SACP method[74].

Up to now, two main strategies have been developed to sustain the protection current for the SACP method used in atmospheric environments. The first approach, known as the submerged sacrificial anode method, involves immersing sacrificial anodes in the electrolyte[168]. This method protects the exposed portions of the steel structure by utilizing the cathodic prevention effect of the sacrificial anodes. However, this method has limited application since certain sections of the steel member must still be immersed in the electrolyte, such as seawater[104]. The second approach, referred to as the water-absorbing material-assisted method, employs high water-absorbing materials as electrolyte carriers. Examples of such materials include absorbent fiber sheets or water-swelling rubber. These materials retain the electrolyte within their structure and establish direct contact with the steel surface, ensuring a continuous protective current against corrosion[169]. However, the use of absorbent fiber sheets necessitates bolting them to an Al–Zn alloy plate and a steel member, which potentially compromises the structural integrity of the system. Moreover, as the sacrificial anode reaction proceeds, metal ions such as Al^{3+}, Zn^{2+} will continuously be released into the surrounding environment, leading to contamination issues[170, 171].

Therefore, it is highly desirable to develop a novel electrolyte carrier with superior retention capability, strong adhesive properties with electrodes, high ionic conductivity, and eco-friendly characteristics. Currently, remarkable water uptake performance of hydrogels has garnered significant attention for their potential use in various applications, such as solid electrolytes in battery and energy storage[172, 173]. The sodium polyacrylate (PANa) hydrogel is a widely known superabsorbent hydrogel that exhibits exceptional water uptake, ionic conductivity, and cost-effectiveness[174]. However, several challenges remain in achieving both high mechanical strength and high water

uptake as these properties often conflict with each other.[175, 176]. Moreover, the hydrophilic functional groups in the hydrogel networks, such as hydroxyl and carboxyl, allow for an effective binding of metal ions from aqueous media[177, 178]. This is considered as a preferable strategy to prevent metal ions from releasing into the environment, highlighting the potential of hydrogels as an eco-friendly electrolyte carrier.

This study focused on the development of PANa–CMC hydrogels as electrolytes for the SACP method, with the objective of safeguarding steel against corrosion in high-humidity environments. Various evaluations were performed to assess the efficacy of the SACP method using PANa–CMC hydrogels. First, the water retention capacity of the hydrogels was investigated under the relative humidity of 90%. Mechanical tests were conducted to examine the adhesion properties of the PANa–CMC hydrogel with steel. Furthermore, the electrochemical performance of the hydrogels was analyzed using Electrochemical impedance spectroscopy (EIS) and polarization curves, focusing on parameters such as ionic conductivity, equivalent circuit, corrosion current density of Al-3Zn anodes, and steel. Constant exposure tests were also conducted to evaluate the time-dependent anti-corrosion performance of the hydrogels, considering the characteristics of the steel surface condition and protective current density. Additionally, the impact of PANa–CMC hydrogels on fixing metal ions from anodes and reducing the formation of passive film in the SACP method was discussed. Overall, the results indicate that PANa–CMC hydrogels exhibit promising characteristics as eco-friendly electrolytes and expand the application of the SACP method to high-humidity environments.

4.2 Experimental details

4.2.1 Materials

Materials for hydrogel preparation: Acrylic acid (AA, ≥ 98.0%), sodium hydroxide, (NaOH, ≥ 97.0%), and N, *N*'-Methylenebis(acrylamide) (MBAA, ≥ 97.0%), were purchased from FUJIFILM Wako Pure Chemical Co., Ltd. sodium carboxymethyl cellulose (CMC, ≥ 95.0%) and ammonium peroxodisulfate ($(NH_4)_2S_2O_8$, ≥ 95.0%) were produced from Hayashi Pure Chemical Ind., Ltd. All reagents were obtained and used as received without further purification.

Materials for the SACP system: An Al-based alloy-casting plate was selected as the sacrificial anode, with its performance already validated in the atmospheric environment. additionally, the PANa hydrogel served as the electrolyte. The SM490A steel (according to Japanese Industrial Standard (JIS) G3106) was selected as the cathode. The chemical compositions of the anode and steel material are listed in Table 3- 1.

4.2.2 Synthesis of PANa–CMC hydrogels

The PANa–CMC hydrogels were prepared via a solution polymerization method. As shown in Figure 4- 1, 14.4 ml AA was diluted with 30 ml deionized water. Then, 8 g NaOH slowly added into the above solution for neutralization under vigorous stirring at 0 ℃ (cooled by an ice-water bath). Subsequently, a certain amount of CMC was included in the neutralized solution. Subsequently, 0.4 g $(NH_4)_2S_2O_8$, and 0.008 g MBAA were dissolved into the mixed solution and stirred vigorously for 1 h at 26 ℃. The solution was degassed with nitrogen to eliminate DO, prior to polymerization. Finally, the resulting solution was cast into an acrylic mold and then subjected to polymerization at 26 ℃ for 12 h to achieve the desired shape and thickness. The as-prepared hydrogel electrolytes

were classified into different groups, depending on the ratio of CMC added. These groups included Pure PANa, PANa-1% CMC, PANa-2% CMC, PANa-5% CMC, PANa-10% CMC.

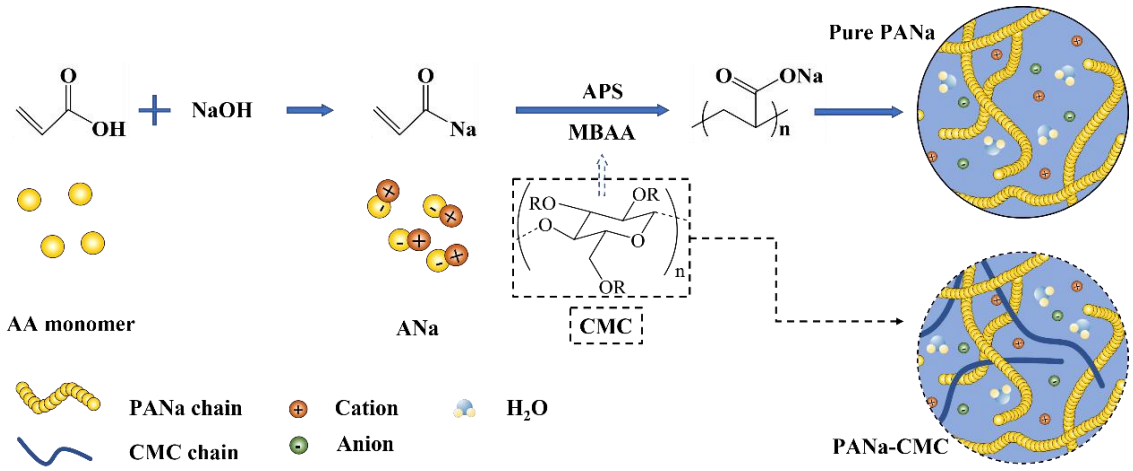

Figure 4- 1 Schematic illustration of synthesis of the pure PANa hydrogel and PANa–CMC hydrogel.

4.2.3 Morphology observation

The morphologies of the dried hydrogels were observed with scanning electron microscopy (SEM, Hitachi SU3500, Japan) operating at 15kV under a low-vacuum condition. Fourier transform infrared spectroscopy (FT/IR 620, Japan.) was used to characterize the chemical properties of the resulting hydrogels with the wavenumber ranging from 4000 to 400 cm^{-1} at 26 ℃. FTIR spectra were obtained after registering 64 scans, with a resolution of 2 cm^{-1}.

4.2.4 Water retention test

To evaluate the water retention capacity of the hydrogels, cylinder-shaped hydrogels (diameter = 12 mm, thickness = 8 mm) were exposed to an environment with the relative humidity (RH) of 90% and a temperature of 30°C. The water retention ratio at time =i (WR_i) is given by:

$$WR_i = (W_{hi} - W_0)/W_0 \quad (4\text{-}1)$$

where W_{hi} and W_0 are the weights of the hydrogel at time = i and 0, respectively.

4.2.5 Adhesion strength test

To determine the correlation between the quantity of CMC and adhesion properties of PANa–CMC hydrogels, dolly pull-off tests were performed between hydrogels and blast steel surface, as shown inFigure 4- 2. The dolly's adhesive surface, comprising of JIS H 4000 Aluminum alloy A2017, had a diameter of 20mm and was uniformly sanded. Afterward, it was washed in an acetone solution and dried. The dolly was then bonded to the core area of the specimen at room temperature with a uniform vertical compressive stress of 0.9 MPa for 30 minutes. The dolly specimen was subsequently cured at 35°C for at least 48 hours, and a circular groove was drilled around the core area before performing the pull-off test. Force and displacement were measured during the loading test using a universal test machine (Tokyo Koki Tester MSC-10/500-2). While testing, the specimens were nipped to the tensile machine and tested at a tensile rate of 100 mm/min.

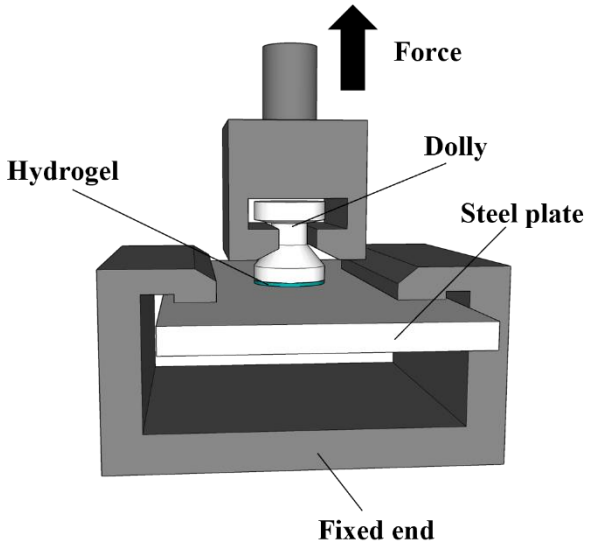

Figure 4- 2 Measurement method of adhesion strength between hydrogels and carbon

steel.

4.2.6 Electrochemical tests

EIS was used to measure the ionic conductivity of the hydrogels to evaluate the impact of the addition of CMC. Two blocking stainless-steel electrodes were set in hydrogel electrolyte, as shown in Figure 4- 3(a). The ionic conductivity σ_{ion} could be expressed as follows:

$$\sigma_{ion} = l/(R \cdot A) \tag{4-2}$$

where l, R, A are the thickness, resistance, and area of the hydrogel electrolyte between the two stainless electrodes, respectively.

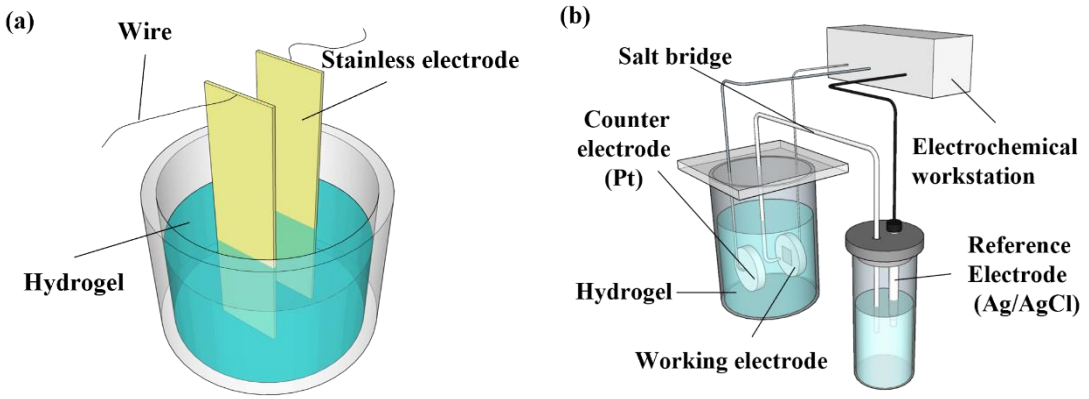

Figure 4- 3 Measurement method of (a) ion conductivity of PANa–CMC hydrogels, (b) electrochemical impedance spectroscopy and polarization curves.

A three-electrode setup was applied to evaluate the electrochemical properties of steel and Al-3Zn coupling with PANa hydrogel using a potentiostate (Princeton Applied Research, Versastat 3), as shown in Figure 4- 3(b). In the apparatus, the steel or Al-3Zn alloy plate was performed as the working electrode, and a platinum plate and Ag/AgCl were chosen as the counter and reference electrodes, respectively. The EIS and polarization curves were measured in a PANa hydrogel electrolyte to evaluate the

electrochemical performance of the SACP system. The frequency ranged from 10^5 to 10^{-2} Hz with an amplitude of 5 mV.

4.2.7 Constant exposure test

To assess the protection area, durability, and effectiveness of the SACP system incorporating PANa–CMC hydrogels, an indoor exposure test was conducted. Figure 4-4 illustrates the setup used to measure the anti-corrosion current between an Al-3Zn alloy plate (15 mm × 15 mm × 5 mm) and a steel plate (150 mm × 70 mm × 6 mm) coupled with PANa hydrogel (diameter = 30 mm, thickness = 20 mm). A zero-resistance ammeter was employed to measure the anti-corrosion current. The specimens were placed uunder a constant temperature of 30 °C and humidity chamber with a relative humidity (RH) of 90%. The anti-corrosion current was monitored and recorded every 10 minutes for 168 hours. Prior to testing, the steel plate and Al-3Zn plate were cleaned using an ultrasonic cleaning machine using acetone as the solvent. The ultrasonic cleaning temperature was set to 25 °C, and the ultrasonic frequency was 40 kHz.

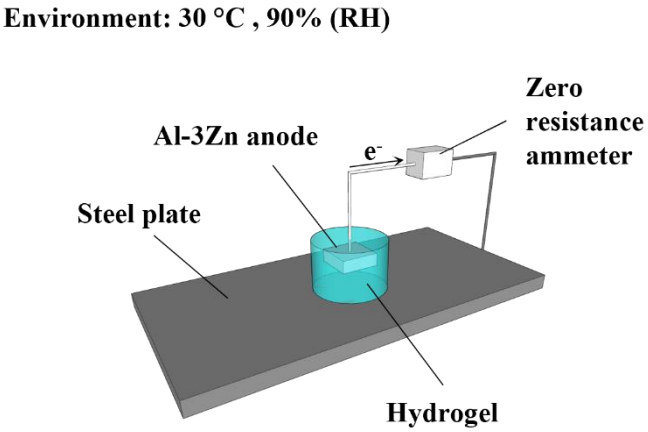

Figure 4- 4 Measurement method of cathodic protection current density in constant exposure test.

4.3 Performance of the PANa-CMC hydrogels in SACP method

4.3.1 Morphology analysis

Figure 4- 5(a) presents the FTIR spectra of pure PANa hydrogel, CMC powder, and PANa–CMC hydrogels. The results indicated that the functional groups of PANa and CMC exhibited characteristic absorption peaks at 1551 cm^{-1} and 3740 cm^{-1}, respectively. The peak at 1551 cm^{-1} was attributed to the carboxylate ion (COO-) from PANa, while the peak at 3740 cm^{-1} was related to the hydroxyl group (-OH) from CMC[179-181]. In the spectrum of PANa-5%CMC, no new absorption peak was observed that differed from that of pure PANa and CMC, suggesting that the connection between PANa and starch molecules was mainly through physical entanglement and hydrogen bonding[182].

Figure 4- 5(b) to (f) illustrates the microstructure of the pure PANa hydrogel and PANa–CMC hydrogels with varying ratios of CMC. The cross-sectional morphology of the pure PANa hydrogel was observed as relatively flat. However, the addition of CMC induces roughness on the surface of the PANa hydrogel, thereby enhancing its water retention capacity and adhesion strength[182-184].

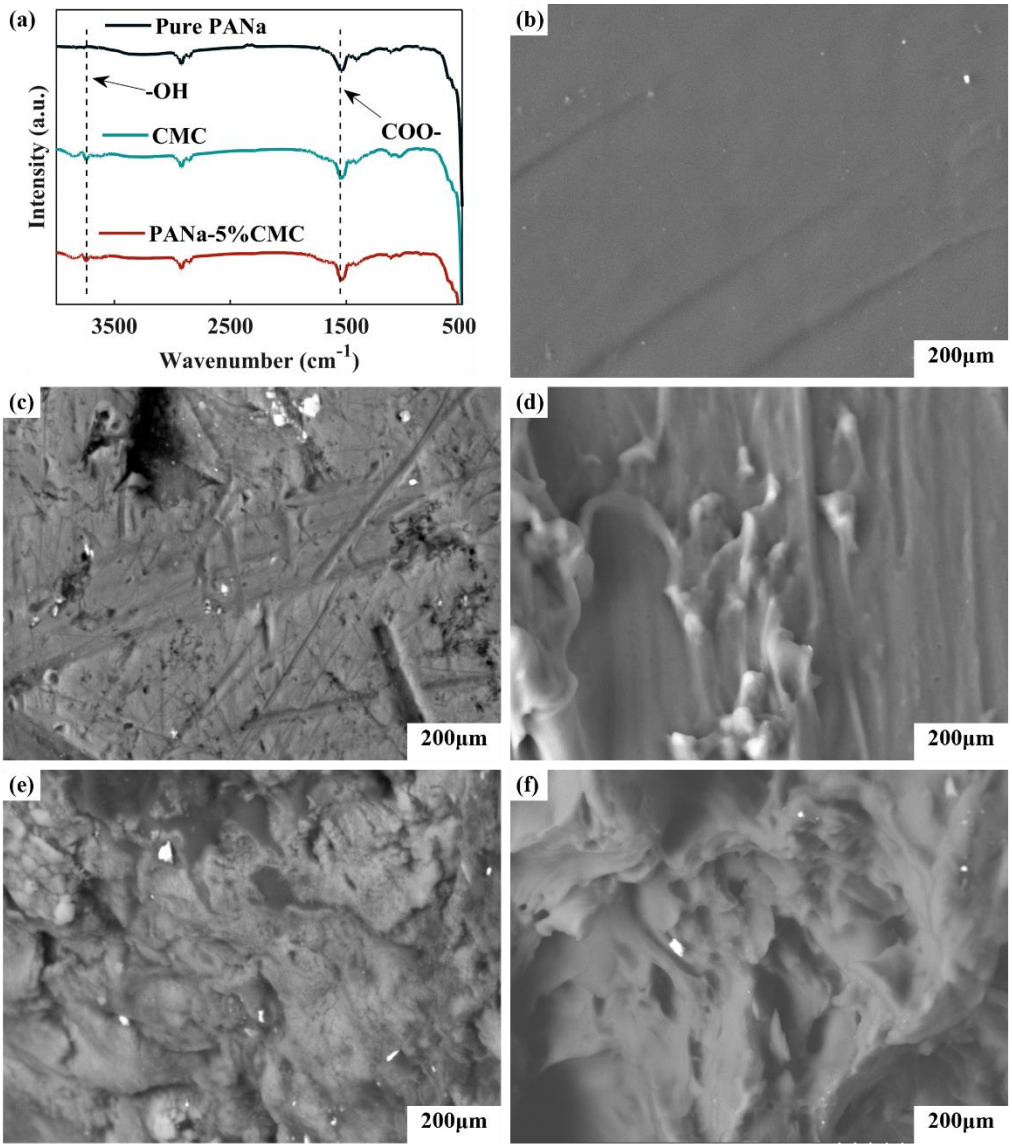

Figure 4- 5 (a) FTIR spectra of CMC, pure PANA hydrogel and PANa–CMC hydrogels. (b) The SEM images of the Pure PANa, (c) PANa-1%CMC, (d) PANa-2%CMC, (e) PANa-5%CMC, and (f) PANa-10%CMC.

4.3.2 Electrochemical performance

EIS analysis was conducted on the Al-3Zn alloy to measure the impedance at the interface of the anode electrode and PANa–CMC hydrogels, as shown in Figure 4- 6(a). The impedance measured is defined as the charge transfer resistance (Rct) of the anode, which is the most important kinetic limitation due to the slow rate of activation reaction

on the anode surface [185]. The Nyquist plots for the Al–3Zn anodes showed a single capacitance loop in the entire frequency range, indicating that the system can be described by a single time constant model. The results showed that the increase in CMC content resulted in a significant reduced diameter in the Nyquist plot, suggesting that the Al–3Zn is more prone to dissolving. A similar trend was also observed in the blast steel samples, as depicted in Figure 4- 6(b).

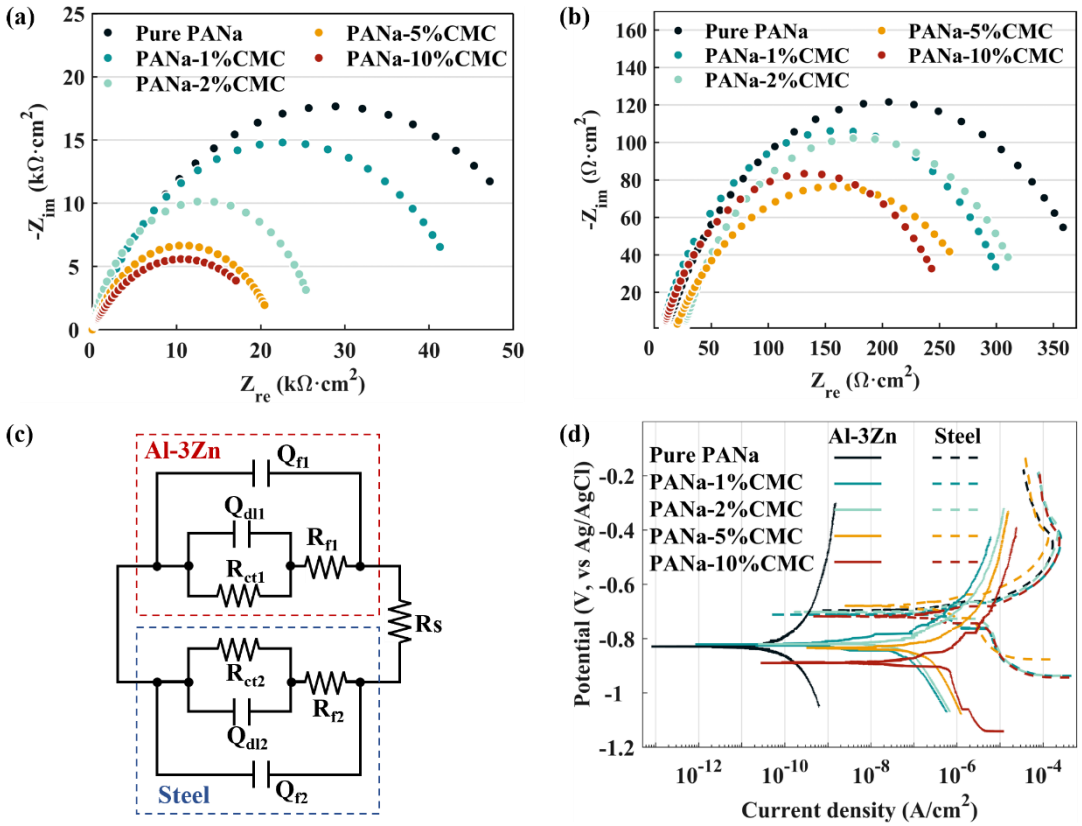

Figure 4- 6 Nyquist plot of Al–3Zn alloy and (b) blast steel immersed in PANa–CMC hydrogels. (c) Equivalent circuit for the EIS data. (d) Potentiodynamic polarization plot of Al–3Zn alloy and blast steel immersed in PANa–CMC hydrogels.

The EIS analysis led to the creation of an equivalent circuit (Figure 4- 6(c)) that models the data, as shown in Table 4- 1. In the equivalent circuit, R_s, R_{ct1}, R_{ct2} represent the solution resistance and the pseudo resistance associated with the electrochemical

reactions at the film/interface, respectively[186]. While R_{f1} and R_{f1} represent the film resistances, and Q_{f1} and Q_{f2} represent the film capacitances, Q_{dl1} and Q_{dl2} correspond to the electric double layer capacitance of Al–3Zn and carbon steel, respectively.

Table 4- 1 EIS fitted parameters for coupled Al-3Zn alloy and blast steel PANa–CMC hydrogels.

Materials	Hydrogel	R_s ($\Omega\cdot cm^2$)	Q_f ($\Omega^{-1}\cdot cm^{-2}\cdot s^n$)	n_1	R_f ($\Omega\cdot cm^2$)	Q_{dl} ($\Omega^{-1}\cdot cm^{-2}\cdot s^n$)	n_2	R_{ct} ($\Omega\cdot cm^2$)
Al-3Zn	Pure PANa	50.80	5.57×10^{-5}	0.62	2.10×10^{4}	1.30×10^{-5}	0.81	231.6
	PANa-1%CMC	34.01	3.67×10^{-5}	0.77	1.57	2.07×10^{-2}	0.72	0.07
	PANa-2%CMC	22.67	4.96×10^{-5}	0.83	2.52×10^{2}	4.33×10^{-10}	0.36	2.66×10^{4}
	PANa-5%CMC	6.67	3.88×10^{-5}	0.80	0.01	4.36×10^{-5}	0.80	5.72×10^{4}
	PANa-10%CMC	11.20	3.12×10^{-5}	0.80	3.04×10^{2}	6.06×10^{-18}	0.80	1.51×10^{4}
Blast Steel	Pure PANa	0.15	3.40×10^{-19}	0.80	10.93	3.57×10^{-3}	0.80	384.7
	PANa-1%CMC	6.91	3.44×10^{-3}	0.77	1.25	1.92×10^{-5}	0.76	308.8
	PANa-2%CMC	25.96	4.05×10^{-3}	0.75	0.14	1.74×10^{-5}	0.77	306.8
	PANa-5%CMC	18.16	4.85×10^{-3}	0.64	36.04	2.06×10^{-5}	0.67	242.6
	PANa-10%CMC	8.14	4.88×10^{-3}	0.74	251.6	6.11×10^{-3}	0.64	3.49

The polarization curves of the Al-3Zn alloy and blast steel in PANa–CMC hydrogels are presented in Figure 4- 6(d), and the fitting parameters are listed in Table 4- 2. It is evident from the plot that the potential of the Al-3Zn alloy is more negative than that of the blast steel, indicating that the Al-3Zn alloy can provide protection current for the blast steel. The addition of CMC had negligible effect on the potential and corrosion current of the blast steel. Furthermore, in the anode area, the steel exhibited a passivation effect, suggesting that the hydrogel can effectively prevent further corrosion of the underlying steel even without the installation of an anode or in the event of a sacrificial anode system failure. This indicates that the hydrogel functions similarly to a protective coating, offering additional corrosion resistance to the steel surface[187]. However, with the increase of CMC, the corrosion current of Al–3Zn alloy was significantly improved to

provide protection for steel.

Table 4- 2 Polarization curve fitted parameters for Al-3Zn alloy and blast steel.

Materials	Hydrogel	β_a (mV/dec)	β_c (mV/dec)	E_{corr} (V)	i_{corr} (A/cm^2)
Al-3Zn	Pure PANa	436.60	423.55	-0.83	2.46×10^{-9}
	PANa-1%CMC	59.12	76.13	-0.82	3.98×10^{-8}
	PANa-2%CMC	118.59	306.61	-0.82	6.52×10^{-7}
	PANa-5%CMC	82.15	137.56	-0.83	6.90×10^{-7}
	PANa-10%CMC	74.43	99.72	-0.88	5.44×10^{-7}
Blast steel	Pure PANa	49.59	78.51	-0.70	1.68×10^{-6}
	PANa-1%CMC	52.41	87.87	0.71	2.85×10^{-6}
	PANa-2%CMC	40.78	56.28	-0.70	3.66×10^{-7}
	PANa-5%CMC	54.86	90.86	-0.68	1.89×10^{-6}
	PANa-10%CMC	55.74	90.37	-0.72	3.58×10^{-6}

4.3.3 Cathodic protection performance

Figure 4- 7(a) presents the time-dependent changes in the anti-corrosion current density of the SACP method using PANa–CMC hydrogels. The results clearly indicate that hydrogels provide adequate protection against corrosion in high-humidity environments of 90% relative humidity. Even the pure PANa hydrogel exhibited a sustained protection current density slightly greater than 1 μA/cm². When the CMC content was below 2%, no substantial change in the current density was observed. Additionally, the current density for all three samples reached its peak within a day. With an increase in the CMC content to 5%, the stabilized current density reached 3 μA/cm², approximately three times that of

the pure PANa hydrogel. This indicates that the addition of CMC at this ratio effectively enhances the protective current density However, when the ratio of CMC exceeded 5%, the current density slightly decreased. This observation suggests that increasing the CMC ratio further did not lead to a proportional increase in the protective current density.

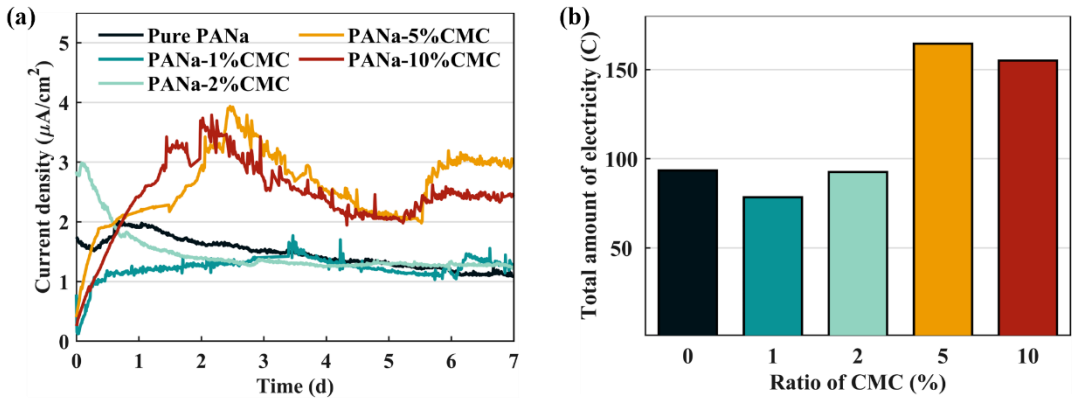

Figure 4- 7 (a) Anti-corrosion current densities provided by the SACP method using PANa–CMC hydrogels. (b) Total transferred electric charge for 7 days.

Based on the currents measured in the constant exposure test, the total electric charge can be calculated by multiplying the current by time. To assess the performance of the SACP method with PANa–CMC hydrogels, a comparison of the total electric charge over a period of seven days is presented in Figure 4- 7(b). It was observed that when the CMC ratio is below 2%, the measured total electric charge remains relatively constant at around 90 C. However, when the CMC ratio exceeds 2%, the measured total electric charge increases sharply, approximately doubling the previous value. This suggests that increasing the CMC ratio beyond 2% significantly enhances the overall electrical performance of the SACP method.

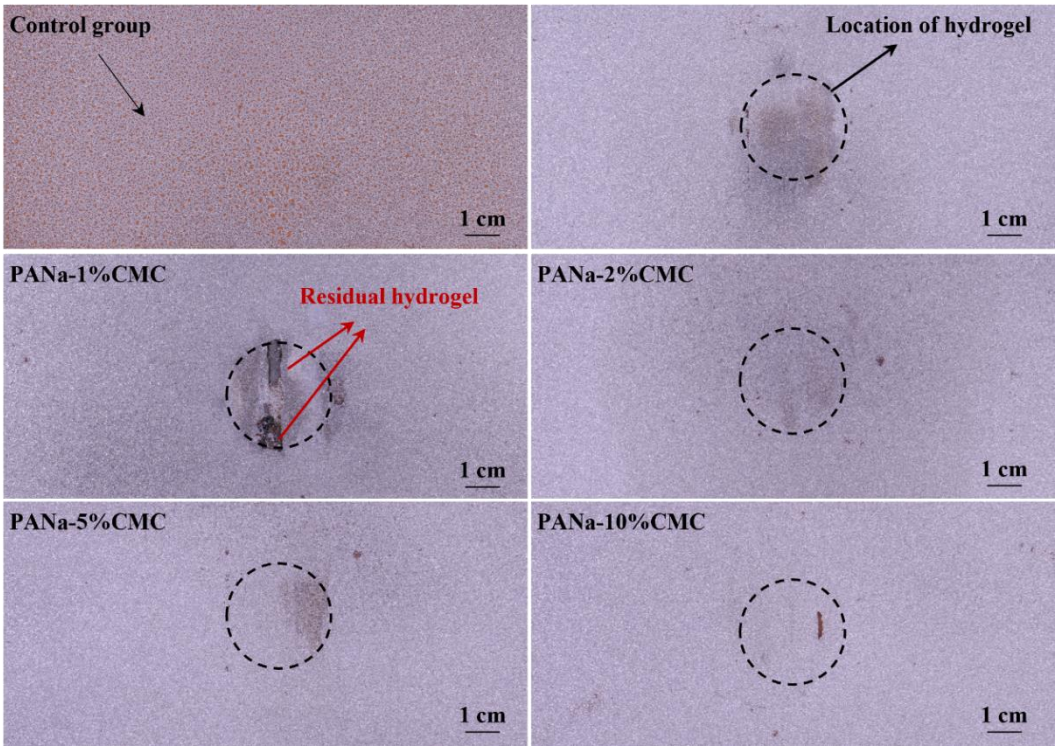

Figure 4- 8 Steel surface condition after 7 days' exposure.

The placement locations of the hydrogel were indicated in red circles on the surface, as depicted in Figure 4- 8. The findings demonstrated a stark contrast between the control group and the steel substrate protected by the SACP method using hydrogels. The control group displayed significant rust formation on the surface, whereas the steel substrate with the SACP method exhibited limited rust formation across the entire area of the steel substrate. This highlights the effectiveness of the SACP method in inhibiting corrosion when utilizing hydrogels as the electrolyte carrier. The generation and sustainability of the protective current can be attributed to the superior water retention properties and excellent conductivity of PANa–CMC hydrogels. Moreover, the hydrogel showed minimal presence of dissolved iron ions, indicating corrosion resistance of steel, as shown in Figure 4- 9(c).

Figure 4- 9 presents the SEM images of the central position in the steel plate and the

central position of the hydrogel cross-section. As shown in Figure 4- 9(a), the control group displayed prominent rust formation on the steel surface after seven days of exposure, as indicated by the high percentage (18.65 wt%) of oxygen (O) element in the element mapping images. Conversely, the experimental group utilizing the SACP method with PANa-5%CMC exhibited minimal rust formation on the steel surface, evident from the low O element percentage (2.75 wt%), as shown in Figure 4- 9(b). This demonstrates the efficacy of the SACP method with PANa-5%CMC in mitigating steel corrosion in high-humidity environments.

The distribution and content of aluminum (Al) and zinc (Zn) elements on the surfaces of the two steel plates in the control group and the PANa-5% CMC hydrogel group exhibited no significant differences, thus indicating that the metal cations released during anodic dissolution were primarily confined to the hydrogel. Interestingly, a substantial amount of aluminum (Al) element, accounting for 24.36 wt%, was detected in the hydrogel, as shown in Figure 4- 9(c). However, the content of Zn elements was relatively low, approximately 1.39 wt% of the Al element content, which exceeds the typical ratio in Al–3Zn alloy. These findings emphasize the potential of hydrogel as a material for fixing metal ions and minimizing contamination in the SACP method.

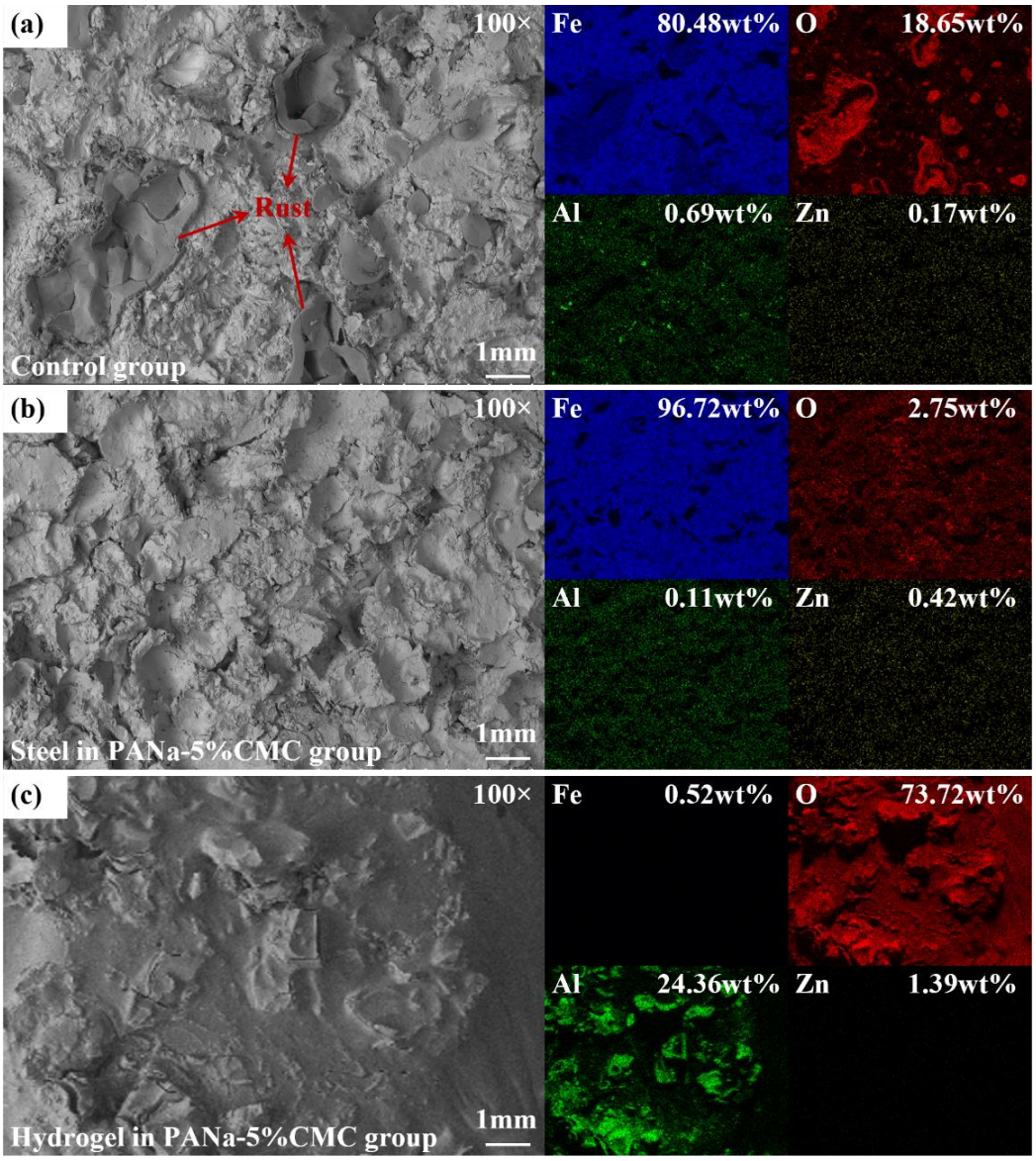

Figure 4- 9 (a) Element mapping images of the steel surface of control group, (b) PANa-5%CMC group, and hydrogel sectional surface of (c) PANa-5%CMC group.

4.3.4 Mechanism of the SACP method using PANa–CMC hydrogels

In this study, PANa–CMC hydrogels are utilized as an electrolyte in the SACP method to provide passive protection to steel in high-humidity environments. The hydrogels can sustain water within themselves and absorb moisture from the surrounding environment to sustain the protection current. Figure 4- 10(d) depicts a schematic diagram that helps

to comprehend the corrosion mechanism of the Al-3Zn alloy in PANa–CMC hydrogels. Since the potential of Al-3Zn alloy is more negative than that of iron, in a hydrogel environment, the Al–3Zn alloy tends to lose electrons preferentially, as shown in Figure 4- 6(d). Consequently, the Al–3Zn alloy in PANa–CMC hydrogels underwent anodic dissolution based on the following reaction:

$$Zn \rightarrow Zn^{2+} + 2e^{-} \quad (4\text{-}2)$$

$$Al \rightarrow Al^{3+} + 3e^{-} \quad (4\text{-}3)$$

Meanwhile, on the steel substrate, the cathodic reaction occurs, involving the reduction of oxygen. This reaction contributes to the water retention capacity of hydrogels. The reaction can be represented as follows:

$$O_2 + 2H_2O + 2e^{-} \rightarrow 4OH^{-} \quad (4\text{-}4)$$

After the constant exposure tests, the surface of Al–3Zn underwent oxidation, forming a layer of white corrosion product. However, as the CMC content in hydrogels increased, the visible amount of corrosion product decreased, as depicted in Figure 4- 9(a). The XRD pattern analysis revealed that the main products formed on the surface were γ-Al_2O_3, ZnO, and $Zn(OH)_2$, as shown in Figure 4- 10(b). Therefore, The Al^{3+} and Zn^{2+} ions released during the anodic dissolution reacted with the hydroxyl ion (OH^{-}) to form a porous corrosion product, $Al(OH)_3$, and passive corrosion product, $Zn(OH)_2$, which could also undergo dehydration to form γ-Al_2O_3 and ZnO, respectively, as described in the following reactions:

$$Al^{3+} + 3OH^{-} \rightarrow Al(OH)_3 \quad (5\text{-}8)$$

$$Zn^{2+} + 2OH^{-} \rightarrow Zn(OH)_2 \quad (5\text{-}9)$$

$$2Al(OH)_3 \rightarrow \gamma\text{-}Al_2O_3 + 3H_2O \quad (5\text{-}10)$$

$$Zn(OH)_2 \rightarrow ZnO + H_2O \quad (5\text{-}11)$$

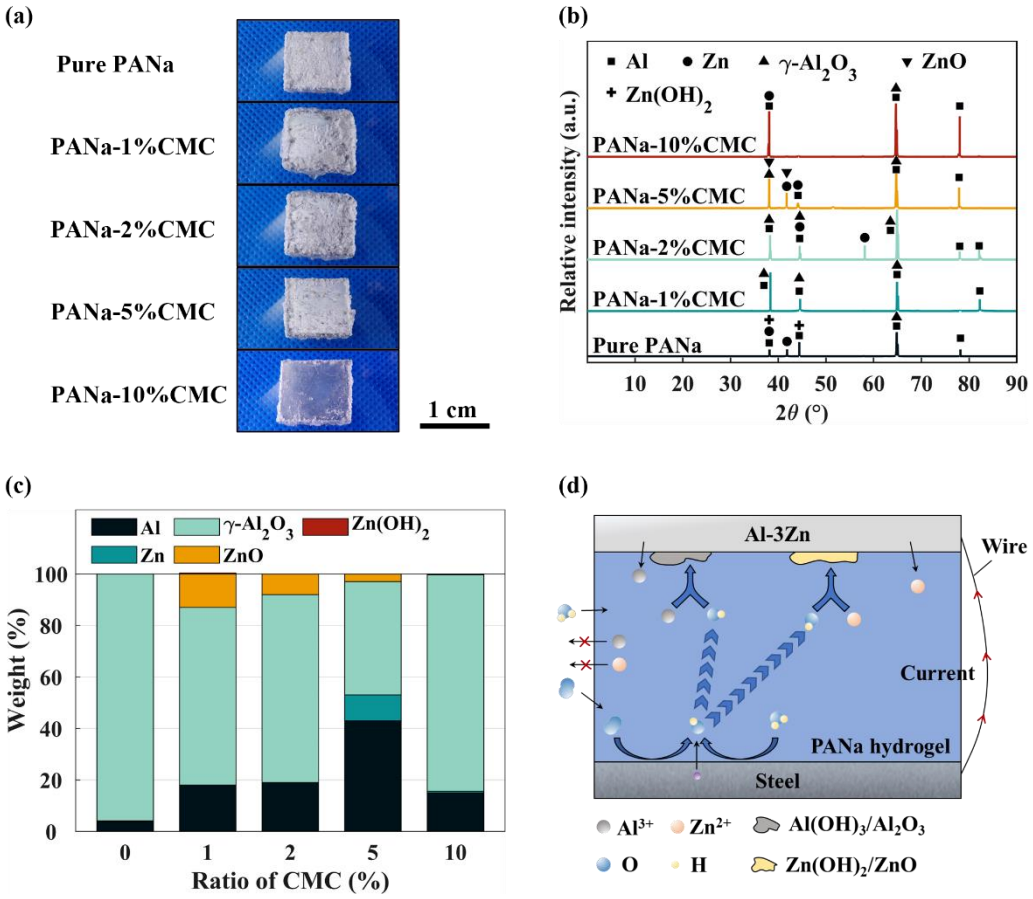

Figure 4- 10 (a) Al-3Zn anode surface condition, (b) XRD patterns and (c) XRD quantitative result after SACP test. (d) Schematic illustrating the corrosion mechanism of the SACP system with PANa–CMC hydrogels.

The XRD quantitative results of the Al–3Zn anodes are shown in Figure 4- 10(c). Furthermore, as the ratio of CMC increased, a notable reduction in the formation of a passive film composed of ZnO and $Zn(OH)_2$ was observed despite the fact that the Zn corrosion product, $Zn(OH)_2$/ZnO, is generally impervious in nature and hinders the dissolution of anodes[166]. However, the addition of CMC can decrease the passive formation of $Zn(OH)_2$/ZnO on the steel substrate to sustain the protection current.

4.4 Summary

In this research, a sodium polyacrylate hydrogel electrolyte carrier was developed in the SACP system to protect steel in the atmospheric environment. The performance of the PANa–CMC hydrogels was verified via water retention tests, adhesion strength tests, electrochemical tests, and constant exposure tests. The main results can be concluded as following:

(1) PANa–CMC hydrogels coupled with Al–3Zn alloy generate and sustain a protective current to safeguard steel in high-humidity environments. Adding 5% CMC in hydrogels increases the density of the protective current up to about 3 μA/cm².

(2) Hydrogels can effectively immobilize the metal ions released from Al–Zn anodes into the surrounding environment, thus reducing its susceptibility for environmental contamination.

(3) The proposed corrosion mechanism of Al–3Zn involves the formation of a passive film composed of Al2O3, ZnO and $Zn(OH)_2$. Adding a certain amount of CMC can reduce the formation of passivation films.

(4) PANa–CMC hydrogels have demonstrated potential as electrolytes in the SACP method. This innovative application will allow for the expansion of SACP methods to high-humidity environments and potentially other atmospheric environments in the future.

CHAPTER 5 DISCUSSION ON APPLICABILITY OF ELECTROLYTE CARRIERS APPLIED IN SACP METHOD UNDER ATMOSPHERIC ENVIRONMENTS

5.1 Introduction

In the realm of safeguarding steel structures from corrosion in atmospheric conditions, the SACP method emerges as a highly effective strategy. Investigated in Chapter 2-4, this innovative technique utilizes sacrificial anodes to divert corrosive reactions away from the protected metal. While previous studies have delved into the protective effects of three electrolytes in the SACP system, exploring their roles, including electrochemical characteristics and protective current density, remains a valuable area for further investigation. A central and indispensable element within SACP systems is the electrolyte carrier, acting as the conduit for ion transport between sacrificial anodes and the metallic structures under protection.

The significance of electrolyte carriers within SACP systems cannot be overstated. Their selection, configuration, and integration into the cathodic protection framework are decisions grounded in a deep understanding of material properties, electrochemical principles, and environmental considerations. This foundational role of electrolyte carriers underscores the necessity for ongoing research, innovation, and optimization to enhance the durability, efficiency, and adaptability of SACP systems in safeguarding our valuable metallic infrastructures against the inevitable advance of corrosion. As we delve into the intricacies of these systems, it becomes clear that the electrolyte carrier is not just a component; it is the critical link that enables sacrificial anodes to fulfill their protective mandate, making it an indispensable element in the quest for long-term corrosion

prevention.

As outlined in Chapter 1, the three primary corrosion locations - the boundary with the ground, enclosed sections, and high-humidity areas - each present unique configuration. This diversity necessitates distinct arrangements for electrolyte carriers to effectively address the specific corrosion challenges posed by each location. Moreover, whether the electrolyte carrier can ensure sufficient contact between the electrolyte and the electrodes (i.e., the protected steel and the anode material providing protection) is an important aspect of achieving SACP. For example, in the application of fiber sheets, the fiber sheets need to be fixed through bolts, which brings the risk of reducing the strength of the steel structure[115, 118, 119]. Furthermore, the water absorption and retention capabilities of the electrolyte carrier directly determine the effectiveness of the electrolyte carrier in the SACP method. In previous studies, it has been observed that once the water retention rate decreases, the cathodic protection current density also significantly decreases[152]. Meanwhile, the ionic conductivity of the electrolyte carrier after absorbing the electrolyte has a profound impact on the effectiveness and efficiency of the SACP system. For example, the protective area in which the SACP method can be effectively applied may still be limited owing to the high resistivity of concrete[111, 150].

This chapter delves into the nuanced aspects that significantly influence the performance of electrolyte carriers within the challenging context of atmospheric environments. A comprehensive exploration encompasses the configuration of these carriers, the fixation between carriers and electrodes, considerations of hydrophilicity, and an in-depth examination of ionic conductivity. Understanding these critical factors is pivotal for optimizing the effectiveness of SACP systems and ensuring the enduring protection of metallic structures against the pervasive threat of corrosion. The results

shows that the configuration of three electrolyte carriers can be adapted to their application environments, respectively. Moreover, these three electrolyte carriers exhibit a level of adhesion to steel members to sustain cathodic protection current. Notably, the PANa-5%CMC hydrogel demonstrates a higher bonding strength, reaching 603.6 kPa. Furthermore, each materials shows remarkable water absorption and retention capability, due to the functional groups such as -OH and -COOH. Additionally, the electrochemical properties including OCP, ionic conductivity ensure that the effectiveness of SACP reaction can also be guaranteed in atmospheric environments.

5.2 Configuration of the electrolyte carriers to adapt atmospheric environments

The of electrolyte carriers such as water-swelling rubber, cotton-like fiber, and PANa-CMC hydrogels in SACP systems plays a crucial role in their effectiveness and adaptability to atmospheric environments. These carriers facilitate the conductive path between the anode and the cathode (the metal structure being protected), and their physical shape can significantly influence the efficiency and durability of the protection provided.

5.2.1 Water-swelling rubber with shrinkage and expansion

The configuration of water-swelling rubber as an electrolyte carrier in SACP systems is critical for adapting to and effectively functioning within various atmospheric environments. Water-swelling rubber, due to its unique property of absorbing water and swelling, can play a pivotal role in maintaining a conducive path for the protective current in environments where the moisture content can vary significantly. This adaptability is essential for the long-term protection of metal structures against corrosion.

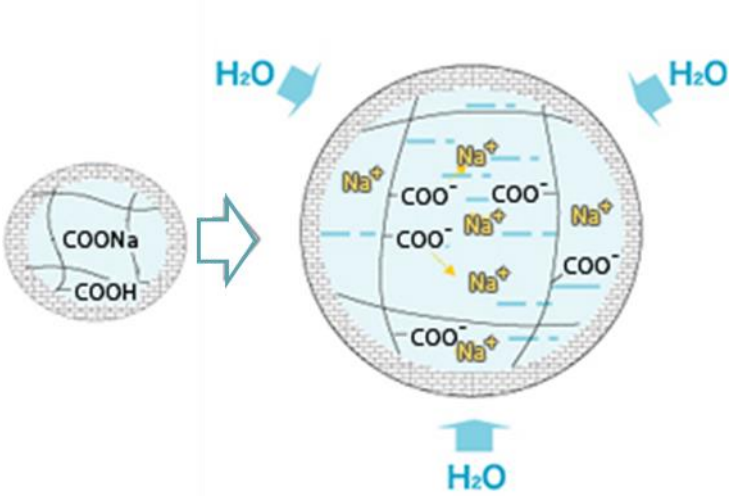

Figure 5- 1 Expansion mechanism of the water-swelling rubber

The degree to which water-swelling rubber can absorb moisture and swell impacts its electrical conductivity. The performance of water-swelling rubber in SACP systems is significantly influenced by its moisture absorption and expansion properties, as shown in Figure 5- 1. In environments with high humidity, the rubber expands more, enhancing its contact with electrodes. This increased contact ensures the efficacy of the SACP by maintaining a continuous protective circuit. Additionally, the expansion and subsequent moisture absorption improve the system's conductivity, effectively reducing the resistance between the anode and cathode, thus optimizing the protection against corrosion. The configuration must ensure that the rubber does not swell excessively, which could compromise mechanical stability or cause delamination from the metal surface. Furthermore, the thickness of the water-swelling rubber layer influences its ability to absorb water and, subsequently, its electrical conductivity. A thicker layer might offer more consistent conductivity over time as it can hold more moisture. However, too thick a layer might also slow the rate of moisture absorption and release, potentially reducing the system's responsiveness to changes in atmospheric humidity. Moreover, the configuration must ensure maximal and uniform contact between the water-swelling

rubber and the metal surfaces (both anode and cathode). Inadequate contact may lead to areas of poor protection, accelerating localized corrosion, as shown in Figure 2- 8 and Figure 2- 9.

5.2.2 Cotton-like fiber with self-adaptive shape

The use of cotton-like fiber as an electrolyte carrier in SACP systems presents unique considerations due to its organic nature, moisture retention capabilities, and structural properties. The configuration of this material significantly influences its effectiveness in adapting to various atmospheric environments and in facilitating the protective electrochemical reactions necessary to prevent metal corrosion.

The design aspects of cotton-like fibers, including porosity and weave density, play a pivotal role in their ability to retain moisture, which is crucial for the effective application of SACP systems. However, these same properties make it challenging for cotton-like fibers to retain their shape upon water absorption, as depicted in Figure 5- 2. Despite this limitation, cotton-like fibers demonstrate a remarkable capacity to adapt to various surrounding environments upon absorbing water, as shown in Figure 5- 3. This adaptability is particularly advantageous for steel members located in enclosed sections, where the flexible nature of cotton-like fibers allows for a snug fit around irregular shapes and configurations, ensuring consistent moisture provision and effective corrosion protection.

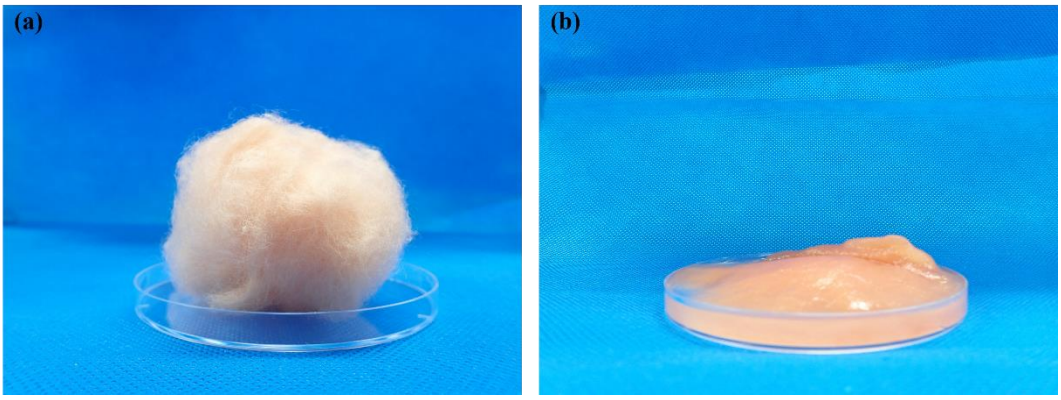

Figure 5- 2 The configuration of cotton-like fiber (a) before and (b) after water absorption.

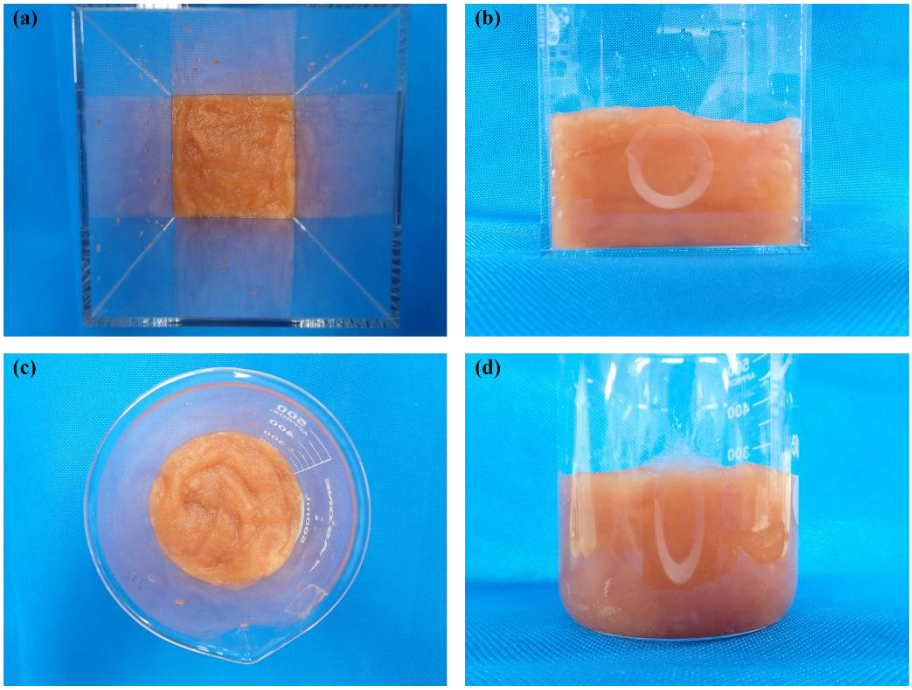

Figure 5- 3 The configuration of cotton-like fiber after water absorption in different containers with diffferent shape. (a) upside and (b) side snapshots of square container, (c) upside and (d) side snapshots of roundness container.

Hydrogels in various forms

Hydrogels as electrolyte carriers in SACP systems offer unique benefits due to their high-water content, flexibility, and ability to form conformal coatings over metal surfaces.

These properties make hydrogels particularly useful in adapting to various atmospheric environments for the protection of metals against corrosion. The configuration of hydrogels — including their chemical composition, physical structure, and integration with the cathodic protection system — plays a pivotal role in their effectiveness and adaptability. Hydrogels can be applied in various forms, such as triangle, tetragon, hexagon, and star, from sheets to beads, affecting their surface area exposure and interaction with atmospheric conditions[188, 189]. The choice of form factor influences how effectively hydrogels can adapt to and mitigate changes in humidity and temperature.

The type of polymers used in forming the hydrogel can influence its water absorption capacity, mechanical strength, and chemical stability. Polymers that can absorb significant amounts of water without dissolving are ideal for maintaining a conducive path for ion transport in dry conditions, while also preventing the hydrogel from becoming too fluid in high humidity. And the degree of crosslinking within the hydrogel network affects its structural integrity and porosity. A higher crosslinking density can lead to a more robust hydrogel that is less likely to degrade in harsh environmental conditions, but it might also reduce the hydrogel's ability to absorb water and swell, which can limit its effectiveness as an electrolyte carrier.

5.3 Fixation between electrolyte carriers and electrodes

The interface or fixation between electrolyte carriers (such as water-swelling rubber, cotton-like fiber, and hydrogels) and electrodes (sacrificial anodes and steel need to protect) the SACP systems is pivotal for the efficacy of corrosion protection, especially when adapting to varied atmospheric environments. This fixation influences the physical contact, electrical conductivity, and overall stability of the protection system under different environmental conditions.

5.3.1 Adherence and gap between water-swelling rubber and electrodes

Ensuring a robust electrical contact between the water-swelling rubber and the electrodes is critical. Poor contact may result in inefficient electron transfer, reducing the protective capability of the SACP system. As shown in Figure 2- 8(f), as with the specimen with the Zn plate, the corrosion protection effect can be seen in most of the rubber contact areas. This is considered to be due to the fact that the rubber adhered to the steel plate, which reduced the amount of DO in contact with the steel plate.

SEM-EDX analysis results for Dew1.0 and Dew1.0-0.1 are presented in Figure 5- 4. In areas ①, ③, and ④ on the contact surface, residue of adhered rubber material (Si) is observed due to the tight adherence of the rubber. In the uncontacted area ②, chloride ions (Cl) from the 3.5 wt% NaCl aq immersion environment are observed, and oxide (O, Fe) is generated on the steel substrate. The upper black part ④ on the contact surface has a high content of oxide (O), suggesting that due to the drying of the rubber during air curing, gaps occurred between the rubber and the steel plate.

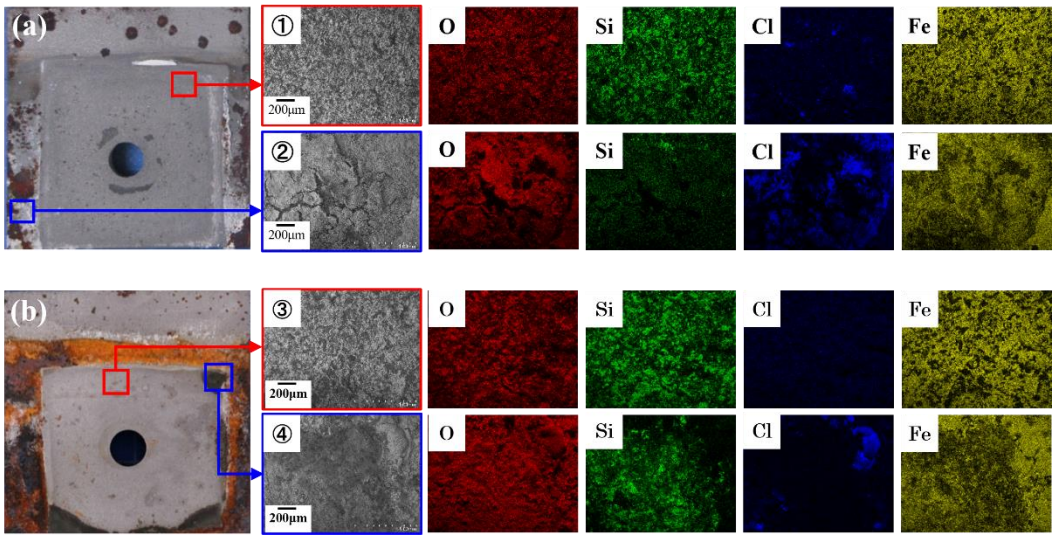

Figure 5- 4 Surface elemental analysis results of (a) Dew1.0 specimen and (b) Dew1.0-X specimen.

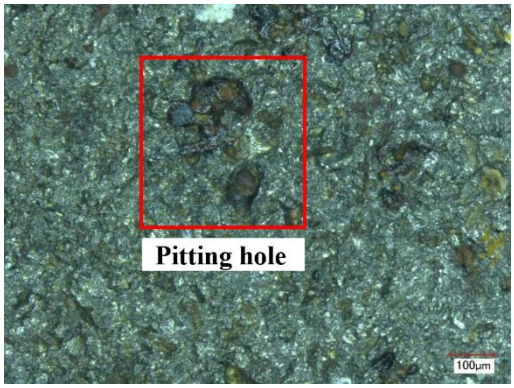

Figure 5- 5 Enlarged view of specimen Dew1.0-X. (×500).

An enlarged view of the upper black part is shown in Figure 5- 5. In the red-framed area in Figure 5- 5, partial corrosion progression is visible. Unlike specimens with a Zn plate, no such corrosion progression is observed, indicating sufficient corrosion protection even at the edge of the steel plate. This is attributed to the use of an anode material, which ensures corrosion protection even in minimal gaps through sacrificial anode action.

5.3.2 Weak adhesion of cotton-like fiber

As discussed in Chapter 5.2.2, cotton-like fibers tend to lose their configuration and adapt to various surrounding environments upon absorbing water, as illustrated in Figure 5- 2 and Figure 5- 3. Consequently, cotton-like fibers lack inherent mechanical strength. However, observations also indicate that fibers exhibit weak adhesion to the steel surface, possibly due to coordination bonds, as shown in Figure 5- 6.

Figure 5- 6 The weak adhesion of cotton-like fibers to the steel surface after SACP tests.

5.3.3 Adhesion strength of PANa-CMC hydrogels

As evident in Figure 5- 7(a), the PANa–CMC hydrogel exhibited remarkable self-adhesiveness, allowing it to adhere to blast steel surface, which makes the PANa–CMC hydrogel a promising candidate for an electrolyte in the SACP method. Figure 5- 7(b) reveals the influence of the ratio of CMC added in PANa–CMC hydrogels on their adhesion strength to blast steel surfaces. Tensile-adhesion tests were performed to quantitatively evaluate the adhesion strength of the hydrogel to the substrate. The results indicated that the adhesion strength increases on increasing the CMC content up to 5% and further decreases. Specifically, when the CMC ratio reached 5%, the adhesive strength increased significantly from 426.8 kPa to 603.6 kPa, demonstrating the existence of an optimal CMC concentration for maximizing the adhesion strength.

The PANa–CMC hydrogels exhibit a strong affinity for the steel substrate, leading to tight adhesion to the surface, which can be attributed to its chemical and structural properties[183, 184, 190], as shown in Figure 5- 7(c). The presence of carboxyl groups inherent in PANa hydrogel, along with the introduction of hydroxyl groups by CMC,

facilitates the formation of various non-covalent bonds, including hydrogen bonds and coordination bonds[191, 192]. These interactions are instrumental in ensuring effective adhesion of the hydrogel to the steel surface. Additionally, increasing the CMC ratio up to 5% results in a rougher surface of PANa–CMC hydrogels, as illustrated in Figure 4-5(b)–(f). Consequently, factors such as negative pressure, capillary force, and mechanical interlocking between the hydrogels and steel are enhanced[193]. However, when the CMC ratio exceeds 5%, an increase in pore quantity on the hydrogel surface may reduce the effective contact area between the hydrogel and the steel substrate, potentially leading to weaker adhesion strength.

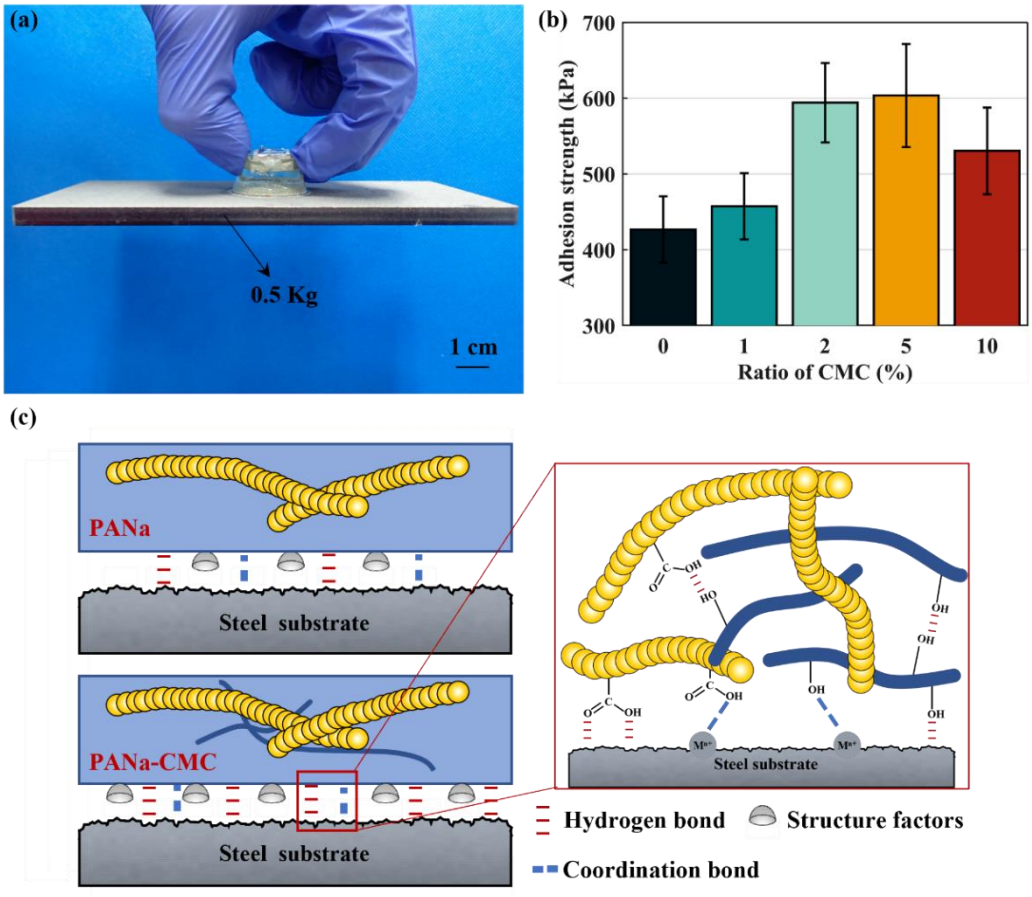

Figure 5- 7 (a) Hydrogel adhered to blast steel surfaces. (b) Adhesion strength between PANa–CMC hydrogels and blast steel. (c) Schematic illustration of the adhesion

mechanism of PANa–CMC hydrogels considering the ratio of CMC.

In summary, the fixation between electrolyte carriers and electrodes in SACP systems significantly influences their ability to adapt to and function effectively within various atmospheric environments. A well-designed fixation ensures optimal contact and conductivity, accommodates the physical and chemical properties of the electrolyte carrier, and withstands environmental challenges, thereby enhancing the protective capabilities of the SACP system.

5.4 Hydrophilicity of electrolyte carriers' materials

5.4.1 Wet-dry cycling hydrophilicity of water-swelling rubber

Figure 5- 8 depicts the temporal weight changes during water absorption and drying tests of water-swelling rubber. The rubber immersed in distilled water reaches near equilibrium in approximately 40 days, exhibiting a maximum weight increase of about 20g compared to its pre-water absorption state. Conversely, in a 3.5 wt% NaCl solution, the weight change stabilizes around 50 days, with an increase in weight of approximately 9g. The highly water-absorbing polymer's cations within the rubber are more soluble in distilled water than in NaCl solution, leading to a larger concentration difference and increased osmotic pressure, enhancing water absorption.

In NaCl solutions, rubber's water absorption increases with decreasing concentration. The lower ion concentration in a 0.1 wt% NaCl solution results in higher osmotic pressure, making water absorption more efficient.

Both specimens soaked in distilled water and a 3.5 wt% NaCl solution exhibit a substantial weight decrease in the initial 30 days during drying. However, rubber soaked in NaCl solution shows a reduced rate of weight loss after 30 days, requiring more time

for drying compared to rubber soaked in distilled water. The affinity of the high water-absorbing polymer with Na^+ ions leads to a slower release of Na+ ions in NaCl solution, slowing down the drying process.

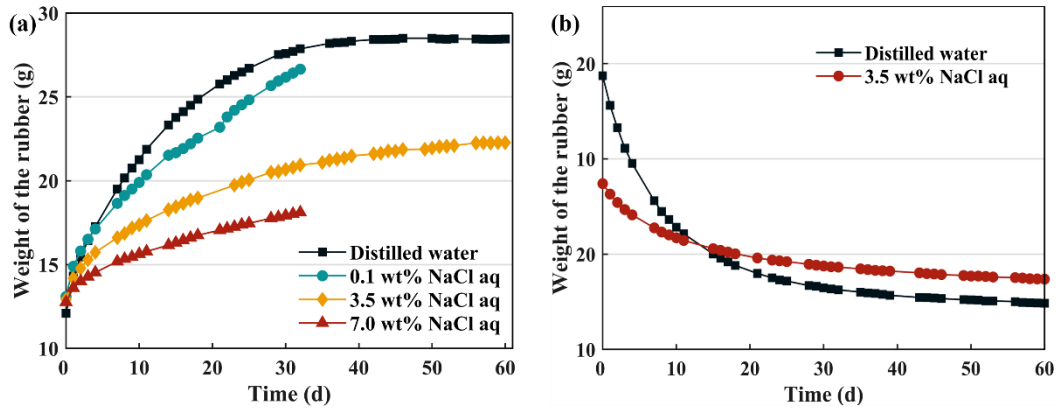

Figure 5- 8 The time-dependence of weight for the water-swelling rubber in (a) absorbing test and (b) drying test.

These observations suggest that when water-swelling rubber absorbs water, it tends to absorb electrolytes with lower ion concentrations in the electrolyte. Conversely, during drying, electrolytes containing ions slow down the process compared to distilled water.

In the SACP technology, the rubber serves as an electrolyte burden medium. Its water absorption performance is influenced by the immersion environment's concentration, and waterproofing performance determines the continuity of SACP. Proper electrolyte concentrations must be explored to strike a balance between water absorption and moisture retention capabilities for the intended application.

5.4.2 Water absorption and retention capacity of cotton-like fiber

As depicted in Figure 5- 9(a), the cotton-like fibers demonstrate an impressive water absorption capacity, capable of absorbing nearly 7 times their weight in 0.1 wt% NaCl aq within the initial 10-minute interval. Furthermore, Figure 5- 9(b) illustrates that even after exposure to an environment of 26 ℃ and 30% humidity for 15 days, the cotton-like fibers

retain over 50% of their maximum water absorption capacity. These outstanding water absorption and retention capabilities underscore the potential applicability of cotton-like fibers in atmospheric environments.

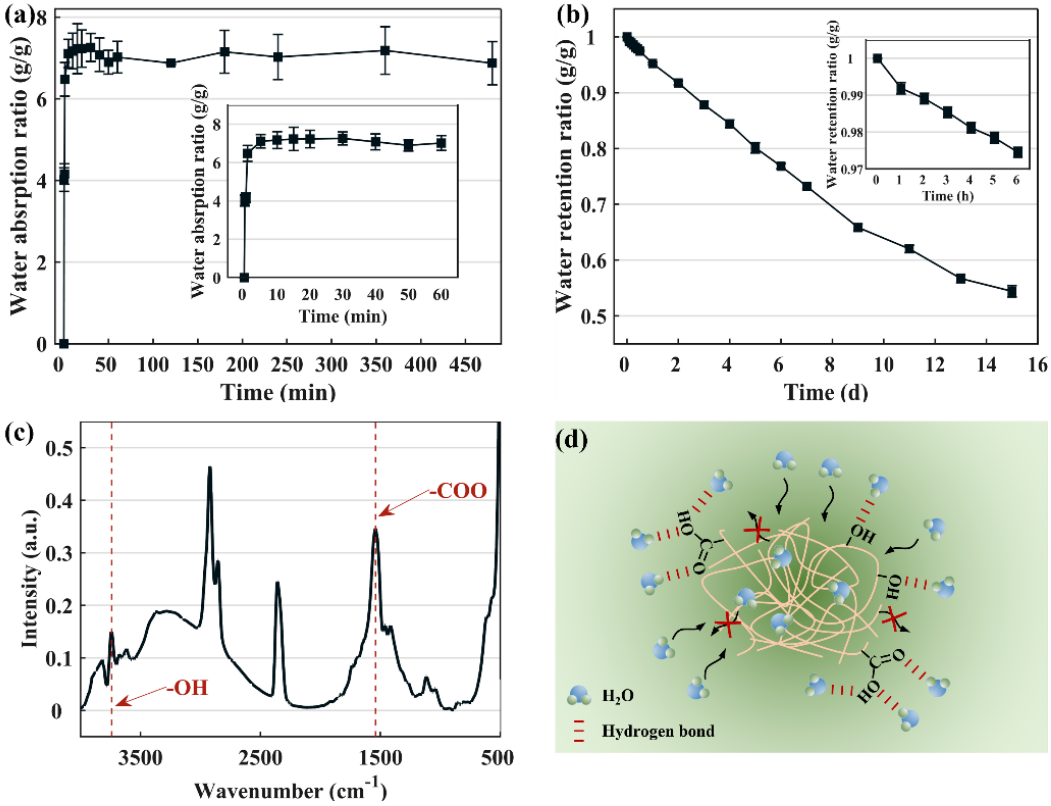

Figure 5- 9 Time-dependent (a) water absorption and (b) retention ratio. (c) FTIR spectra of cotton-like fiber. (d) schematic illustration of the water retention properties of cotton-like fiber.

The impressive water absorption and retention capabilities of the cotton-like fiber stem from its chemical composition. As illustrated in Figure 5- 9(c), the FTIR spectra of the fiber revealed characteristic absorption peaks at 1551 cm^{-1} and 3740 cm^{-1}, respectively. The peak at 1551 cm^{-1} corresponds to the carboxylate ion (COO-) while the peak at 3740 cm^{-1} is attributed to the hydroxyl group (-OH). These functional groups are known for their hydrophilic nature, contributing significantly to the fiber's water-attracting properties, as depicted in Figure 5- 9(d).

5.4.3 Hydrophilicity of PANa–CMC hydrogels

Figure 5- 10 depicts the exceptional water absorption capacity of pure PANa hydrogel, as evidenced by its ability to absorb water at a rate of 1.08, 1.15, 1.24, and 2.91 times its weight after 10, 20, 30, and 60 minutes of immersion in deionized water, respectively. As shown in Figure 5- 10(g), this impressive property arises from the presence of hydroxyl groups that enable efficient interaction with water molecules through hydrogen bonding[194]. Furthermore, during the water absorption process, the size of the hydrogel increased, and its transparency improved, as evidenced by Figure 5- 10(b).

The incorporation of 1% CMC in the PANa hydrogel resulted in a slight increase in water absorption capacity, as revealed by the presence of carboxyl groups (Figure 5- 10 (g)) and rough surface and porous channels, as illustrated in Figure 4- 5(b)-(f), respectively. This enhancement can be attributed to the unique properties of CMC, which facilitate increased interaction with water molecules, resulting in greater water absorption capacity[195]. However, when the CMC ratio exceeded 1%, the water absorption capacity declined with an increase in the CMC ratio, resulting from the density of macromolecular chains becomes too high, hindering penetration of water molecules into the PANa, and hydrogen bonding interactions between PANa and CMC chains[161, 196], as shown in Figure 5- 10(g).

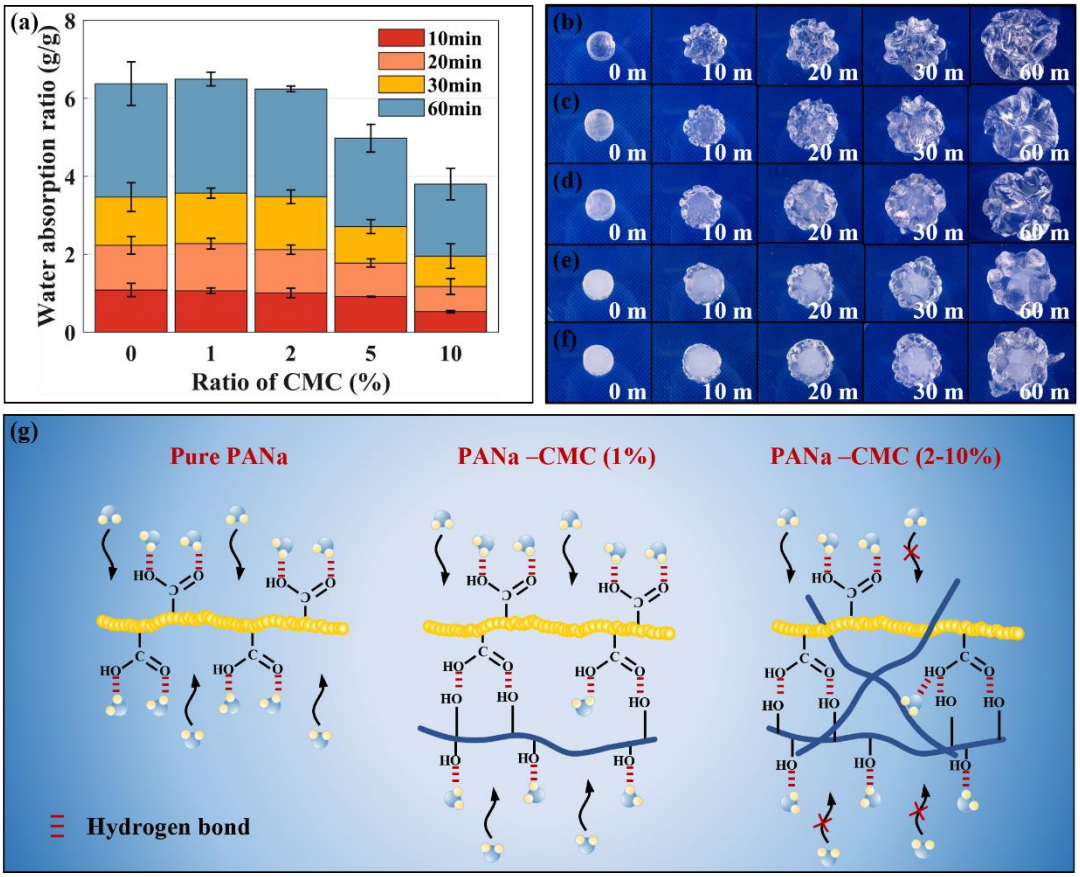

Figure 5- 10 (a) The water absorption ratio of PANa hydrogels immersed in deionized water. (b) Comparison of the water absorbing properties of the pure PANa hydrogel, (c) PANa-1%CMC, (d) PANa-2%CMC, (e) PANa-5%CMC, and (f) PANa-10%CMC. (g) Schematic illustration of the water-absorbing properties considering the ratio of CMC.

Figure 5- 11(a) demonstrates the exceptional water retention capacity of PANa–CMC hydrogels, with pure PANa hydrogel losing only 2% of its water content after seven days. The addition of CMC further improved the water retention capacity, even to the point where hydrogels with 5% and 10% CMC ratios could absorb a certain amount of water from the surrounding humidity. These findings suggest that the incorporation of CMC into the PANa hydrogel can significantly enhance its water retention capabilities. Figure 5- 11(b) clearly shows that the surface of pure PANa hydrogel becomes swollen and soft,

which can potentially impact its mechanical properties[197]. However, with an increase in the CMC ratio, PANa–CMC hydrogels exhibited better moisture retention, maintaining its original shape. This is evident from Figure 5- 11(b), where the hydrogels with higher CMC ratios retain their sharpness, indicating improved stability in their mechanical properties.

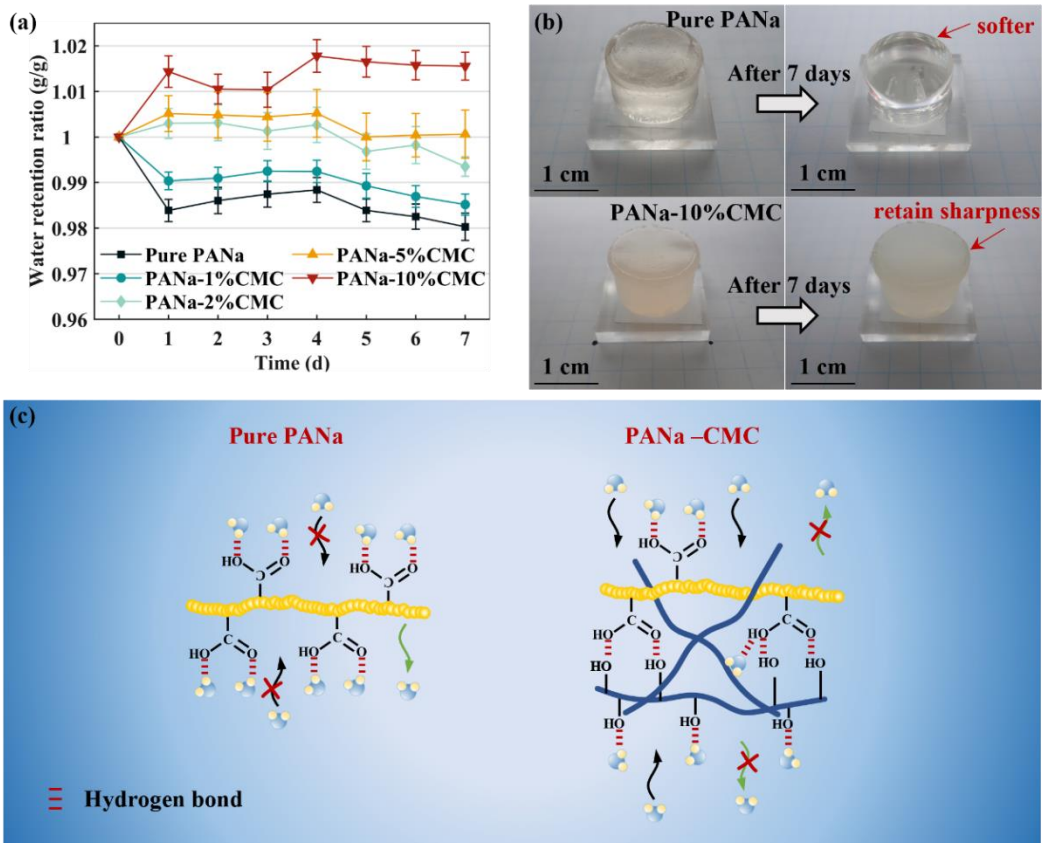

Figure 5- 11 (a) The water retention ratio of PANa–CMC hydrogels . (b) Comparison of surface condition of the pure PANa hydrogel and PANa-10%CMC. (c) Schematic illustration of the water retention properties considering the ratio of CMC.

The addition of CMC to the PANa hydrogel has been found to improve its water retention capacity. This improvement is attributed to the presence of carboxyl groups in CMC (Figure 4- 5(c)) and its rough surface (Figure 4- 5(b)–(f)). The carboxyl groups in CMC enabled stronger interactions with water molecules, leading to an increased ability

of the hydrogel to retain water[195]. Notably, when the CMC ratio exceeded 5%, the water retention ratio exceeded 1, indicating that the hydrogel not only hinders the evaporation of water molecules into the surrounding environment but can also absorb moisture from the environment into the hydrogel. This demonstrates the exceptional water retention capability of the hydrogel, which has potential applications in preserving moisture and preventing dehydration in various settings.

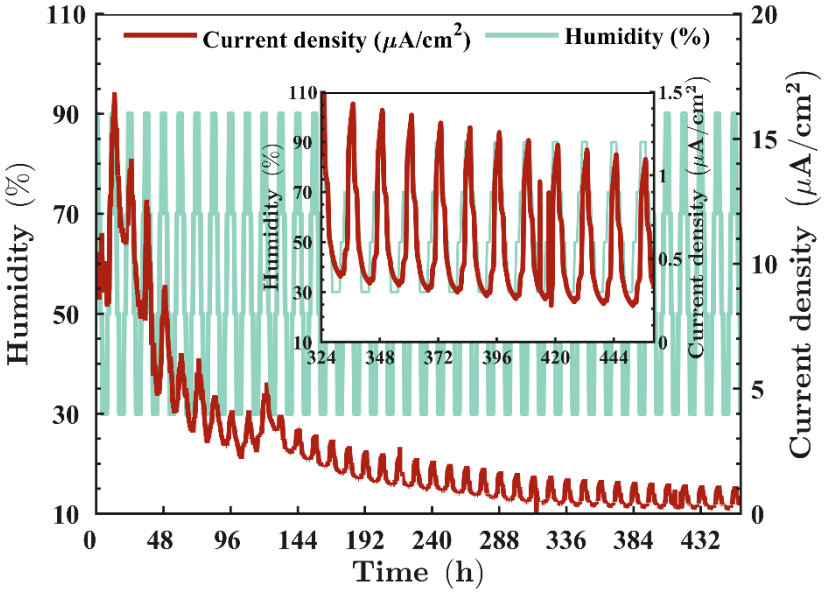

Figure 5- 12 The time-dependent protective current density of the SACP method in different relative humidity environments.

In addition, hydrogels emonstrate sensitivity to humidity, as indicated in Figure 5-14. While the overall current density initially decreased, it stabilized after 300 hours. Notably, the peaks in current density and humidity remained almost identical throughout the test period. This suggests that hydrogels can adapt and provide protective current density in response to changes in humidity.

5.5 Ionic conductivity of electrolyte carriers' materials

The ionic conductivity of electrolyte carriers' materials (such as water-swelling rubber,

cotton-like fiber, and hydrogels) and electrodes is a crucial factor influencing the effectiveness of SACP systems. Ionic conductivity refers to the ability of a material to allow the flow of ions, which is essential for the electrochemical reactions involved in cathodic protection.

5.5.1 Ionic conductivity of water-swelling rubber under different pressure

The ionic conductivity of seawater is 50 mS/cm. σ is significantly influenced by the density of free electrons, with higher σ indicating a more easily flowing cathodic protection current. Regardless of the type of electrolyte, σ increases with an increase in concentration, as shown in Figure 5- 13. The relatively low σ of the rubber soaked in 0.1 wt% electrolyte suggests that when the concentration of the electrolyte used to swell the rubber is low, the SACP system may not provide sufficient corrosion current. Compared to NaCl, $NaNO_2$ shows a similar decreasing trend in σ under different stress conditions. The significantly small σ of 1.0– 10.0 wt% $NaNO_2$ aq suggests that the cathodic protection current flows easily.

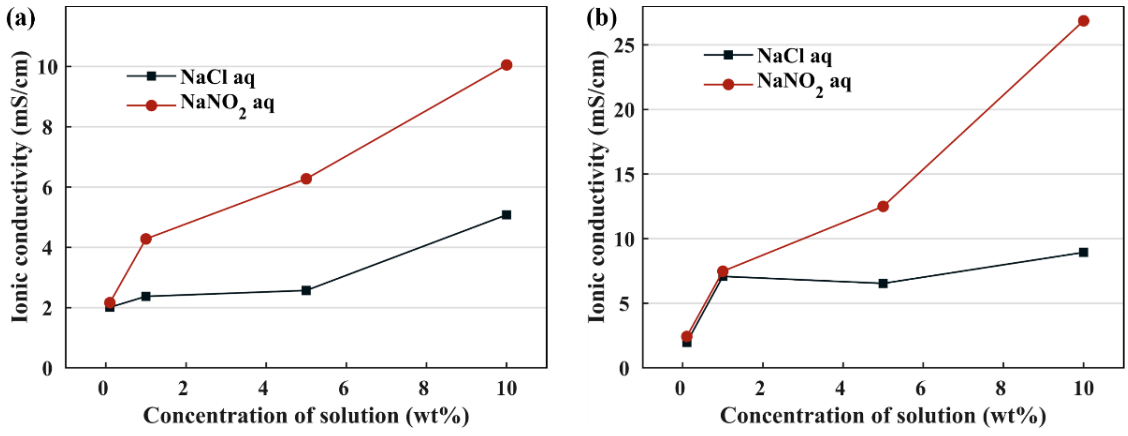

Figure 5- 13 Ionic conductivity of the specimens of (a) intensity of pressure 1.2×10^{-2} MPa, and (b) intensity of pressure 3.7×10^{-2} MPa.

Furthermore, σ increases with an increase in stress. When using rubber soaked in

$NaNO_2$, the σ with a load of 6 kg is approximately 1–3 times larger than with a load of 2 kg. It is presumed that placing stress on the rubber enhances the contact between the rubber surface and the steel member, thereby increasing the cathodic protection current.

5.5.2 Ionic conductivity of cotton-like fiber with different electrolyte content

The ionic conductivity of the cotton-like fibers, acting as electrolyte carriers, is pivotal in ensuring the efficacy of the SACP method by directly influencing the ion transfer between the anodes and cathodes. The ionic conductivity values of the cotton-like fiber, absorbing distinct ratios of 0.1 wt% NaCl aq, were assessed through EIS, with corresponding Nyquist plots and Bode plots depicted in Figure 5- 14(a) and (b), respectively.

Notably, all plots demonstrated a linear trend, indicative of a non-Faradaic process, with no charge crossing the electrode-conductor interface. The impedance values of the electrolyte carrier can be construed as the points of intersection of EIS plots with the X-axis[198]. It can be clearly found that the ionic conductivity of the fiber fully absorbing 0.1 wt% NaCl aq was almost double the conductivity of 0.1 wt% NaCl aq, as shown in Figure 5- 14(c), which can be ascribed to the effects of fiber side chains on ion transport[199]. However, as the electrolyte content of the fibers decreases, the ion conductivity also decreases. When the fiber electrolyte content drops to around 10%, the ion conductivity is approximately one-fifth of that of a 0.1% NaCl solution. Therefore, the water retention capability of the fibers is a crucial criterion for ensuring their effectiveness as an electrolyte carrier.

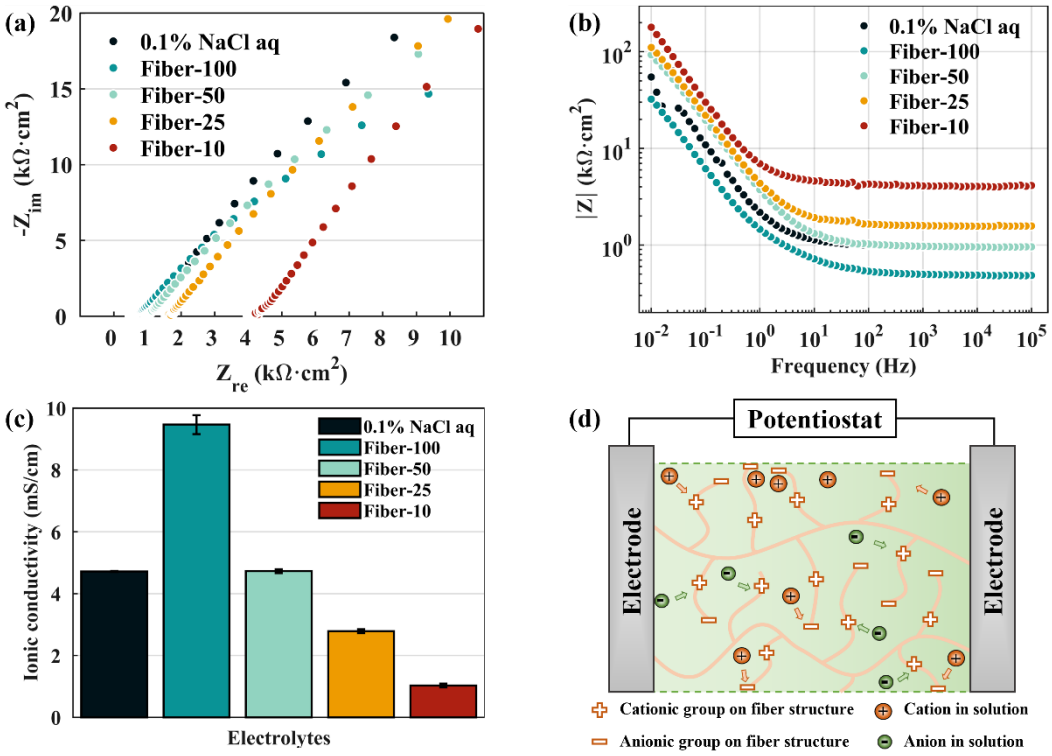

Figure 5- 14 (a) Nyquist plots, (b) Bode plots and (c) ion conductivity of cotton-like fiber absorbing different electrolyte content. (d) Schematic illustration of ionic conductivity mechanism in cotton-like fiber with electrolyte content.

5.5.3 Ionic conductivity of PANa-CMC hydrogels with different CMC ratio

The ionic conductivity of the hydrogel electrolyte plays a critical role in the efficient functioning of the SACP method, as it directly affects the transfer of ions between anodes and cathodes. The AC impedance tests were conducted to measure the Nyquist plot and ionic conductivity of PANa–CMC hydrogels with varying CMC ratios, as depicted in Figure 5- 15(a) and (b). Pure PANa hydrogel exhibited the lowest ionic conductivity of 16.135 mS/cm in comparison to the hydrogels containing CMC. As the CMC content increased, the ionic conductivity also significantly increased. Remarkably, the hydrogel with 10% CMC showed the highest ionic conductivity of 29.160 S/cm, almost double the

conductivity of pure PANa hydrogel. This improvement in conductivity can be attributed to the ability of CMC to penetrate the hydrogel, creating a continuous ionic fluid that ensures stable and strong ionic conductivity[200]. These findings suggest that the addition of CMC can effectively enhance the ionic conductivity of the hydrogel electrolyte, thereby improving the overall performance of the SACP method.

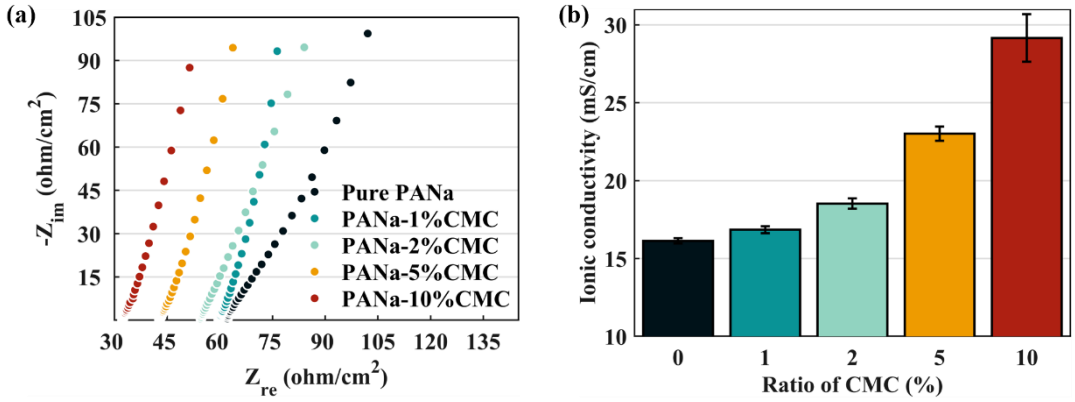

Figure 5- 15 (a) Alternating current impedance spectra of the hydrogel electrolyte at the frequency range from 100 kHz to 0.01 Hz. (b) The ionic conductivity of PANa–CMC hydrogels considering the ratio of CMC.

5.6 Summary

This chapter evaluates the applicability of three electrolyte carrier materials—water-swelling rubber, cotton-like fiber, and PANa-CMC hydrogels—for mitigating atmospheric corrosion in three classical locations. The assessment considers factors such as configuration, fixation, hydrophilicity, and ionic conductivity. The key findings can be summarized as follows:

(1) The configuration of three types of electrolyte carriers including water- swelling rubber, cotton-like fiber and PANa-CMC hydrogels can be adapted to three kinds of corrosion locations of in boundary with ground, enclosed sections and high-humidity areas, respectively.

(2) All three electrolyte carriers exhibit a level of adhesiveness, ensuring effective contact between the electrolyte and the electrode material to sustain SACP. However, it's notable that water-absorbing rubber and cotton-like fibers maintain relatively weak adhesion, whereas the PANa-5%CMC hydrogel demonstrates a higher bonding strength, reaching 603.6 kPa.

(3) The amount of water absorbed by the rubber increases as the ion concentration of the electrolyte decreases, and the rubber takes more time to dry with the electrolyte concentration inside rubber increasing. An appropriate electrolyte concentration should take both water absorption and retention into consideration.

(4) The cotton-like fiber displayed a remarkable water absorption capability, absorbing nearly seven times its weight of the electrolyte within a 10-min interval. Moreover, it retained over 50% of its maximum water absorption even after 15-day exposure.

(5) The composition of CMC increases the surface roughness and introduces hydroxyl groups to hydrogels, enhancing water retention capacity. At a CMC ratio up to 5% or higher, the hydrogel achieves a water retention ratio exceeding 1.

(6) In the water-swelling rubber, the ionic conductivity of $NaNO_2$ aq is superior to that of NaCl aq, but both increase with the increase in pressure.

(7) The ionic conductivity of the fiber, when fully saturated with 0.1 wt% NaCl aq, was nearly twice that of the same concentration without fibers, diminishing as the electrolyte content decreased.

(8) As the CMC content increases, the ionic conductivity of hydrogels improves and Nyquist curve radius decreases. Additionally, Al–Zn exhibits a more negative polarization potential than steel in the hydrogel.

CHAPTER 6 CONCLUSIONS AND FUTURE WORK

6.1 Summary and main conclusions

For steel structures exposed to the atmosphere, corrosion prevention usually relies on surface coatings such as paint. However, the quality of surface preparation and coating is difficult to ensure in many specialized parts of steel structures, especially in areas such as narrow sections and plate nodes. In this dissertation, three electrolyte carriers are developed for three typical corrosion locations, and the SACP method, which is commonly used in aqueous or soil environments, is applied to atmospheric environments to avoid coating defects.

In this study, the protection capability of the three electrolyte carriers in atmospheric environments in terms of the effect of SACP, the electrochemical behavior of the anode material and steel in the electrolyte carriers, and the cathodic protection current were evaluated. Finally, the research explained the suitability of each electrolyte carrier material for the respective corrosion site by discussing the morphology of the electrolyte carrier material, the fixation mode with the electrode, the hydrophilic properties and the ionic conductivity.

Based on the above studies, we can draw the following conclusions

6.1.1 Effectiveness of water-swelling rubber in SACP method applied in boundary with ground

(1) Unless completely dry, rubber retains sufficient moisture for the maintenance of the sacrificial anode corrosion protection circuit.

(2) Transitioning from a water-submerged to a dry environment is facilitated by the high-water retention capability of the rubber, ensuring the continuity of sacrificial anode

action.

6.1.2 Effectiveness of cotton-like fiber in SACP method applied in closed-sections

(1) The OCP of the Al-3Zn sacrificial anode was approximately −0.2 V relative to steel when immersed in the cotton-like fiber, indicating the effectiveness of the SACP method.

(2) Both the Al-3Zn alloy and steel were more resistant to dissolution immersed in the cotton-like fiber, based on Nyquist plots.

(3) The Al-3Zn alloy exhibited the ability to provide adequate and relatively stable protective current density and potential for steel members, mitigating corrosion risks within the cotton-like fiber environment.

6.1.3 Effectiveness of PANa-CMC hydrogels in SACP method applied in high-humidity areas

(1) As the CMC content increases, the ionic conductivity of hydrogels improves and Nyquist curve radius decreases. Additionally, Al–Zn exhibits a more negative polarization potential than steel in the hydrogel.

(2) PANa–CMC hydrogels coupled with Al–3Zn alloy generate and sustain a protective current to safeguard steel in high-humidity environments. Adding 5% CMC in hydrogels increases the density of the protective current up to about 3 μA/cm².

(3) Hydrogels can effectively immobilize the metal ions released from Al–Zn anodes into the surrounding environment, thus reducing its susceptibility for environmental contamination.

(4) The proposed corrosion mechanism of Al–3Zn involves the formation of a passive film composed of Al2O3, ZnO and $Zn(OH)_2$. Adding a certain amount of CMC can reduce the formation of passivation films.

(5) PANa–CMC hydrogels have demonstrated potential as electrolytes in the SACP method. This innovative application will allow for the expansion of SACP methods to high-humidity environments and potentially other atmospheric environments in the future.

6.1.4 Configuration of the electrolyte carriers

the configuration of three types of electrolyte carriers including water- swelling rubber, cotton-like fiber and PANa-CMC hydrogels can be adapted to three kinds of corrosion locations of in boundary with ground, and high-humidity areas.

6.1.5 Fixation of electrolyte carriers

All three electrolyte carriers exhibit a level of adhesiveness, ensuring effective contact between the electrolyte and the electrode material to sustain SACP. However, it's notable that water-absorbing rubber and cotton-like fibers maintain relatively weak adhesion, whereas the PANa-5%CMC hydrogel demonstrates a higher bonding strength, reaching 603.6 kPa.

6.1.6 Hydrophilicity of electrolyte carriers' materials

(1) The amount of water absorbed by the rubber increases as the ion concentration of the electrolyte decreases, and the rubber takes more time to dry with the electrolyte concentration inside rubber increasing. An appropriate electrolyte concentration should take both water absorption and retention into consideration.

(2) The cotton-like fiber displayed a remarkable water absorption capability, absorbing nearly seven times its weight of the electrolyte within a 10-min interval. Moreover, it retained over 50% of its maximum water absorption even after 15-day exposure.

(3) The composition of CMC increases the surface roughness and introduces hydroxyl groups to hydrogels, enhancing water retention capacity. At a CMC ratio up to 5% or

higher, the hydrogel achieves a water retention ratio exceeding 1.

6.1.7 Ionic conductivity of electrolyte carriers' materials

(1) In the water-swelling rubber, the ionic conductivity of $NaNO_2$ aq is superior to that of NaCl aq, but both increase with the increase in pressure.

(2) The ionic conductivity of the fiber, when fully saturated with 0.1 wt% NaCl aq, was nearly twice that of the same concentration without fibers, diminishing as the electrolyte content decreased.

(3) As the CMC content increases, the ionic conductivity of hydrogels improves and Nyquist curve radius decreases. Additionally, Al–Zn exhibits a more negative polarization potential than steel in the hydrogel.

6.2 Recommendations for future work

This dissertation had developed the three types of electrolyte carriers to expand the application of the SACP method to atmospheric environments. However, limitations existed in the work which worthy for future work:

6.2.1 Effect of alkaline environments on the performance of water-swelling rubber

To ensure effective cathodic protection in alkaline environments, it is essential to carefully select materials with suitable resistance to alkaline conditions and regularly monitor the condition of the sacrificial anode system to address any potential issues that may arise over time. Additionally, proper installation and maintenance practices play a crucial role in maximizing the performance and longevity of SACP systems employing water-swelling rubber.

6.2.2 The performance of the three types of electrolyte carriers applied in tidal zone

In the tidal zone, which is characterized by periodic exposure to saltwater and

atmospheric conditions, the performance of these electrolyte carriers will depend on their specific material properties, such as water absorption, resistance to degradation, adhesion, and mechanical strength. Factors such as wave action, salinity, temperature variations, and exposure to sunlight can affect the durability and effectiveness of these carriers in providing cathodic protection or serving other purposes.

It's essential to consider the unique challenges posed by the tidal zone environment and conduct thorough testing and monitoring to assess the long-term performance of electrolyte carriers in such conditions. Additionally, regular maintenance and replacement of these materials may be necessary to ensure continued effectiveness in protecting metal structures from corrosion.

6.2.3 The long-term performance of the three types of electrolyte carriers

The long-term performance of electrolyte carriers in the SACP method depends on the specific material properties, environmental conditions, and the corrosive potential of the protected structure. Regular monitoring and maintenance practices are essential to assess the condition of the carriers and sacrificial anodes over time. Some key considerations for ensuring the effectiveness of electrolyte carriers in the SACP method, including material selection, compatibility, monitoring. By addressing these considerations, it is possible to enhance the long-term performance of electrolyte carriers in SACP method and effectively mitigate corrosion in protected structures.

6.2.4 Development of environmentally friendly hydrogel for SACP method

As the sacrificial anode reaction proceeds, metal ions such as Al^{3+}, Zn^{2+} will continuously be released into the surrounding environment, leading to contamination issues. Therefore, it is highly desirable to develop a novel electrolyte carrier, such as

hydrogels, that not only effectively supports sacrificial anode reactions but also addresses environmental concerns by minimizing metal ion release and contamination issues. The goal is to strike a balance between effective cathodic protection and environmentally friendly characteristics in marine or similar environments.

REFERENCE

[1] F. Mansfeld, J. Kenkel, Electrochemical monitoring of atmospheric corrosion phenomena, Corrosion Science, 16 (1976) 111-122.

[2] I.S. Cole, T. Muster, N. Azmat, M. Venkatraman, A. Cook, Multiscale modelling of the corrosion of metals under atmospheric corrosion, Electrochimica Acta, 56 (2011) 1856-1865.

[3] L. Veleva, R.D. Kane, Atmospheric corrosion, (2003).

[4] I. Cole, N. Azmat, A. Kanta, M. Venkatraman, What really controls the atmospheric corrosion of zinc? Effect of marine aerosols on atmospheric corrosion of zinc, International materials reviews, 54 (2009) 117-133.

[5] T. Graedel, Corrosion mechanisms for aluminum exposed to the atmosphere, Journal of the Electrochemical Society, 136 (1989) 204C.

[6] J. Alcántara, D. de la Fuente, B. Chico, J. Simancas, I. Díaz, M. Morcillo, Marine atmospheric corrosion of carbon steel: A review, Materials, 10 (2017) 406.

[7] T. Graedel, Corrosion mechanisms for silver exposed to the atmosphere, Journal of the Electrochemical Society, 139 (1992) 1963.

[8] P. Albrecht, T.T. Hall Jr, Atmospheric corrosion resistance of structural steels, Journal of materials in civil engineering, 15 (2003) 2-24.

[9] G. Batis, E. Rakanta, Corrosion of steel reinforcement due to atmospheric pollution, Cement and concrete composites, 27 (2005) 269-275.

[10] Y. Qian, C. Ma, D. Niu, J. Xu, M. Li, Influence of alloyed chromium on the atmospheric corrosion resistance of weathering steels, Corrosion Science, 74 (2013) 424-429.

[11] A.N. Kallias, B. Imam, M.K. Chryssanthopoulos, Performance profiles of metallic bridges subject to coating degradation and atmospheric corrosion, in: Bridge Design, Assessment and Monitoring, Routledge, 2018, pp. 24-37.

[12] P. Dillmann, F. Mazaudier, S. Hœrlé, Advances in understanding atmospheric corrosion of iron. I. Rust characterisation of ancient ferrous artefacts exposed to indoor atmospheric corrosion, Corrosion science, 46 (2004) 1401-1429.

[13] E. Hidaka, Report on measures and observation of corrosion at the base of road lighting poles, Collection of Papers from the Ministry of Land, Infrastructure, Transport and Tourism's Technical Research Council, (2013) 9-14.

[14] I. Ministry of Land, Transport and Tourism, Inspection Guidelines for Fixtures (Signs, Lighting Facilities, etc.), in, 2019.

[15] U.M. Angst, Challenges and opportunities in corrosion of steel in concrete,

Materials and Structures, 51 (2018) 1-20.

[16] W. Aperador, R.M. de Gutiérrez, D.M. Bastidas, Steel corrosion behaviour in carbonated alkali-activated slag concrete, Corrosion Science, 51 (2009) 2027-2033.

[17] W. Tahri, X. Hu, C. Shi, Z. Zhang, Review on corrosion of steel reinforcement in alkali-activated concretes in chloride-containing environments, Construction and Building Materials, 293 (2021) 123484.

[18] Y. Cai, W. Zhang, L. Yu, M. Chen, C. Yang, R. Francois, K. Yang, Characteristics of the steel-concrete interface and their effect on the corrosion of steel bars in concrete, Construction and Building Materials, 253 (2020) 119162.

[19] T.A. Soylev, R. François, Quality of steel–concrete interface and corrosion of reinforcing steel, Cement and Concrete Research, 33 (2003) 1407-1415.

[20] A. Goyal, H.S. Pouya, E. Ganjian, P. Claisse, A review of corrosion and protection of steel in concrete, Arabian Journal for Science and Engineering, 43 (2018) 5035-5055.

[21] A. Afshar, S. Jahandari, H. Rasekh, M. Shariati, A. Afshar, A. Shokrgozar, Corrosion resistance evaluation of rebars with various primers and coatings in concrete modified with different additives, Construction and Building Materials, 262 (2020) 120034.

[22] L. Fan, X. Shi, Techniques of corrosion monitoring of steel rebar in reinforced concrete structures: A review, Structural Health Monitoring, 21 (2021) 1879-1905.

[23] W.P. Iverson, Microbial Corrosion of Metals, in: A.I. Laskin (Ed.) Advances in Applied Microbiology, Academic Press, 1987, pp. 1-36.

[24] Y. Ohara, H. Endo, T. Mihara, K. Yamanaka, Ultrasonic Measurement of Closed Stress Corrosion Crack Depth Using Subharmonic Phased Array, Japanese Journal of Applied Physics, 48 (2009) 07GD01.

[25] H. El Hajj, A. Abdelouas, Y. El Mendili, G. Karakurt, B. Grambow, C. Martin, Corrosion of carbon steel under sequential aerobic–anaerobic environmental conditions, Corrosion Science, 76 (2013) 432-440.

[26] Z. Salarvand, M. Amirnasr, M. Talebian, K. Raeissi, S. Meghdadi, Enhanced corrosion resistance of mild steel in 1M HCl solution by trace amount of 2-phenyl-benzothiazole derivatives: Experimental, quantum chemical calculations and molecular dynamics (MD) simulation studies, Corrosion Science, 114 (2017) 133-145.

[27] T.E. Graedel, R.P. Frankenthal, Corrosion Mechanisms for Iron and Low Alloy Steels Exposed to the Atmosphere, Journal of The Electrochemical Society, 137 (1990) 2385.

[28] P.R. Roberge, R.D. Klassen, P.W. Haberecht, Atmospheric corrosivity modeling — a review, Materials & Design, 23 (2002) 321-330.

[29] Y. Ma, Y. Li, F. Wang, Corrosion of low carbon steel in atmospheric environments of different chloride content, Corrosion Science, 51 (2009) 997-1006.

[30] C. Han, Z. Li, X. Yang, J. Wang, Corrosion behavior and mechanical performance of weathering steel in industrial and rural atmospheric environments, Construction and Building Materials, 411 (2024) 134284.

[31] E. Bernardi, I. Vassura, S. Raffo, L. Nobili, F. Passarini, D. de la Fuente, M. Morcillo, Influence of inorganic anions from atmospheric depositions on weathering steel corrosion and metal release, Construction and Building Materials, 236 (2020) 117515.

[32] G. Li, L. Niu, J. Lian, Z. Jiang, A black phosphate coating for C1008 steel, Surface and Coatings Technology, 176 (2004) 215-221.

[33] D. Mizuno, S. Suzuki, S. Fujita, N. Hara, Corrosion monitoring and materials selection for automotive environments by using Atmospheric Corrosion Monitor (ACM) sensor, Corrosion Science, 83 (2014) 217-225.

[34] S.J. Oh, D.C. Cook, H.E. Townsend, Atmospheric corrosion of different steels in marine, rural and industrial environments, Corrosion Science, 41 (1999) 1687-1702.

[35] T.E. Graedel, Corrosion Mechanisms for Zinc Exposed to the Atmosphere, Journal of The Electrochemical Society, 136 (1989) 193C.

[36] R. Bender, D. Féron, D. Mills, S. Ritter, R. Bäßler, D. Bettge, I. De Graeve, A. Dugstad, S. Grassini, T. Hack, Corrosion challenges towards a sustainable society, Materials and Corrosion, 73 (2022) 1730-1751.

[37] A. Williamson, M. Hernandez, C. Arroyave, The Role of the Corrosion Engineer in Contributing Towards the United Nations Sustainable Development Goals, in: NACE CORROSION, NACE, 2020, pp. NACE-2020-14605.

[38] D.-H. Xia, S. Song, Z. Qin, W. Hu, Y. Behnamian, Review—Electrochemical Probes and Sensors Designed for Time-Dependent Atmospheric Corrosion Monitoring: Fundamentals, Progress, and Challenges, Journal of The Electrochemical Society, 167 (2020) 037513.

[39] B.G. Koushik, N. Van den Steen, M.H. Mamme, Y. Van Ingelgem, H. Terryn, Review on modelling of corrosion under droplet electrolyte for predicting atmospheric corrosion rate, Journal of Materials Science & Technology, 62 (2021) 254-267.

[40] J.H. Cho, C. Lee, S.H. Hong, H.Y. Jang, S. Back, M.-g. Seo, M. Lee, H.-K. Min, Y. Choi, Y.J. Jang, S.H. Ahn, H.W. Jang, S.Y. Kim, Transition Metal Ion Doping on ZIF-8 Enhances the Electrochemical CO2 Reduction Reaction, Advanced Materials, 35 (2023) 2208224.

[41] S. Zhang, X. Zheng, P. Wang, D. Zhang, Fabrication of super-hydrophobic micro-needle ZnO surface as corrosion barrier against corrosion in simulated condensation

environment, Colloids and Surfaces A: Physicochemical and Engineering Aspects, 585 (2020) 124087.

[42] H. Wang, J. Zhuang, H. Qi, J. Yu, Z. Guo, Y. Ma, Laser-chemical treated superhydrophobic surface as a barrier to marine atmospheric corrosion, Surface and Coatings Technology, 401 (2020) 126255.

[43] P. Refait, A.M. Grolleau, M. Jeannin, C. Rémazeilles, R. Sabot, Corrosion of Carbon Steel in Marine Environments: Role of the Corrosion Product Layer, Corrosion and Materials Degradation, 1 (2020) 198-218.

[44] Y. Fan, W. Liu, S. Li, T. Chowwanonthapunya, B. Wongpat, Y. Zhao, B. Dong, T. Zhang, X. Li, Evolution of rust layers on carbon steel and weathering steel in high humidity and heat marine atmospheric corrosion, Journal of Materials Science & Technology, 39 (2020) 190-199.

[45] J.S. Lee, R.I. Ray, An Evaluation of Carbon Steel Corrosion under Stagnant Seawater Conditions, in: CORROSION 2004, 2004, pp. NACE-04595.

[46] J. Nawrocki, U. Raczyk-Stanisławiak, J. Świetlik, A. Olejnik, M.J. Sroka, Corrosion in a distribution system: Steady water and its composition, Water Research, 44 (2010) 1863-1872.

[47] R.W. Bradshaw, S.H. Goods, Corrosion of Alloys and Metals by Molten Nitrates, in, United States, 2001.

[48] G. Lazorenko, A. Kasprzhitskii, T. Nazdracheva, Anti-corrosion coatings for protection of steel railway structures exposed to atmospheric environments: A review, Construction and Building Materials, 288 (2021) 123115.

[49] V. Chobaomsup, M. Metzner, Y. Boonyongmaneerat, Superhydrophobic surface modification for corrosion protection of metals and alloys, Journal of Coatings Technology and Research, 17 (2020) 583-595.

[50] Z. Gong, J. Wang, L. Wu, X. Wang, G. LÜ, L. Liao, Fabrication of Super Hydrophobic Surfaces on Copper by Solution-immersion, Chinese Journal of Chemical Engineering, 21 (2013) 920-926.

[51] A. Chakraborty, R. Ghosh, M. Sudan, A. Mondal, Improvement in hot dip galvanized coating microstructure and properties by pre-metallic deposition on steel surface: A comprehensive review, Surface and Coatings Technology, 449 (2022) 128972.

[52] Z. Kamdi, F. Mohd, Case Study in Evaluation and Performance of Metallic and Polymer Coating as Corrosion Protection In Marine Environment, Research Progress in Mechanical and Manufacturing Engineering, 1 (2020) 56-63.

[53] D. Czachor-Jadacka, B. Pilch-Pitera, Progress in development of UV curable powder coatings, Progress in Organic Coatings, 158 (2021) 106355.

[54] S. Rossi, F. Russo, M. Calovi, Durability of vitreous enamel coatings and their resistance to abrasion, chemicals, and corrosion: a review, Journal of Coatings Technology and Research, 18 (2021) 39-52.

[55] H.-F. Chen, C. Zhang, Y.-C. Liu, P. Song, W.-X. Li, G. Yang, B. Liu, Recent progress in thermal/environmental barrier coatings and their corrosion resistance, Rare Metals, 39 (2020) 498-512.

[56] J. Liu, Z. Li, L. Zhang, J. Hou, Z. Lu, P. Zhang, B. Wang, N. Jin, Degradation behavior and mechanism of polyurethane coating for aerospace application under atmospheric conditions in South China Sea, Progress in Organic Coatings, 136 (2019) 105310.

[57] M. Faccini, L. Bautista, L. Soldi, A.M. Escobar, E. Domínguez, Environmentally Friendly Anticorrosive Polymeric Coatings, Applied Sciences, 11 (2021) 3446.

[58] H. Zhang, W. Sun, L. Wang, J. Wang, S. Wang, G. Liu, A Mechanically and Chemically Stable Superhydrophobic Coating for Preventing Marine Atmospheric Corrosion, Surfaces and Interfaces, 27 (2021) 101537.

[59] E. Sadeghi, N. Markocsan, S. Joshi, Advances in Corrosion-Resistant Thermal Spray Coatings for Renewable Energy Power Plants. Part I: Effect of Composition and Microstructure, Journal of Thermal Spray Technology, 28 (2019) 1749-1788.

[60] R.G. Buchheit, Chapter 18 - Corrosion resistant coatings and paints, in: M. Kutz (Ed.) Handbook of Environmental Degradation of Materials, William Andrew Publishing, Norwich, NY, 2005, pp. 367-385.

[61] P. Vijayan, M. Al-Maadeed, Self-Repairing Composites for Corrosion Protection: A Review on Recent Strategies and Evaluation Methods, Materials, 12 (2019).

[62] N. Roghanian, N. Banthia, Development of a sustainable coating and repair material to prevent bio-corrosion in concrete sewer and waste-water pipes, Cement and Concrete Composites, 100 (2019) 99-107.

[63] Y. Jia, C. Zhou, Y. Gao, Y. Zhou, M. Liu, H. Wang, Atmospheric Corrosion Resistance of Weathering Angle Steels in a Simulated Industrial Atmosphere, Journal of Materials Engineering and Performance, 29 (2020) 1225-1234.

[64] S. Guo, D. Xu, Y. Li, Y. Guo, S. Wang, D.D. Macdonald, Corrosion characteristics and mechanisms of typical Ni-based corrosion-resistant alloys in sub- and supercritical water, The Journal of Supercritical Fluids, 170 (2021) 105138.

[65] Q. Liu, J. Qian, R. Barker, C. Wang, A. Neville, F. Pessu, Effect of thermal cycling on the corrosion behaviour of stainless steels and Ni-based alloys in molten salts under air and argon, Solar Energy, 238 (2022) 248-257.

[66] W. Wu, Z. Dai, Z. Liu, C. Liu, X. Li, Synergy of Cu and Sb to enhance the

resistance of 3%Ni weathering steel to marine atmospheric corrosion, Corrosion Science, 183 (2021) 109353.

[67] H. Cheng, Z. Pan, Y. Fu, X. Wang, Y. Wei, H. Luo, X. Li, Review—Corrosion-Resistant High-Entropy Alloy Coatings: A Review, Journal of The Electrochemical Society, 168 (2021) 111502.

[68] S. Zehra, M. Mobin, J. Aslam, 1 - An overview of the corrosion chemistry, in: C.M. Hussain, C. Verma, J. Aslam (Eds.) Environmentally Sustainable Corrosion Inhibitors, Elsevier, 2022, pp. 3-23.

[69] J. Esquivel, R.K. Gupta, Review—Corrosion-Resistant Metastable Al Alloys: An Overview of Corrosion Mechanisms, Journal of The Electrochemical Society, 167 (2020) 081504.

[70] A. Eslamimanesh, A. Anderko, M.M. Lencka, Prediction of General and Localized Corrosion of Corrosion-Resistant Alloys in Aggressive Environments, in: CORROSION 2019, 2019, pp. NACE-2019-12763.

[71] S. Li, L. Zhang, Y. Wang, P. Hu, N. Jiang, P. Guo, X. Wang, H. Feng, Effect of cathodic protection current density on corrosion rate of high-strength steel wires for stay cable in simulated dynamic marine atmospheric rainwater, Structures, 29 (2021) 1655-1670.

[72] P. Astuti, K. Kamarulzaman, R.S. Rafdinal, H. Hamada, Y. Sagawa, D. Yamamoto, Influence of Rust Removal Process on The Effectiveness of Sacrificial Anode Cathodic Protection in Repair Concrete, IOP Conference Series: Materials Science and Engineering, 849 (2020) 012088.

[73] P. Hu, S. Li, N. Jiang, Y. Yan, Investigation of the impressed current cathodic protection method for the cable parallel wires in the rainwater electrolyte based on acoustic emission method, Construction and Building Materials, 229 (2019) 116918.

[74] M. Yang, S. Kainuma, S. Ishihara, A. Kaneko, T. Yamauchi, Atmospheric corrosion protection method for corroded steel members using sacrificial anode of Al-based alloy, Construction and Building Materials, 234 (2020) 117405.

[75] L. Yan, G.-L. Song, P. Wu, Y. Zhu, D. Zheng, A chloride-sensitive corrosion sensor and protector made of an optimized Mg-Al alloy for reinforcing steel, Materials & Design, 210 (2021) 110028.

[76] N.T. Chung, M.S. Hong, J.G. Kim, Optimizing the Required Cathodic Protection Current for Pre-Buried Pipelines Using Electrochemical Acceleration Methods, Materials, 14 (2021) 579.

[77] J.Y. Hu, S.S. Zhang, E. Chen, W.G. Li, A review on corrosion detection and protection of existing reinforced concrete (RC) structures, Construction and Building

Materials, 325 (2022) 126718.

[78] A. Goyal, E.K. Olorunnipa, H.S. Pouya, E. Ganjian, A.O. Olubanwo, Potential and current distribution across different layers of reinforcement in reinforced concrete cathodic protection system- A numerical study, Construction and Building Materials, 262 (2020) 120580.

[79] Y. Zhou, X. Zheng, F. Xing, L. Sui, Y. Zheng, X. Huang, Investigation on the electrochemical and mechanical performance of CFRP and steel-fiber composite bar used for impressed current cathodic protection anode, Construction and Building Materials, 255 (2020) 119377.

[80] F. Wang, J. Xu, Y. Xu, L. Jiang, G. Ma, A comparative investigation on cathodic protections of three sacrificial anodes on chloride-contaminated reinforced concrete, Construction and Building Materials, 246 (2020) 118476.

[81] R. Polder, W. Peelen, Cathodic protection of reinforcement in concrete – experience and development over 30 years, MATEC Web Conf., 289 (2019).

[82] U.M. Angst, A Critical Review of the Science and Engineering of Cathodic Protection of Steel in Soil and Concrete, Corrosion, 75 (2019) 1420-1433.

[83] H. Liu, F. Cao, G.-L. Song, D. Zheng, Z. Shi, M.S. Dargusch, A. Atrens, Review of the atmospheric corrosion of magnesium alloys, Journal of Materials Science & Technology, 35 (2019) 2003-2016.

[84] O.S.I. Fayomi, I.G. Akande, S. Odigie, Economic Impact of Corrosion in Oil Sectors and Prevention: An Overview, Journal of Physics: Conference Series, 1378 (2019) 022037.

[85] M. Strebl, M. Bruns, S. Virtanen, Editors' Choice—Respirometric in Situ Methods for Real-Time Monitoring of Corrosion Rates: Part I. Atmospheric Corrosion, Journal of The Electrochemical Society, 167 (2020) 021510.

[86] Z. Pei, D. Zhang, Y. Zhi, T. Yang, L. Jin, D. Fu, X. Cheng, H.A. Terryn, J.M.C. Mol, X. Li, Towards understanding and prediction of atmospheric corrosion of an Fe/Cu corrosion sensor via machine learning, Corrosion Science, 170 (2020) 108697.

[87] O. Habibzadeh-Bigdarvish, X. Yu, T. Li, G. Lei, A. Banerjee, A.J. Puppala, A novel full-scale external geothermal heating system for bridge deck de-icing, Applied Thermal Engineering, 185 (2021) 116365.

[88] S. Guo, R. Si, Q. Dai, Z. You, Y. Ma, J. Wang, A critical review of corrosion development and rust removal techniques on the structural/environmental performance of corroded steel bridges, Journal of Cleaner Production, 233 (2019) 126-146.

[89] H.A. Kazem, M.T. Chaichan, A.H.A. Al-Waeli, K. Sopian, A review of dust accumulation and cleaning methods for solar photovoltaic systems, Journal of Cleaner

Production, 276 (2020) 123187.

[90] M. Galiński, A. Lewandowski, I. Stępniak, Ionic liquids as electrolytes, Electrochimica Acta, 51 (2006) 5567-5580.

[91] H. Lee, G. Kim, Y. Song, S. Cho, S. Park, Hybrid Liquid–Solid Composite Electrolytes for Sulfide-Based Solid-State Batteries: Advantages and Limitation, Advanced Functional Materials, 33 (2023) 2305373.

[92] T. Famprikis, P. Canepa, J.A. Dawson, M.S. Islam, C. Masquelier, Fundamentals of inorganic solid-state electrolytes for batteries, Nature Materials, 18 (2019) 1278-1291.

[93] E. Peled, D. Golodnitsky, G. Ardel, Advanced Model for Solid Electrolyte Interphase Electrodes in Liquid and Polymer Electrolytes, Journal of The Electrochemical Society, 144 (1997) L208.

[94] K. Xu, Nonaqueous Liquid Electrolytes for Lithium-Based Rechargeable Batteries, Chemical Reviews, 104 (2004) 4303-4418.

[95] Ju, Brushett, R. Fikile, Bazant, Z. Martin, Bai, Peng, Transition of lithium growth mechanisms in liquid electrolytes, Energy & environmental science: EES, (2016).

[96] J.W. Fergus, Ceramic and polymeric solid electrolytes for lithium-ion batteries, Journal of Power Sources, 195 (2010) 4554-4569.

[97] G. Xi, M. Xiao, S. Wang, D. Han, Y. Li, Y. Meng, Polymer-Based Solid Electrolytes: Material Selection, Design, and Application, Advanced Functional Materials, 31 (2021) 2007598.

[98] K.J. Kim, M. Balaish, M. Wadaguchi, L. Kong, J.L.M. Rupp, Solid-State Li–Metal Batteries: Challenges and Horizons of Oxide and Sulfide Solid Electrolytes and Their Interfaces, Advanced Energy Materials, 11 (2021) 2002689.

[99] N. Miura, G. Lu, N. Yamazoe, Progress in mixed-potential type devices based on solid electrolyte for sensing redox gases, Solid State Ionics, 136-137 (2000) 533-542.

[100] J.R. Stetter, W.R. Penrose, S. Yao, Sensors, Chemical Sensors, Electrochemical Sensors, and ECS, Journal of The Electrochemical Society, 150 (2003) S11.

[101] S. Fonna, R. Kurniawan, Israr, R. Fachri, S. Huzni, The Effect of Stray Current from Sacrificial Anode Cathodic Protection (SACP) System on the Adjacent Unprotected Reinforcing Steel, IOP Conference Series: Materials Science and Engineering, 796 (2020) 012013.

[102] E.K. Arya, B.S. Dhanya, Corrosion control of reinforced concrete structures in construction industry: A review, IOP Conference Series: Materials Science and Engineering, 1114 (2021) 012006.

[103] B. Van Belleghem, M. Maes, T. Soetens, Throwing power and service life of galvanic cathodic protection with embedded discrete anodes for steel reinforcement in

chloride contaminated concrete, Construction and Building Materials, 310 (2021) 125187.

[104] L. Bertolini, M. Gastaldi, M. Pedeferri, E. Redaelli, Prevention of steel corrosion in concrete exposed to seawater with submerged sacrificial anodes, Corrosion Science, 44 (2002) 1497-1513.

[105] N. Krishnan, D.K. Kamde, Z. Doosa Veedu, R.G. Pillai, D. Shah, R. Velayudham, Long-term performance and life-cycle-cost benefits of cathodic protection of concrete structures using galvanic anodes, Journal of Building Engineering, 42 (2021) 102467.

[106] X. Cheng, J. Xia, R.-j. Wu, W.-l. Jin, C.-g. Pan, Optimisation of sacrificial anode cathodic protection system in chloride-contaminated reinforced concrete structure, Journal of Building Engineering, 45 (2022) 103515.

[107] A. Torres-Acosta Andrés, R. Sen, M. Martı´nez-Madrid, Cathodic Protection of Reinforcing Steel in Concrete Using Conductive-Polymer System, Journal of Materials in Civil Engineering, 16 (2004) 315-321.

[108] Y. Liu, X. Shi, Cathodic Protection Technologies for Reinforced Concrete: Introduction and Recent Developments, 25 (2009) 339-388.

[109] P. Arito, Discrete sacrificial anodes and their use in service life extension of chloride contaminated reinforced concrete structures, in, University of Cape Town, 2012.

[110] S. Ndeutapo, An economic evaluation on FRP for bridge construction in South African coastal areas, in, 2022.

[111] K. Wilson, M. Jawed, V. Ngala, The selection and use of cathodic protection systems for the repair of reinforced concrete structures, Construction and Building Materials, 39 (2013) 19-25.

[112] M.T. Walsh, A.A. Sagüés, Modeling and Control of Localized Corrosion of Steel in Submerged Reinforced Concrete Structures, in: CORROSION 2016, 2016, pp. NACE-2016-7766.

[113] S.J. Bullard, S.D. Cramer, J.B.S. Covino, G.R. Holcomb, M. Ziomek-Moroz, C.C. B, M.L. Gallardo, Corrosion prevention of Oregon's reinforced coastal bridges, in, Seoul National University, Korea Concrete Institute, Seoul, Korea, United States, 2004.

[114] S.C. Das, H.S. Pouya, E. Ganjian, Corrosion mitigation of chloride-contaminated reinforced concrete structures: a state-of-the-art review, Construction Materials, 164 (2011) 21-28.

[115] S. Kainuma, Y. Tsuchihashi, S. Ishihara, D. Uchida, A. Kaneko, T. Yamauchi, Study on Atmospheric Corrosion Protection Method with Al-Zn Sacrificial Anode and Fiber Sheet for Steel Members, Journal of Japan Society of Civil Engineers, Ser. A1 (Structural Engineering & Earthquake Engineering (SE/EE)), 73 (2017) 313-329.

[116] S. Kainuma, K. Utsunomiya, S. Ishihara, D. Uchida, A. Kaneko, T. Yamauchi,

Influences of Mixing and Porosity Ratios of Porous Sintered Al-Zn Plate and Material Property of Fiber Sheet on Anticorrosive Effects of Sacrificial Anode for Carbon Steel in Atmospheric Environment, Zairyo-to-Kankyo, 62 (2013) 278-288.

[117] S. Kainuma, K. Utsunomiya, S. Ishihara, D. Uchida, A. Kaneko, Fundamental Study on Corrosion Protection Method with Sacrificial Anode of Steel Members using Porous Sintered Plate and Fiber Sheet in Atmospheric Environment, Zairyo-to-Kankyo, 60 (2011) 535-540.

[118] S. Kainuma, Y. Tsuchihashi, S. Ishihara, D. Uchida, A. Kaneko, T. Yamauchi, Fundamental Study on Anti-corrosive Method with Sacrificial Anode for Steel Members using Al-Zn Alloy Casting Plate and Fiber Sheet in Atmospheric Environment, Zairyo-to-Kankyo, 65 (2016) 390-397.

[119] S. Ishihara, S. Kainuma, M. Kinoshita, D. Uchida, A. Kaneko, T. Yamauchi, Fundamental Study on Corrosion Protection Effect with Sacrificial Anode for Corroded Steel Members using Porous Sintered Plate and Fiber Sheet in an Atmospheric Environment, Zairyo-to-Kankyo, 63 (2014) 609-615.

[120] S. Kainuma, M. Yang, S. Ishihara, Corrosivity Evaluation for Steel Members near the Atmosphere-liquid Interface Using the Ground Corrosion Sensor, Zairyo-to-Kankyo, 67 (2018) 404-415.

[121] S. Kainuma, N. Hosomi, Fatigue life evaluation of corroded structural steel members in boundary with concrete, International Journal of Fracture, 157 (2009) 149-158.

[122] S. Kainuma, N. Hosomi, I.-T. Kim, Y. Itoh, Time-dependent Corrosion Behavior of Structural Steel Members in Boundary with Concrete, Doboku Gakkai Ronbunshu, 2005 (2005) 780_797-780_114.

[123] I. Iwaki, A. Kamiharako, Y. Koda, H. Naito, H. Minagawa, M. Suzuki, Evaluation on Properties o Concrete and Steel in Pc Bridge Girders Severely Damaged by Chloride Induced Deterioration, Doboku Gakkai Ronbunshuu E, 66 (2010) 413-432.

[124] C. Jiang, Y.-F. Wu, G. Wu, Plastic Hinge Length of FRP-Confined Square RC Columns, Journal of Composites for Construction, 18 (2014) 04014003.

[125] C. Jiang, Y.-F. Wu, M.-J. Dai, Degradation of steel-to-concrete bond due to corrosion, Construction and Building Materials, 158 (2018) 1073-1080.

[126] W. Kurz, C. Kessler, L. Geiss Paul, S. Turcinskas, Evaluation of Adhesive Bonding between Steel and Concrete, Composite Construction in Steel and Concrete VI, (2012) 669-679.

[127] X. Wang, Y. Liu, F. Yang, Y. Lu, X. Li, Effect of concrete cover on the bond-slip behavior between steel section and concrete in SRC structures, Construction and Building

Materials, 229 (2019) 116855.

[128] J. Kere Kiswendsida, Q. Huang, Life-Cycle Cost Comparison of Corrosion Management Strategies for Steel Bridges, Journal of Bridge Engineering, 24 (2019) 04019007.

[129] S.D. Cramer, B.S. Covino, S.J. Bullard, G.R. Holcomb, J.H. Russell, F.J. Nelson, H.M. Laylor, S.M. Soltesz, Corrosion prevention and remediation strategies for reinforced concrete coastal bridges, Cement and Concrete Composites, 24 (2002) 101-117.

[130] A.M. Rajab, Cathodic Protection Design & Commissioning for Sheet Piles Using SACP Aluminum Anodes, in: AMPP Middle East Corrosion Conference and Exhibition, 2023, pp. AMPP-MECC-2023-19890.

[131] K. Suzumura, S.-i. Nakamura, Environmental Factors Affecting Corrosion of Galvanized Steel Wires, Journal of Materials in Civil Engineering, 16 (2004) 1-7.

[132] E. Oguzie, C. Enenebeaku, C. Akalezi, S. Okoro, A. Ayuk, E. Ejike, Adsorption and corrosion-inhibiting effect of Dacryodis edulis extract on low-carbon-steel corrosion in acidic media, Journal of Colloid and interface Science, 349 (2010) 283-292.

[133] M. Moradi, M. Rezaei, Construction of highly anti-corrosion and super-hydrophobic polypropylene/graphene oxide nanocomposite coatings on carbon steel: Experimental, electrochemical and molecular dynamics studies, Construction and Building Materials, 317 (2022) 126136.

[134] X. Wang, R.E. Melchers, Corrosion of carbon steel in presence of mixed deposits under stagnant seawater conditions, Journal of Loss Prevention in the Process Industries, 45 (2017) 29-42.

[135] W. Zhang, S. Yang, W.-T. Geng, Q. Hu, Corrosion behavior of the low alloy weathering steels in stagnant water, Materials Chemistry and Physics, 302 (2023) 127745.

[136] G.A. El-Mahdy, A. Nishikata, T. Tsuru, Electrochemical corrosion monitoring of galvanized steel under cyclic wet–dry conditions, Corrosion Science, 42 (2000) 183-194.

[137] L. Hao, S. Zhang, J. Dong, W. Ke, Evolution of corrosion of MnCuP weathering steel submitted to wet/dry cyclic tests in a simulated coastal atmosphere, Corrosion science, 58 (2012) 175-180.

[138] C. Li, Y. Ma, Y. Li, F. Wang, EIS monitoring study of atmospheric corrosion under variable relative humidity, Corrosion Science, 52 (2010) 3677-3686.

[139] B. Hou, X. Li, X. Ma, C. Du, D. Zhang, M. Zheng, W. Xu, D. Lu, F. Ma, The cost of corrosion in China, npj Materials Degradation, 1 (2017) 4.

[140] D. De la Fuente, I. Díaz, J. Simancas, B. Chico, M. Morcillo, Long-term atmospheric corrosion of mild steel, Corrosion Science, 53 (2011) 604-617.

[141] C.A. Vázquez-Rodríguez, M. De La Garza-Garza, C. Gaona Tiburcio, B.E. Maldonado, M.A. Baltazar-Zamora, G.C.R. de J, R.O. García, N.F. Garza-Montes-de-Oca, R.J.L. Ramirez, F. Almeraya-Calderón, Characterization of Corrosion Behavior of Painted Galvanized Steel under Accelerated Conditions, International Journal of Electrochemical Science, 10 (2015) 4654-4665.

[142] R. Vera, E. Cruz, M. Bagnara, R. Araya, R. Henríquez, A. Díaz-Gómez, P. Rojas, Evaluation of Anticorrosive Coatings on Carbon Steel in Marine Environments: Accelerated Corrosion Test and Field Exposure, International Journal of Electrochemical Science, 13 (2018) 898-914.

[143] W. Thandar, K.K. Thaw, T. Tomiyama, The Effect of Substrate's Preparation on Repainting Degradation, Structural Safety and Reliability: Proceedings of the Japan Conference on Structural Safety and Reliability (JCOSSAR), 10 (2023) 46-53.

[144] E.S. Kline, Steel bridges: Corrosion protection for 100 years, Journal of Protective Coatings & Linings, (2008) 20.

[145] R.P. Nicolai, R. Dekker, J.M. van Noortwijk, A comparison of models for measurable deterioration: An application to coatings on steel structures, Reliability Engineering & System Safety, 92 (2007) 1635-1650.

[146] W. Guo, X. Li, M. Chen, L. Xu, L. Dong, X. Cao, W. Tang, J. Zhu, C. Lin, C. Pan, Electrochemical cathodic protection powered by triboelectric nanogenerator, Advanced Functional Materials, 24 (2014) 6691-6699.

[147] T. Zhang, W. Zhao, T. Li, Y. Zhao, Q. Deng, Y. Wang, W. Jiang, Comparison of hydrogen embrittlement susceptibility of three cathodic protected subsea pipeline steels from a point of view of hydrogen permeation, Corrosion Science, 131 (2018) 104-115.

[148] X. Mu, J. Wei, J. Dong, W. Ke, In situ corrosion monitoring of mild steel in a simulated tidal zone without marine fouling attachment by electrochemical impedance spectroscopy, Journal of Materials Science & Technology, 30 (2014) 1043-1050.

[149] C. Yao, X. Wang, W. Zhang, W. Xia, Z. Chen, B. Han, Formation of calcareous deposits in the tidal zone and its effect on cathodic protection, npj Materials Degradation, 7 (2023) 30.

[150] K. Hornbostel, C.K. Larsen, M.R. Geiker, Relationship between concrete resistivity and corrosion rate–A literature review, Cement and concrete composites, 39 (2013) 60-72.

[151] I.-C. Park, S.-J. Kim, Determination of corrosion protection current density requirement of zinc sacrificial anode for corrosion protection of AA5083-H321 in seawater, Applied Surface Science, 509 (2020) 145346.

[152] S. Kainuma, M. Yang, S. Ishihara, A. Kaneko, T. Yamauchi, Corrosion protection

of steel members using an Al-Zn base sacrificial anode and fiber sheet in an atmospheric environment, Construction and Building Materials, 224 (2019) 880-893.

[153] Z. Pei, X. Cheng, X. Yang, Q. Li, C. Xia, D. Zhang, X. Li, Understanding environmental impacts on initial atmospheric corrosion based on corrosion monitoring sensors, Journal of Materials Science & Technology, 64 (2021) 214-221.

[154] Q. Wang, S. Kainuma, P. Huo, R. Morikawa, Quantitative evaluation of surface cleanliness of weathering steel treated by continuous wave laser, Optics & Laser Technology, 158 (2023) 108864.

[155] S.B. Lyon, R. Bingham, D.J. Mills, Advances in corrosion protection by organic coatings: What we know and what we would like to know, Progress in Organic Coatings, 102 (2017) 2-7.

[156] C.S. Witharamage, M.A. Alrizqi, J. Chirstudasjustus, A.A. Darwish, T. Ansell, A. Nieto, R.K. Gupta, Corrosion-resistant metallic coatings for aluminum alloys by cold spray, Corrosion Science, 209 (2022) 110720.

[157] M. Zhang, S. Huang, P. Li, K.W. Shah, X. Zhang, Application of dehumidification as anti-corrosion technology on suspension bridges: A review, Applied Thermal Engineering, 199 (2021) 117549.

[158] L. Guo, S.R. Street, H.B. Mohammed-Ali, M. Ghahari, N. Mi, S. Glanvill, A. Du Plessis, C. Reinhard, T. Rayment, A.J. Davenport, The effect of relative humidity change on atmospheric pitting corrosion of stainless steel 304L, Corrosion Science, 150 (2019) 110-120.

[159] J. Cui, X. Li, Z. Pei, Y. Pei, A long-term stable and environmental friendly self-healing coating with polyaniline/sodium alginate microcapsule structure for corrosion protection of water-delivery pipelines, Chemical Engineering Journal, 358 (2019) 379-388.

[160] F. Deflorian, S. Rossi, M. Fedel, Organic coatings degradation: Comparison between natural and artificial weathering, Corrosion Science, 50 (2008) 2360-2366.

[161] A. Bajpai, A. Giri, Water sorption behaviour of highly swelling (carboxy methylcellulose-g-polyacrylamide) hydrogels and release of potassium nitrate as agrochemical, Carbohydrate polymers, 53 (2003) 271-279.

[162] K.M. Zmetra, K.F. McMullen, A.E. Zaghi, K. Wille, Experimental study of UHPC repair for corrosion-damaged steel girder ends, Journal of Bridge Engineering, 22 (2017) 04017037.

[163] M. Shamsuddoha, M.M. Islam, T. Aravinthan, A. Manalo, K.-t. Lau, Effectiveness of using fibre-reinforced polymer composites for underwater steel pipeline repairs, Composite Structures, 100 (2013) 40-54.

[164] D. Xue, J. Liu, Y. Song, X. Zhang, Performance Analysis of a Hybrid Dehumidification System Adapted for Suspension Bridge Corrosion Protection: A Numerical Study, Applied Sciences, 13 (2023) 4219.

[165] M.M. Rafique, P. Gandhidasan, H.M. Bahaidarah, Liquid desiccant materials and dehumidifiers–A review, Renewable and Sustainable Energy Reviews, 56 (2016) 179-195.

[166] N.K. Prasad, A. Pathak, S. Kundu, K. Mondal, Novel hybrid sacrificial anodes based on high phosphorus pig iron and Zn, Corrosion Science, 189 (2021) 109616.

[167] H.M.H. Farh, M.E.A.B. Seghier, T. Zayed, A comprehensive review of corrosion protection and control techniques for metallic pipelines, Engineering Failure Analysis, (2022) 106885.

[168] L. Bertolini, E. Redaelli, Throwing power of cathodic prevention applied by means of sacrificial anodes to partially submerged marine reinforced concrete piles: Results of numerical simulations, Corrosion Science, 51 (2009) 2218-2230.

[169] M. Yang, S. Kainuma, S. Zhuang, S. Ishihara, A. Kaneko, T. Yamauchi, Cathodic protection system applied to steel using fiber sheet and Al-based alloy anode in atmospheric environment, Int. J. Electrochem. Sci, 14 (2019) 9858-9875.

[170] C. Rousseau, F. Baraud, L. Leleyter, O. Gil, Cathodic protection by zinc sacrificial anodes: Impact on marine sediment metallic contamination, Journal of hazardous materials, 167 (2009) 953-958.

[171] J. Richir, S. Bray, T. McAleese, G.J. Watson, Three decades of trace element sediment contamination: the mining of governmental databases and the need to address hidden sources for clean and healthy seas, Environment International, 149 (2021) 106362.

[172] Y. Huang, Z. Li, Z. Pei, Z. Liu, H. Li, M. Zhu, J. Fan, Q. Dai, M. Zhang, L. Dai, Solid‐state rechargeable Zn//NiCo and Zn–air batteries with ultralong lifetime and high capacity: the role of a sodium polyacrylate hydrogel electrolyte, Advanced Energy Materials, 8 (2018) 1802288.

[173] A. Ortiz-Ozuna, F. Godínez, B. Ramírez-Barat, M. Garcia-Alonso, M. Escudero, S. Fajardo, J. Genesca, R. Montoya, pH evolution around the AZ31/Steel galvanic couple under gelled-electrolytes: A numerical and experimental study, Corrosion Science, 178 (2021) 109061.

[174] S. Zhao, Y. Zuo, T. Liu, S. Zhai, Y. Dai, Z. Guo, Y. Wang, Q. He, L. Xia, C. Zhi, Multi‐functional hydrogels for flexible zinc‐based batteries working under extreme conditions, Advanced Energy Materials, 11 (2021) 2101749.

[175] J.R. Witono, I. Noordergraaf, H. Heeres, L. Janssen, Water absorption, retention and the swelling characteristics of cassava starch grafted with polyacrylic acid,

Carbohydrate polymers, 103 (2014) 325-332.

[176] G.K. Tummala, T. Joffre, R. Rojas, C. Persson, A. Mihranyan, Strain-induced stiffening of nanocellulose-reinforced poly (vinyl alcohol) hydrogels mimicking collagenous soft tissues, Soft Matter, 13 (2017) 3936-3945.

[177] Z. Darban, S. Shahabuddin, R. Gaur, I. Ahmad, N. Sridewi, Hydrogel-based adsorbent material for the effective removal of heavy metals from wastewater: a comprehensive review, Gels, 8 (2022) 263.

[178] J. Kaur, P. Sengupta, S. Mukhopadhyay, Critical review of bioadsorption on modified cellulose and removal of divalent heavy metals (Cd, Pb, and Cu), Industrial & Engineering Chemistry Research, 61 (2022) 1921-1954.

[179] W. Rengga, A. Seubsai, S. Roddecha, S. Azizah, D. Rosada, Kinetic study of adsorption carboxylic acids of used cooking oil using mesoporous active carbon, in: IOP Conference Series: Earth and Environmental Science, IOP Publishing, 2021, pp. 012035.

[180] G. Chitra, M. Selvi, D. Franklin, S. Sudarsan, M. Sakthivel, S. Guhanathan, pH-sensitive biopolymeric hydrogel-based on indole-3-acetic acid for wound healing and anti-cancer applications, SN Applied Sciences, 1 (2019) 1-15.

[181] N. Xue, L. Wang, M. Pei, Y. He, Y. Du, W. Guo, Preparation and characterization of sodium polyacrylate-grafted bentonite and its performance removing Pb 2+ from aqueous solutions, Rsc Advances, 6 (2016) 98945-98951.

[182] Y. Zhang, Y. Chen, M. Alfred, F. Huang, S. Liao, D. Chen, D. Li, Q. Wei, Alkaline sodium polyacrylate-starch hydrogels with tolerance to cold conditions for stretchable zinc-air batteries, Composites Part B: Engineering, 224 (2021) 109228.

[183] J. Yang, R. Bai, B. Chen, Z. Suo, Hydrogel adhesion: a supramolecular synergy of chemistry, topology, and mechanics, Advanced Functional Materials, 30 (2020) 1901693.

[184] S. Yashima, N. Takase, T. Kurokawa, J.P. Gong, Friction of hydrogels with controlled surface roughness on solid flat substrates, Soft Matter, 10 (2014) 3192-3199.

[185] H. Sun, L. Liu, Y. Li, L. Ma, Y. Yan, The performance of Al–Zn–In–Mg–Ti sacrificial anode in simulated deep water environment, Corrosion science, 77 (2013) 77-87.

[186] P.-P. Wu, G.-L. Song, Y.-X. Zhu, L. Yan, Z.-L. Feng, D.-J. Zheng, Improvement of intelligent corrosivity-detection and corrosion-protection for reinforcing steel, Corrosion Science, 184 (2021) 109396.

[187] J. Wen, J. Lei, J. Chen, J. Gou, Y. Li, L. Li, An intelligent coating based on pH-sensitive hybrid hydrogel for corrosion protection of mild steel, Chemical Engineering

Journal, 392 (2020) 123742.

[188] W. Gao, J. Chang, X. Li, S. Li, Y. Zhou, X. Hou, L. Long, J. Zhao, X. Yuan, A Quenched Double-Hydrophilic Coating for the Enhancement of Water Retention of Hydrogels, Advanced Functional Materials, 33 (2023) 2303306.

[189] T. Zhu, C. Jiang, M. Wang, C. Zhu, N. Zhao, J. Xu, Skin-Inspired Double-Hydrophobic-Coating Encapsulated Hydrogels with Enhanced Water Retention Capacity, Advanced Functional Materials, 31 (2021) 2102433.

[190] J. Li, A. Celiz, J. Yang, Q. Yang, I. Wamala, W. Whyte, B. Seo, N. Vasilyev, J. Vlassak, Z. Suo, Tough adhesives for diverse wet surfaces, Science, 357 (2017) 378-381.

[191] Z. Jia, X. Lv, Y. Hou, K. Wang, F. Ren, D. Xu, Q. Wang, K. Fan, C. Xie, X. Lu, Mussel-inspired nanozyme catalyzed conductive and self-setting hydrogel for adhesive and antibacterial bioelectronics, Bioactive Materials, 6 (2021) 2676-2687.

[192] G. Wang, Y. Liu, B. Zu, D. Lei, Y. Guo, M. Wang, X. Dou, Reversible adhesive hydrogel with enhanced sampling efficiency boosted by hydrogen bond and van der Waals force for visualized detection, Chemical Engineering Journal, 455 (2023) 140493.

[193] W. Li, X. Yang, P. Lai, L. Shang, Bio‐inspired adhesive hydrogel for biomedicine—principles and design strategies, Smart Medicine, 1 (2022) e20220024.

[194] H. Kono, Characterization and properties of carboxymethyl cellulose hydrogels crosslinked by polyethylene glycol, Carbohydrate Polymers, 106 (2014) 84-93.

[195] S. Dong, S. Feng, F. Liu, R. Li, W. Li, F. Liu, G. Shi, L. Chen, Y. Zhang, Factors influencing the adhesive behavior of carboxymethyl cellulose-based hydrogel for food applications, International Journal of Biological Macromolecules, 179 (2021) 398-406.

[196] A. Bajpai, A. Mishra, Ionizable interpenetrating polymer networks of carboxymethyl cellulose and polyacrylic acid: evaluation of water uptake, Journal of applied polymer science, 93 (2004) 2054-2065.

[197] Y. Gao, N.K. Chai, N. Garakani, S.S. Datta, H.J. Cho, Scaling laws to predict humidity-induced swelling and stiffness in hydrogels, Soft matter, 17 (2021) 9893-9900.

[198] D. Wang, Z. Li, L. Yang, J. Zhang, Y. Wei, Q. Feng, Q. Wei, Hydrogel electrolyte based on sodium polyacrylate/KOH hydrogel reinforced with bacterial cellulose aerogel for flexible supercapacitors, Chemical Engineering Journal, 454 (2023) 140090.

[199] C.-J. Lee, H. Wu, Y. Hu, M. Young, H. Wang, D. Lynch, F. Xu, H. Cong, G. Cheng, Ionic Conductivity of Polyelectrolyte Hydrogels, ACS Applied Materials & Interfaces, 10 (2018) 5845-5852.

[200] J. Liu, Z. Chen, Y. Chen, H.U. Rehman, Y. Guo, H. Li, H. Liu, Ionic Conductive Organohydrogels with Dynamic Pattern Behavior and Multi‐Environmental Stability, Advanced Functional Materials, 31 (2021) 2101464.

ACKNOWLEDGEMENT

Foremost, I would like to express my deepest appreciation to my supervisor, Prof. Shigenobu Kainuma, whose expertise was invaluable in formulating the research and methodology. His guidance helped me in all the time of research and writing this dissertation.

Besides my supervisor, I would like to thank the dissertation examining committee: Prof. Hiroaki Nakano and Prof. Takahiro Nishida. Your insightful feedback pushed me to sharpen my thinking and brought my work to a higher level.

I would like to acknowledge Daichi Inoue from Sumitomo Mitsui Construction Steel Structures Engineering Co., Ltd.,, Shuji Ishihara from Mitsui Engineering & Shipbuilding Co., Ltd. for their wonderful collaboration. I would particularly like to single out Associate Professor Muye Yang, and Associate Professor Aran Kim, Secretary Ms. Reiko Kato and Ms. Kumi Kawano in structural design laboratory, for their patient support.

My sincere thanks also goes to fellow labmates: Qidi Wang, Sanghong Park, Yang Gao, Jiajing Xie, Lianheng Cai, Jian tang, Shengyue Li, Kaishi Takaki and Daiki Hashimoto, for the stimulating discussions, for the sleepless nights we were working together, and for all the fun we have had.

Last but not the least, I would like to thank my wife and parents, for supporting me throughout my life.